U S

FACULTY OF SCIENCE AND TECHNOLOGY

MASTER THESIS

Study programme / specialisation: Robot technology and signal processing

The spring semester, 20.23.

<u>Open</u> / Confidential

Author:	Espen Myrset

Espen Myrset
....
(signature author)

|	
Course coordinator:	Sven Ole Aase – UiS
Supervisor(s):	Kjetil Oftedal – Easee
Thesis title:	Detecting series electric arcs by using digital signal processing in Easee chargers
Credits (ECTS):	30

Keywords:

electric arc, arcing, arc fault,
electric arc detection algorithm,
AFDD, arc fault detection device,
AFCI, arc fault circuit interrupter,
digital signal processing, EV,
electric vehicle, charger

Pages: ....91..........

+ appendix: ....28..........

Stavanger, ...05.06.2023..........
date/year

Detecting series electric arcs by using digital signal processing in Easee chargers
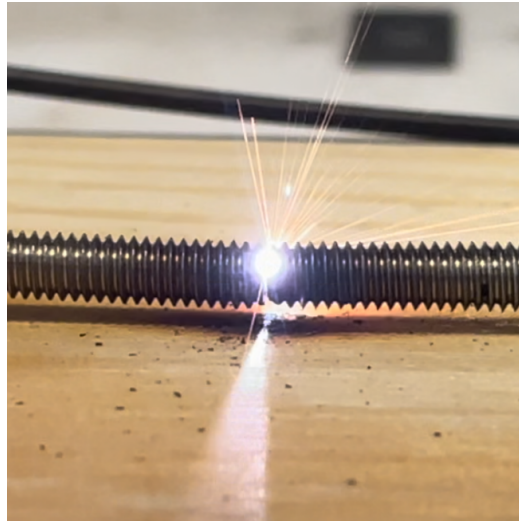
Author:

Name	Student number
Espen Myrset	247712

University of Stavanger

easee®

Master thesis
Department of Electrical Engineering and Computer Science
June 2023

Abstract

Series electric arcs can occur in a circuit by wrongly installed, damaged or ageing electrical equipment. It is the most common electrical cause of fires, and realizing series electric arc detection can improve the safety of the circuit.

In this thesis an algorithm is developed that detects series electric arcs based on current measurements by utilizing digital signal processing. It guaranties a relay release within 120 ms from when arcing starts.

The algorithm is specifically developed for Easee chargers to be implemented on its embedded microcontroller, by using its available resources and measurements, without changing its hardware. In this way, the detection can be implemented as a built-in function on both new and existing chargers in the field through over-the-air updates. Ever though it is designed for Easee chargers, the principle may be converted to other electrical equipment or measuring systems as well.

Feature extraction is the essential part of the algorithm, and five methods are developed and compared. The chosen method is based on high-pass filtering, but all the methods shows promising results and can be used in future development.

A dataset of measurements taken by the charger was collected of normal and arcing signals using an electric arc generator. The algorithm is tested using the dataset and manages to detect all the arcing signals without any false positives. However, the dataset is too small to conclude that the algorithm works sufficiently, but it indicates very promising results.

There is still more work to be done before the algorithm can be realized. This thesis forms a basis for further development and is a step towards realizing built-in series electric arc detection in Easee chargers.

Acknowledgements

I would like to thank my supervisors Sven Ole Aase from UiS and Kjetil Oftedal from Easee. They have supported me with valuable input throughout the semester and helped me through hard times. I am grateful that they have prioritized this project and all the time that they have spent on me.

I would also like to thank Easee for providing me with an office and all the necessary equipment. My gratitude also goes to Easeetonians (Easee employees) for including me in their everyday life and making me a part of the culture. I would like to give an extra thanks to Daniel Fedai Larsen, Jarand Kennedy and Vegard Pettersen for among other things helping me with 3D printing, programming tools and lab tests.

Contents

Chapter 1

Introduction

1.1 Outline

The chapter outline for the thesis is as follows:

Chapter 1 **Introduction**: The goal of the thesis, what electric arcs are and why it is desired to protect against it.

Chapter 2 **Electric arc theory**: Physics of electric arcs and some history about its study. Existing protection devices, the requirement standard IEC 62606 and today's requirement for using such protection devices.

Chapter 3 **The Easee charger**: Introduction to the Easee charger and its electrical specifications related to electric arc detection.

Chapter 4 **Data collection**: The setup of how data from electric arcs are collected using an electric arc generator and some important observations.

Chapter 5 **Detection algorithm**: Development of the electric arc detection algorithm going through each step of its structure.

Chapter 6 **Discussion**: Conclusion and further work.

1.2   Electric arcs

An electric arc (or *arcing*) is a phenomenon that occur under certain conditions where current travels through air which is normally non-conductive. It creates a bright light and a high temperature in a focused spot which can damage nearby materials as shown in figure 1.1, and in the worst case lead to fire.
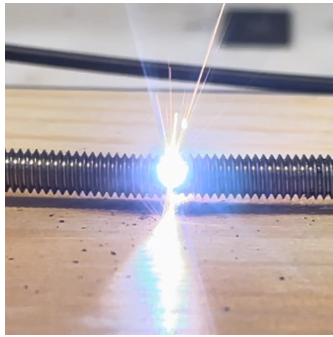
(a) Electric arcs generated at the lab by two bolts with a tiny air-gap in between.
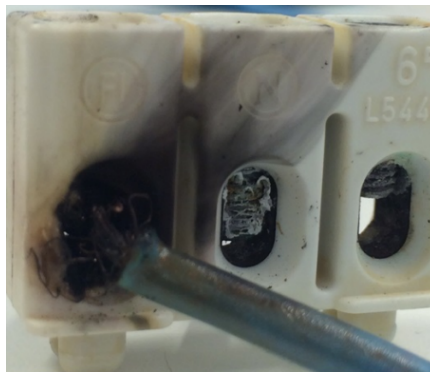
(b) Damage caused by electric arcs. From [18, fig. 6.6].

Figure 1.1: Electric arcs can cause damage.

Because of the hazard associated with electric arcs, they are undesired in electric circuits, and occurrences fall under the term *arc faults*. Arc faults are divided into three categories depending on where they occur shown in figure 1.2:

1. **Series arc fault**: Something causes the wire in the circuit to get an open connection in form of a tiny air gap where arcing occurs. The gap is in series with the load, and the supplied energy is distributed between the load and the arcing gap. Series arc faults cannot be detected by any other protection devices than an AFDD[1].

2. **Parallel arc fault**: The isolation between the live and neutral wire (L and N in figure 1.2) is insufficient causing electric arcs. Usually the current gets so high that the fuse of the circuit trips, protecting it

---

[1]AFDD (Arc fault detection and protection device) will be described in section 2.4.

against further damage. But in special circumstances the arc may have high enough and stable impedance which will not trip the fuse.

3. **Ground arc fault**: Similar to a parallel arc fault, but the arcing is from live or neutral to ground (PE in figure 1.2). Circuits that are protected with ground-fault protection will usually be protected against further damage unless the arc has high enough and stable impedance.
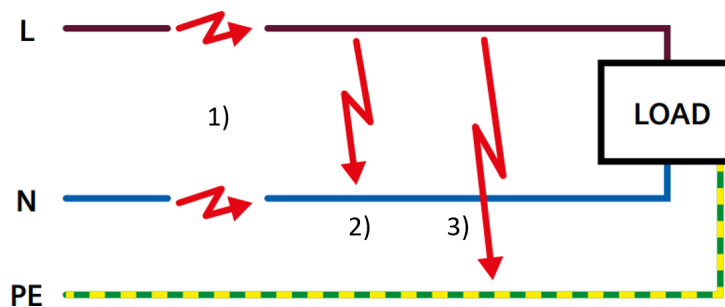
Figure 1.2: Three types of arcing faults; 1) series, 2) parallel and 3) ground arc fault. From [34, fig. 11].

The Easee charger has a built-in ground-fault protector and is installed with an individual fuse which will help protect against parallel- and ground arc faults. Having this in mind, to narrow the scope of the thesis, it is chosen to only focus on series arc faults. From now on "series electric arcs" will go under the terms "electric arcs" or "arcing".

The following list gives some examples of how series arc faults can occur:

- **Production**: Insufficient contact in PCB-tracks or relays.

- **Installation**: Cable terminals are connected to screw terminals with too low (or too high) torque making the wires loose.

- **Cable damage**: Nails, screws or clips are by accident inserted through the cable damaging the wires.

- **Use**: Charging cable exposed to too much mechanical stress which damages its wires.

1.3 Protection

Arc faults can lead to damage and fires. Statistics from DSB (Norwegian Directorate for Civil Protection) shows that electrical equipment is the cause of 21 % of fires in Norway and within that category series arc faults are the cause of 35 % (where 51 % is categorized as *other/unknown*). There are especially a higher risk of starting fires in circuits where there is a high load.

In the USA and Canada it is a requirement for most of the branch circuits to be protected by AFDDs. The question about introducing a requirement in Norway has been in the spotlight for the past years. A comprehensive study from 2021 [37] concluded that the production tests of AFDDs should change to situations that better reflects actual conditions, a large scale test of AFDDs should be done over a long time, and it should be documented that AFDDs are an effective fire prevention before introducing a requirement.

Easee facilitates for electric arcs not to occur in a charging circuit. This includes comprehensive testing of the chargers at the factory, making products and instructions that are easy to understand by electricians and using robust materials on their equipment. However, with an increase in number of installed chargers with over half a million so far, the risk is also increasing, especially as adjacent equipment start ageing.

Today there is no requirement for AFDDs in EV (Electric vehicle) charging circuits, and it is currently not known that any EV chargers on the market has built-in electric arc detection. It is through this study desired to implement it as an extra safety function to improve the safety even further.

1.4 Objective

The objective of the thesis is to make an algorithm that can detect series electric arcs in a charging circuit using measurements taken by the Easee charger. The algorithm is supposed to be executed on the charger's microcontroller using embedded software. It is desired not to make any changes in the hardware so that the functionality can be realized on existing chargers in the field using over-the-air updates as well as new products. An alternative could be to insert AFDDs into charger circuits, but this would result in great economical costs and this study will research the possibility to implement electric arc detection as a built-in functionality.

Figure 1.3 shows an example of a measurement taken by the charger where it is easy for us humans to separate a normal and an arcing signal. The idea is that digital signal processing can be utilized to automatically detect when arcing occurs.
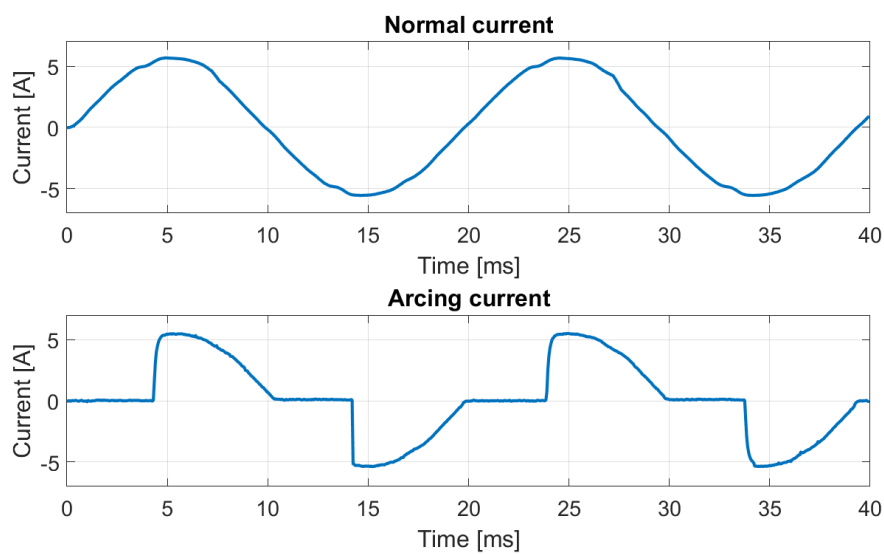
Figure 1.3: Current measurements taken by the charger where one easily can separate a normal and an arcing signal.

Chapter 2

Electric arc theory

This chapter will describe the physics of electric arcs and some history about its study. Existing protection devices are presented together with the requirement standard IEC 62606 and today's requirement for using such protection devices.

2.1 History and discovery

In the 1700s numerous phenomena related to electricity were discovered. Among other the well known experiment by Benjamin Franklin in 1752 where he proved that lightning is a form of electricity by flying a kite with a metal tip into a thunderstorm and was credited for discovering electricity [36].

Alessandro Volta invented the voltaic pile in 1799 which was the first battery. This was an essential building block for other discoveries in the early 19th century that relied on using electricity [10, p. 19]. The unit volt from the internal system of units is named after Volta which describes electric potential.

Figure 2.1: An old voltaic pile on display in museum Tempio Voltiano in Italy near where Volta lived. From [4].

Humphry Davy is credited for discovering the electric arc as early as 1800 by using his voltaic pile [6, p. 1]. In the aftermath, it is known that what Davy discovered at this time was technically speaking only short pulses of electric discharge and not a continuous electric arc. This was because of the high internal resistance and low capacity of the batteries used in the experiments which was made up of coins and cardboard soaked in dilute acid forming a voltaic pile [10, p. 21].

It is said that unaware of Davy's work the Russian experimental physicist Vasilii Petrov in 1802 created continuous electric arcs by using 4200 battery cells. The next year Petrov published his work, but it appeared only in Russian, and his work was ignored for over century [6, p. 1].

At that same time Davy increased the battery size in his experiments. Using a 2000-cell battery he demonstrated a continuous electric arc in the

Royal Institution theatre in front of a large audience. In 1812 he published the book "Elements of Chemical Philosophy" [15], and thereby establishing arc physics as a lasting science [6, p. 1]. Although Davy is generally credited for discovering the electric arc, it remains a mystery which person was the first to obtain a continuous electric arc.

(a) A packed theatre watching Davy's demonstration. Notice the shadow from underneath the table and in front of Davy, emphasizing the brightness of the electric arc.
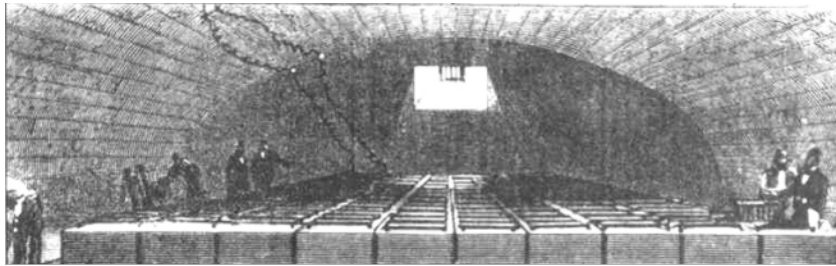
(b) The huge 2000-cell battery that was used to make the electric arc.

Figure 2.2: Davy's demonstration of the electric arc in the Royal Institution theatre in 1809 or later. From [6, Fig. 5(a)].
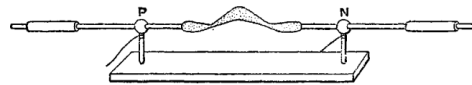
(a) A drawing of a six- to seven-inches (15-18 cm) electric arc that Davy created in one of his experiments. He gave it the name "electric arc" as the arc of flame bent upwards like an arc [10, p. 27]. From [15, Fig. 18].
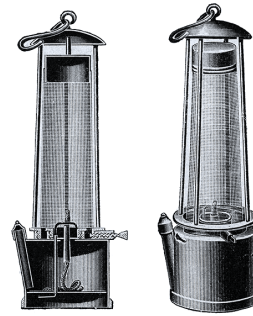
(b) Davy is also known for the invention of the carbon arc lamp which was widely used for lighting up streets, buildings and coal mines in the 1870s. From [1].

Figure 2.3: Some of Davy's contribution to research of the electric arc.

A German physicist Friedrich Paschen released an article in 1889 where he presented the equation known as Paschen's law. This equation can be used to calculate the breakdown voltage of a gas as a function of pressure and gap length. The breakdown voltage is the minimum voltage required to start an electric arc through a specific medium, and will be further discussed in section 2.2.4.

In 1902 Hertha Ayrton published the book "The Electric Arc" [10] covering her research and her husband William Edward Ayrton's experiments. At that time the electric arc was well known but not fully understood, and the book was one of the first systematic investigations of it.
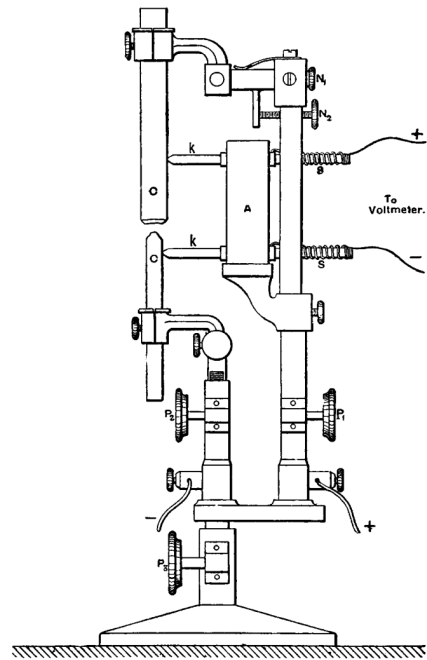
Figure 2.4: An arc lamp made by William Edward Ayrton in 1890. It was used in experiments to generate electric arcs so that characteristics could be observed. Two carbon rods were used to make a gap for the electric arc and various adjustment knobs could be used to adjust their positions and angles relative to each other. From [10, p. 98].

2.2 The quantum physics behind the electric arc phenomena

2.2.1 Introduction

An electric arc is created when a normally non-conductive material such as air starts conducting electric current [10, p. 1]. It is often known for producing heat, a bright light and making a hissing noise. Most people have seen electric arcs being created in welding, lightning or railway tracks when a train arrives.

An electric arc is a complex physical phenomenon. There are a lot of parameters affecting it, and it is today still not fully understood. The main parameters are type of gas, pressure of gas, arc length and the amount of

current passing through it [27, p. 7]. Other parameters that affect the electric arc are magnetic field, type and shape of material on the terminals, temperature and voltage potential between the terminals (which is related to the current passing through).

2.2.2   Creation and destruction

There are three main ways of creating an electric arc [27, p. 4]:

1. Raising the voltage between the terminals high enough to cause an electric discharge.

2. Raising the temperature of the air until it starts ionizing.

3. By bringing the terminals into contact establishing a current flow, then separate them.

After creation, as the gas is in a state where it is electrically conductive, it is easier to maintain an electric arc rather than creating it.

One of the most common ways to destruct an electric arc is to limit the current travelling through it by increasing the series resistance in the circuit or using some sort of switch to open the circuit. When the current is reduced the electric arc will finally blow out. The other common way is to increase the length of the air-gap so that the electric arc will increase its resistance which eventually leads to the same outcome as the previous mentioned case. An electric arc can sometimes increase its length by itself when influenced by magnetic fields or heat. When for instance the temperature of air is increased (by the electric arc), it will drift upward. The resulting curved path constitutes a longer length than the initial straight path which again will eventually blow it out at a specific length.

In AC-circuits (alternating current) the voltage alternates between a positive and negative voltage in cycles following a frequency of typically 50 or 60 Hz. The voltage will have two zero-crossings during a period, and any electric arcs will blow out at each zero-crossing and ignite again when the voltage increases over the breakdown voltage again. The higher the frequency is, the easier an electric arc will occur after each zero-crossing because of high temperature and ionisation of the air from the previous electric arcs [11, p. 1283].

2.2.3   Types of electric discharges

An electric arc is in one stage of the three types of electric discharges. The first stage is dark discharge followed by glow, and then arc discharge. An electric arc needs to go through all these stages when being created and each of them are associated with a respectively low to high current and power. Depending on the circuit, the electric discharge can be held stable in one of the three stages [22, chap. 7, 8]. This section will introduce some of the characteristics in each of these three stages.

Figure 2.5 shows the shape of the voltage-current characteristics of an electric discharge. Table 2.1 summarise typical electrical parameters. They give an idea of how any of the three electric discharge stages impact the circuit.
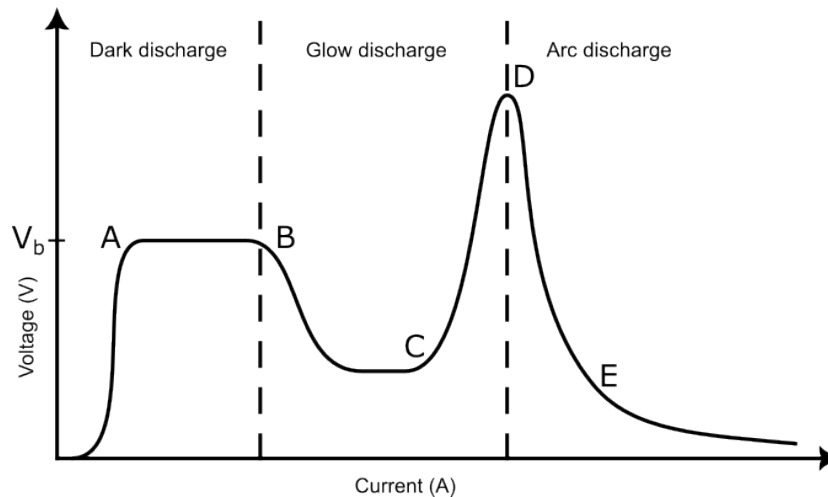

Figure 2.5: Approximation of the voltage-current characteristics to an electric discharge. The current-axis is of logarithmic scale. The different stages of the characteristic are split into dark-, glow-, and arc discharges.

	Dark discharge	Glow discharge	Arc discharge
Voltage across gap	< 500 V	100-1000 V	10-100 V
Current	< 1 μA	0.1-500 mA	1 A-30 kA
Power	< 1 mW	~100 W	1 kW/cm
Temperature	Close to ambient		Up to 20 000 °C

Table 2.1: Electrical characteristics of conventional dark-, glow-, and arc discharges. From [22, table 7.1, 8.1].

Dark discharge

An air gap in an electric circuit is often said to not conduct current. But if there is a voltage potential between the terminals very small pulses (below a pico ampere) of electrons will randomly be sent over the gap by cosmic radiation. Such discharge is called a dark discharge and is not associated with any danger.

Glow discharge

If any series resistance is reduced, or in general if the voltage across the gap is increased, the electric discharge will transfer state to a glow discharge. The threshold voltage required for the transition is called the *breakdown voltage* (A in figure 2.5). At this voltage the electrons are sent over the gap with so high energy that when it collides into other molecules it will free other electrons and so on. The gas between the gap will now contain positive ions and electrons which is electrically conductive. This ionisation process is called *secondary emission* and will evolve quickly. A small change in the voltage across the gap will significantly increase the current passing through as shown in the area AB in figure 2.5. This is called *Townsend discharge* and the hill at B is called *corona discharge* and transits the dark discharge into the glow discharge [22, chap. 7.1.4].

A glow discharge is self-sustaining meaning that once in this state it can be held stable (typically around C in figure 2.5) by less voltage that the breakdown voltage. In contrast to the dark discharge it is luminous which is the background of their names.

As shown in table 2.1 a glow discharge allows higher current to pass through and higher power than a dark discharge. But the temperature is still relatively low, so the glow discharge is also not associated with any danger.

Arc discharge

If the current increases even more, the terminals will start to heat, and the discharge will transit from the glow (CD in figure 2.5) to arc state (E in figure 2.5). This transition is triggered by thermionic emission[1] of the terminals and depends on the terminals material and shape [22, chap. 8.1.4]. The transition will for instance happen at lower current if the terminals are made up of a metal with a low melting point compared to a metal with higher melting point. In such case the voltage between the terminals does not necessarily need to exceed the voltage at D in figure 2.5, but quickly transits from C to E. Unless the circuit is carefully designed to stabilize in the glow state a discharge will typically end in the arc state.

The difference between glow and arc discharge is the type of ionisation they are sustained by. The ionisation process in a glow discharge is collisions of cold atoms (so-called secondary emission) while hot atoms in the arc discharge which is more electrical conductive [22, chap. 7.1.1].

An arc discharge is more powerful than glow and creates intense heat which evaporates[2] and erodes[3] the terminals releasing smoke and a hissing noise. The arc state is also self-sustaining like the glow, but requires an even lower voltage (see table 2.1). The electrical resistance of the arc makes it release energy, mostly heat and some radiation.

The arc as a part of an electric circuit is said to be a "negative resistor" because, unlike a normal resistance, an increase in the current will reduce the voltage across the terminals (as the region around E in figure 2.5 shows). Because of this, the arc itself is not limiting the current, only the external circuit is [22, chap. 8.6.3].

2.2.4 Breakdown voltage

The breakdown voltage is the minimum voltage required to start an electric arc through a specific medium. Paschen's law is shown in equation 2.1 and can be used to calculate the breakdown voltage as a function of gas pressure p (in Pa) and gap length d (in m).

The constants A, B and γ are dependent on the specific gas and can be found experimentally. For air A = 15 Torr^{-1}cm^{-1}, B = 365 Torr^{-1}cm^{-1} and

---

[1]Release of the materials electrons because of its high temperature.

[2]Change the state of a material into gas.

[3]Dissolve parts of the material.

γ=0.01 which simplifies the equation to 2.2 [35, chap. II A]. It is reasonable to assume constant atmospheric pressure (101 325 Pa), and the equation can be rewritten to only be dependent on distance d as shown in equation 2.3 and figure 2.6.

$$V_b = \frac{Bpd}{\ln(Apd) - \ln(\ln(1 + 1/\gamma))} \tag{2.1}$$

$$V_b = \frac{365pd}{\ln(pd) + 1.18} \tag{2.2}$$

$$V_b = \frac{37 \cdot 10^6 d}{\ln(d) + 12.71} \tag{2.3}$$

By setting the derivative of equation 2.3 equal to zero its minimum point can be found to be 304 V at 8.21 µm. This point is called *Paschen's minimum* and is the minimum breakdown voltage and its optimal gap distance. An increase in distance from Paschen's minimum requires higher voltage potential to breakdown. But a reduction from this point also requires higher voltage because of the low number of atoms between the gap [31, cap. II A].

Although Paschen's law is a reasonable approach for distances larger than Paschen's minimum, recent studies and the availability of MEMS devices (Microelectromechanical systems) have shown that there is a deviation in calculations lower than the minimum. According to [31] electrical breakdown voltage can be divided into three stages depending on the gap distance shown in table 2.2.

Gap distance	Breakdown voltage	Approach
> 8 µm	$V_b = \frac{37 \cdot 10^6 d}{\ln(d) + 12.71}$ V	Paschen's law
1 < 8 µm	$V_b = 304$ V	Paschen's minimum
< 1 µm	$V_b = 350$ V/µm	Based on new studies

Table 2.2: Approximation of breakdown voltage in air at atmospheric pressure depending on gap distance [31].

The breakdown voltage is nearly constant at distances from 1 µm to Paschen's minimum , and below 1 µm it seems to have a linear slope. The theoretical breakdown voltage of air (based on new studies) is plotted together with Paschen's law in figure 2.6.
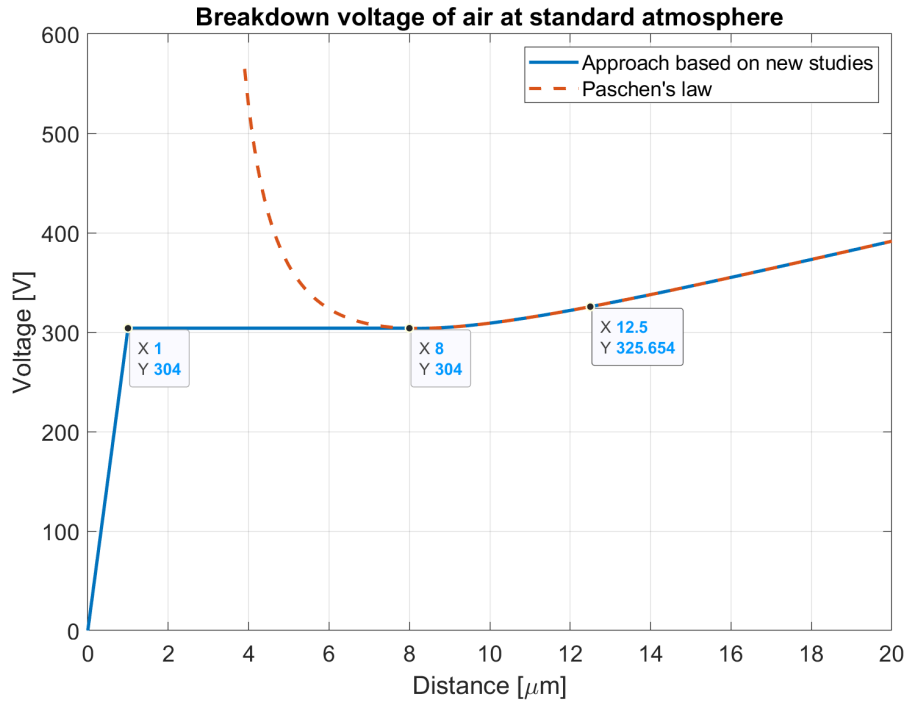
Figure 2.6: Two approaches to approximate the breakdown voltage in air at atmospheric pressure as a function of gap distance.

Breakdown voltage in 230 V AC-systems

230 V AC-systems use an alternating voltage with an RMS-value of 230 V. The voltage amplitude is found by equation 2.4 to be 325.3 V. From figure 2.6 it is shown that all distances lower than approximately 12.5 µm has a breakdown voltage under 325.3 V which theoretically leads to electric arcs in 230 V AC-systems.

$$V_{max} = 230 \cdot \sqrt{2} = 325.3 \text{ V} \tag{2.4}$$

2.3 Outcome of electric arcs

Electric arcs can lead to both desired and undesired effects. Industrial tools take advantage of the high temperature in electric arcs to melt metals. While uncontrolled arcs can lead to release of heat, fire and explosions if there is high enough current.

2.3.1 Plasma

Electric arcs and plasma are related to each other because electric arcs can be used to create plasma. As the temperature of a substance increases it transfer state in the sequence solid↔liquid↔gas↔plasma, where plasma is the fourth state of matter. Unlike the other three states, plasma consists of a mixture of electrons, ions, and neutral particles, where the electrons are not tightly bound to the atom but free throughout the system [22, chap. 1.0].

Like described in section 2.2.3 ionisation occurs during arcing. If the arc creates enough heat to make the gas thermal equilibrium it is called plasma, but the transition is not well defined.

2.3.2 Heat and fire

In section 2.2.3 it was mentioned that electric arcs creates intense heat up to 20 000 °C. This can damage nearby parts like electronic components, plastic enclosure and insulation. Such damage sets the system out of operation and results in economical costs replacing it.
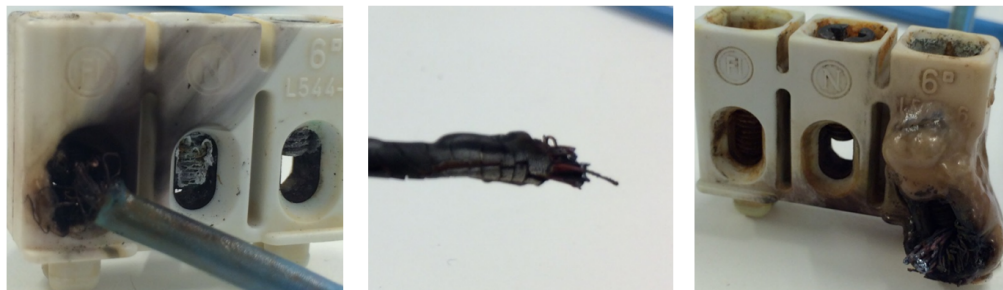
Figure 2.7: Example of damage caused by electric arcs because of loose connection caused by not tightened screw. From [18, fig. 6.6].

In the worst case heat from electric arcs can start a fire. The longer time arcing occurs, the more energy will be released to its surroundings in form of temperature increase. The temperature needed to start a fire depends on the fuel material. Wood ignites at roughly 200 °C and plastic at 400-500 °C, but usually melts and drips away before reaching such temperature [13].

Figure 2.8 shows proportion of where a fire starts in Norway. The statistics are collected from DSB (Norwegian Directorate for Civil Protection) by using fire cases that is publicly available in the period 2009-2022. Electrical equipment is the cause of 21 % of fires (yearly average of 1200 fires) where within that category series arcs are the highest cause of 35 % (yearly average of 420 fires). There are especially a higher risk of electric arc fires in circuits where there is a high load [37, chap. 3.1]. One should note from figure 2.8b that a portion of 51 % of the fires are in the category *other/unknown* and due to the fact that many fires are hard to investigate the number is expected to be even higher.

Where fires starts (2016-2022)
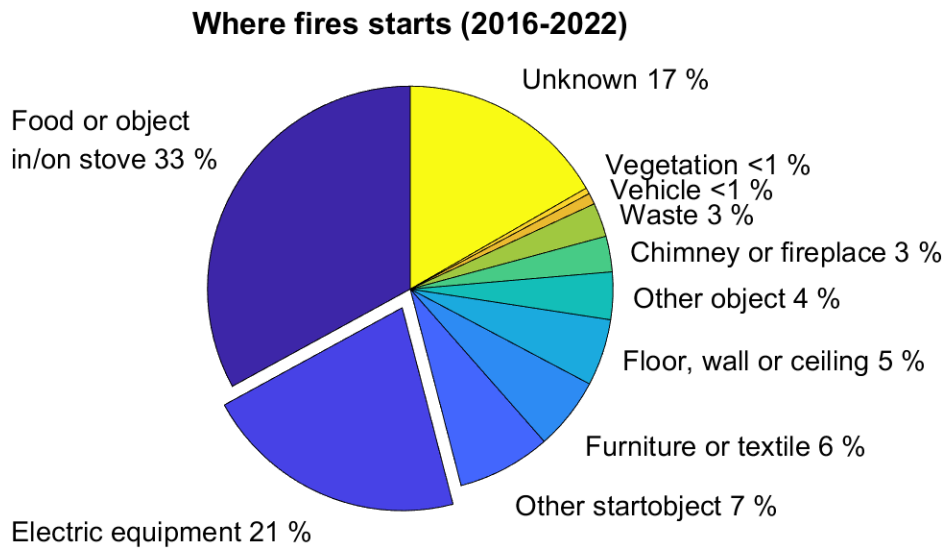
(a) Statistics from [20].

Causes of fires within "Electric equipment" category (2009-2014)
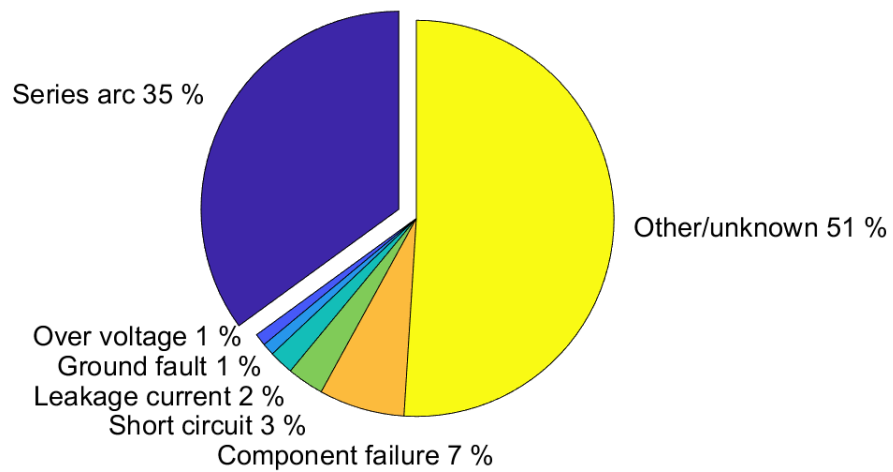
(b) Statistics from [37, chap. 2.1.1].

Figure 2.8: Statistics from where fires starts in Norway and causes of the *Electrical equipment* fires.

2.3.3   Explosion

An electric arc transfers energy into heat. "An arc explosion arises due a very rapid heating of air or other medium"[11, p. 1284]. Similar to when the temperature of a medium increases as the volume increases, a rapid heating of it will cause a form of explosion creating bright light, sound, and a shock wave.

Electric arc explosions usually only takes place in high-voltage supply system from 480 V AC and higher. Care must be taken from personnel when working close to or on high-voltage systems, and the electric arc energy is essential for considering the risk of work tasks. In 230 V AC systems the current have to reach a few kiloamps before explosions are treated as a risk [11, p. 1294], so this is not relevant for this project as the maximum current will be 32 A (will be described in section 3.2.1).

2.3.4   Areas of use

Products can be designed to take advantage of the effects created by electric arcs. Today, many products, especially industrial tools are build up around the electric arc phenomena like shown in figure 2.9. Electric arcs are used in arc welding and steel furnaces to melt metals, spark plugs are used in vehicles to ignite the fuel, and tesla coils are used for entertainment, science and special effects in movies.

(a) Arc welding. From [26].

(b) Electric arc furnace. From [21].
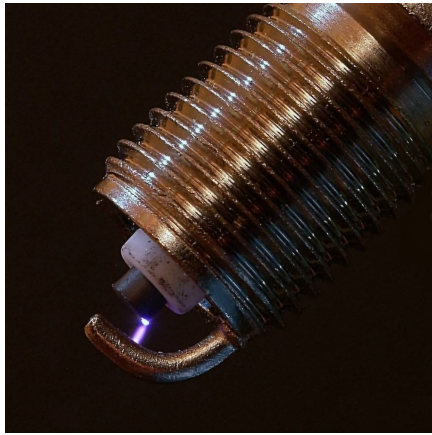
(c) Spark plug. From [33].

(d) Tesla coil. From [19].

Figure 2.9: Examples of use cases where the electric arc has an essential role.

2.4 AFDD - Arc fault detection and protection device

An AFDD is a device that can be installed in fuse cabinets instead of, or in addition to a fuse. It constantly monitors the current and disconnects the

circuit if it senses any dangerous arcing[4]. Some of them like the one shown in figure 2.10 are designed to replace the fuse, making an all-in-one device which protects the circuit against short circuit, over current, ground fault, as well as electric arcs.

Figure 2.10: Eaton AFDD 32/2/B/003-A is an example of an AFDD that can replace a fuse. From [16].

2.4.1 IEC 62606 standard

The first commercial AFDD was released in 1997, but it was not before 2013 that IEC (International Electrotechnical Commission) created the standard IEC 62606 [14] which describes general requirements for AFDDs. The standard is a relatively comprehensive 150-pages paper that describes various requirements and tests that the AFDD has to satisfy.

One of the most essential requirements is shown in table 2.3 which is the maximum time from when arcing starts before the device has to break the circuit. IEC did a lot of lab research trying to define the borderline between a dangerous and a harmless arc. They ended up with a threshold of 100 J dissipated energy from the arc, where higher energy can be treated as a risk of igniting fire in surrounding materials. By assuming a 40 V voltage drop

---

[4]This is just like the objective of this thesis, but instead of using additional equipment like AFDDs, it is desired to implement it on the embedded microcontroller taking advantage of the available resources.

over the arc in a 230 V circuit they defined these limit values of the break time [32].

Test arc current	2.5 A	5 A	10 A	16 A	32 A	63 A
Maximum break time	1 s	0.5 s	0.25 s	0.15 s	0.12 s	0.12 s

Table 2.3: Limit values of break time for 230 V, 50 Hz AFDDs [14, tab. 1]. AFDDs does not need to break immediately, but can measure a couple of periods before reacting.

2.4.2 How an AFDD works

Figure 2.11 shows how an AFDD is build up. A current sensor is used to measure the current going in the circuit, and an HF-sensor separates the high-frequency components (from 100 kHz to tens of MHz depending on the product) from the nominal 50 Hz waveform. A microcontroller processes these signals and has the ability to break the circuit if it detects characteristics associated arcing [34].
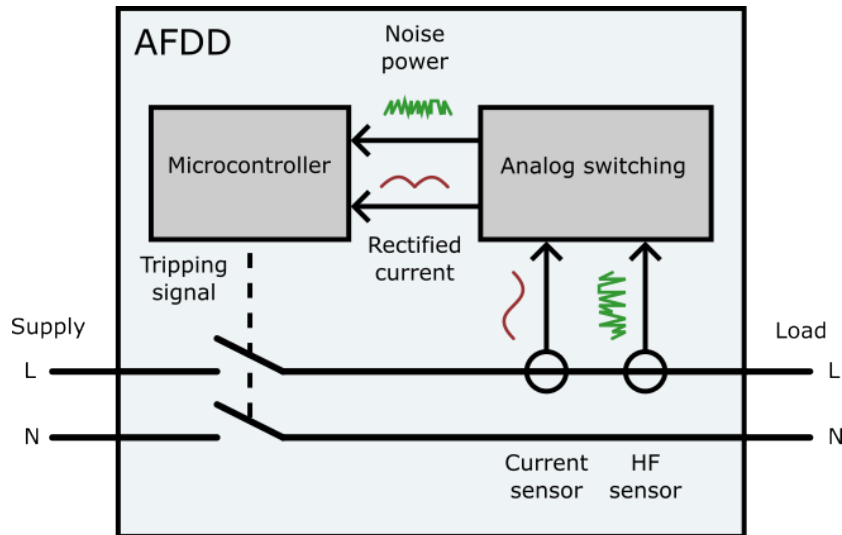
Figure 2.11: Basic structure of an AFDD.

Figure 2.12 shows the current signal that the sensors will be measuring during arcing. There are a lot of ways for the microcontroller to process this data, and each producer has their way of doing it. But common for them all is that they use the high-frequency properties that typically characterizes electric arcs to determine disconnection. However, it is asserted that only the high-frequency noise that takes place in the start of the sparking phase when the arc ignites (during the rising edge in figure 2.12, but too fast to be visible in the figure) is used to detect the arcs, not the overall wave shape [37, chap. 4.4].
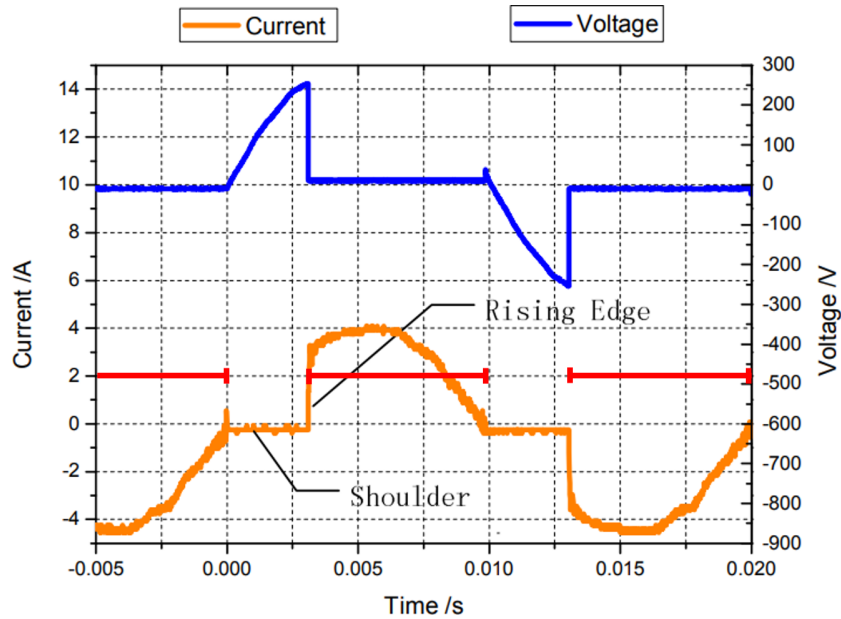
Figure 2.12: Typical voltage and current variation of arcing in AC circuits. From t = 0 s (shoulder) there is no arc and the voltage over the gap is increasing. When the voltage reaches the breakdown voltage of in this case 260 V, an arc is generated. Current starts flowing through the arc (rising edge) and the gap needs a voltage of about 10 V to be sustained. As the current decreases again, the dissipated energy from the arc also decreases and there comes a point where the arc will blow out. Because of this, a tiny voltage pulse can be seen right before t = 0.01 s, then a new half-wave starts. The red lines mark the time where arcing occurs. From [28, fig. 2a].

One of the big challenges is that some household equipment naturally generates electric arcs without being a big risk of starting fire, like brushed motors in vacuum cleaners. To avoid the AFDD to falsely trip, it has to separate between *normal* and *dangerous* arcing [18, chap 4.2].

Some AFDDs have a LED-indicator that will flash when the user flicks the switch on again if it has detected any arcing and tripped. This will make it possible for the user to know if it was tripped because of a short circuit or electric arcs and in the last mentioned case an electrician can be contacted. In addition to the LED-indicator, some AFDDs also comes with a test-button that will generate high-frequency noise which emulates electric arcs, and the device is then expected to trip [37, chap. 4.3].

The costs for an AFDD depends on the load of the circuit and number of phases, but is generally three to four times as expensive as a similar protection device but without arc detection. In addition to that, it takes somewhat more space in the fuse cabinet.

2.4.3 Today's requirements for using AFDDs

USA and Canada

In the 2020 edition of the National Electrical Code (NEC)[5] it states that for dwelling units: "*All 120-volt, single-phase, 15- and 20-ampere branch circuits supplying outlets or devices installed in dwelling unit kitchens, family rooms, dining rooms, living rooms, parlors, libraries, dens, bedrooms, sunrooms, recreation rooms, closets, hallways, laundry areas, or similar rooms or areas shall be protected by AFDDs*" [9, 210.12A].

In their first requirement for AFDDs in the 1999-edition, it was only for bedrooms, but it has been evolving over the years. The initial motivation for setting this requirement was that a study from the 1980s [12] discovered that the mortality rate in the USA was two to four times larger than in Europe, and that fires in electrical installations constituted a great proportion. It is worth mentioning that the grid voltage in the USA and Canada is 120 V and the current in such electrical circuits will therefore be higher compared to Europe where 230 V is used [37, chap. 4.1].

---

[5]NEC is a set of standards and guidelines for safe electrical installations, with its purpose to prevent fires and other electrical accidents. The standard is updated once every three years and electricians in nearly all states in the USA as well as Canada are required to follow it.

Norway

NEK 400[6] introduced in 2022 a requirement to use AFDDs to protect all circuits going to areas with irreplaceable values (e.g. museums, libraries and document centres) and business critical installations (e.g. server centres and warehouses).

In addition to the requirement, it is a recommendation to protect circuits going to areas intended for sleeping people, or in fuse cabinets with a high rated current, typically in commercial or operational buildings [5, chap. 4.42].

In the end of 2021 an independent study was finished called "Status of the use of arc fault detection devices in Norway"[37] from IFE (Institute for Energy Technology). It aimed on researching issues and questions regarding the use of AFDDs in Norway based on *"published research in the field and information obtained from authorities, experts and manufacturers supplying AFDDs to the Norwegian market"*[37, summary].

IFE summarises their study with four recommendations before changing the requirements regarding the use of AFDDs in Norway[37, summary]:

- A review of the causal categories for fires caused by electrical faults is recommended in the Norwegian Directorate for Civil Protection's (DSB) fire statistics, and it should be assessed whether the causal category of 'series arc faults' should be changed to 'series faults'.

- It is recommended that the general requirements for arc fault detection devices (IEC 62606) should be expanded to include new and more comprehensive test requirements that better reflects conditions in actual electrical installations.

- It is recommended that an independent body conducts a test study, in which a large number of AFDDs are fitted to different types of electrical installations and monitored over time.

- It is recommended that documentation should be obtained demonstrating that AFDDs constitute an effective fire prevention measure before any requirements concerning AFDDs in electrical installations are introduced.

---

[6]NEK 400 is a set of standards developed by the Norwegian Electrotechnical Committee. Its purpose is to set requirements and guidelines to ensure that electrical installations maintain safety and functionality. It is updated every fourth year and all engineers and electricians in Norway are required to follow it.

As per change in the NEK 400 2022 version, AFDDs were only changed to be a requirement in areas with irreplaceable values and business critical installations. Future studies will have to decide if AFDDs will be a requirement in future versions of NEK 400.

2.4.4 Alternatives to AFDD
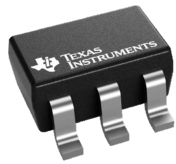
(a) Temperature sensor IC. From [3].

(b) Arc flash optical sensor. From [2].

Figure 2.13: Examples of other devices than AFDDs used to detect electric arcs.

Thermal sensor

AFDDs can be expensive and takes up space. A simple thermal or temperature sensor is cheap, small and can be placed near vulnerable parts for electric arcs on PCBs. Microprocessors and microcontrollers also often have built-in temperature sensors as well.

The problem with using thermal sensors to detect electric arcs is that a lot of heat have to be evolved before it can be noticed. This can do a lot of damage on the equipment and may already have created fire before it is detected.

Optical sensor

Arc flash optical sensors are designed to detect the flash from arcs. They can be placed in enclosures and pointed against the vulnerable area where arcs are most likely to occur. The sensor is connected to an arc flash relay which can rapidly trip the circuit, and together they constitute an arc flash monitoring system. A gas pressure sensor can also be connected to the system which can detect the shock waves of electric arcs in the enclosure.

Arc flash monitoring system are mostly used in supply enclosures for large buildings where the current is very high.

Current/voltage sensors and digital signal processing

Like in this thesis, it is studied if the data from current- and/or voltage sensors can be used with digital signal processing to detect the shape of arcing-waveforms. Realizing this would also be an alternative to AFDDs.

Chapter 3

The Easee charger

This chapter introduces the Easee charger, its electrical specifications and measurements that is available on its microcontroller that can be used for electric arc detection.

3.1 Introduction to the Easee charger

Figure 3.1: Easee Charging Robot. From [8].

The Easee Charging Robot is a smart charger used to charge all types of electric vehicles. It can charge the vehicle much faster than charging from a

standard household socket. Through Wi-Fi or built-in 4G eSim, it is always connected to the internet and can be controlled using an app. From there, the user can control and monitor the charging, make an automatic charging schedule or lock/unlock the charging cable among other things.

Because of its connection to the internet it supports various smart features. For instance load balancing, where the amount of power is adjusted according to the available power in the local grid or household. It can also be set to charge when the electricity price is at its cheapest. Both of these features help balance the electrical grid which lower the probability of a power outage.

Safety mechanisms are some of the main prioritized functions and is summarised in section 3.2.2. In addition to the smart- and safety functions, it is also popular for its small and beautiful design.

3.1.1   Parts structure

Figure 3.2 shows the three main parts of an Easee charger. The backplate in figure 3.2a is mounting the charger to the surface where it sits. A cable is inserted through one of the entries (top or bottom) and connected to the screw terminals from the bottom shown in the middle of figure 3.2a.

The Chargeberry in figure 3.2b encapsulates all the electronics into an IP54 degree of protection. It has a couple of metal rods sticking out on the back, which when it is attached into the backplate get electrical contact with the backplate terminals. Finally, the front cover in figure 3.2c is attached on the front covering the inside of the charger.

(a) **Backplate**: For attaching and connecting to the charging infrastructure.

(b) **Chargeberry**: Contains the electronics for charging the vehicle.

(c) **Front cover**: Protects the electronics from external influences.
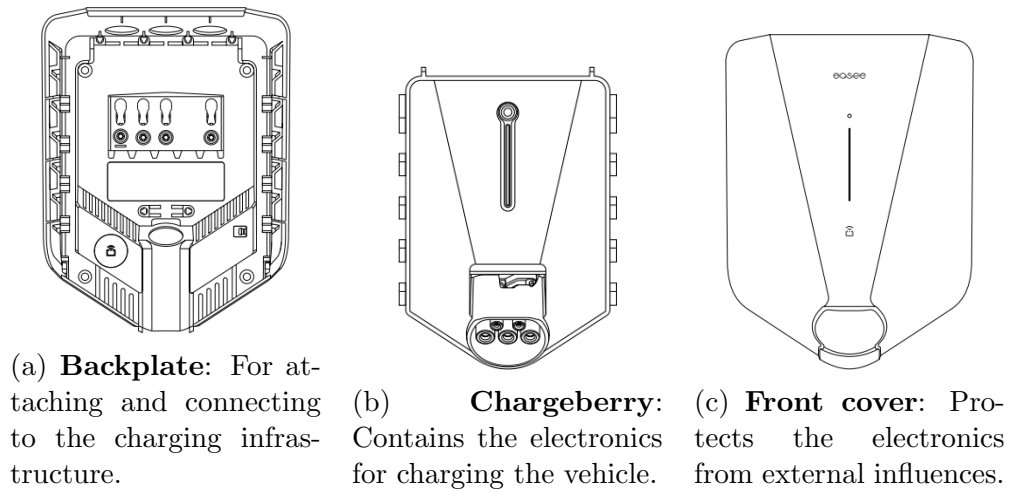
Figure 3.2: The three main parts of an Easee charger. Images and caption from installation manual [7].

Charging cable

The charging cable consists of two type 2 sockets like shown in figure 3.3a. It provides five power pins; protective earth (PE), neutral (N), and line 1-3 (L1, L2, L3) which supports various grid types and three-phase charging. There are also two signal wires: proximity pilot (PP) and control pilot (CP).

Proximity pilot tells the charger that a cable is connected by the use of resistors connected to ground internally in the socket. The value of the resistors tells the charging cable capacity and a button on the charging cable or in the vehicle can signal that charging should stop, and the cable should be unlocked.

Control Pilot is used as a communication line from the vehicle to the charger. It is used to tell the charger presence of the vehicle, maximum allowed charging current and control begin or end of a charging session.
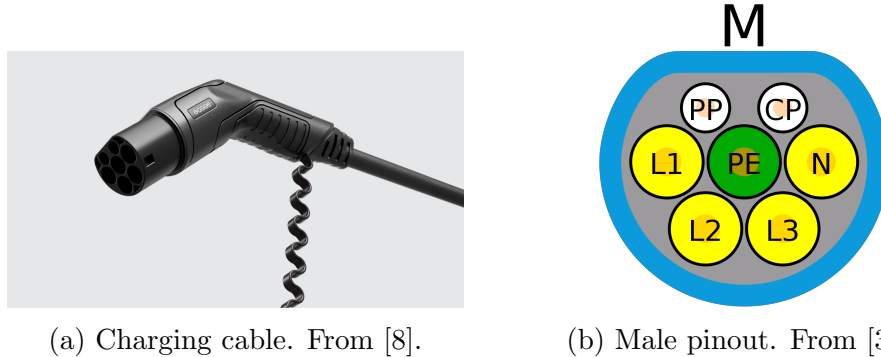
(a) Charging cable. From [8].   (b) Male pinout. From [30].

Figure 3.3: Type 2 socket in charging cables.

When a charging cable is connected between the charger and vehicle, charging will start automatically. Once the cable is attached, it will lock the cable before it can start charging. Any ongoing charging have to be stopped (e.g. via the app or the vehicle) before the cable is unlocked and can be removed.

3.2 Specifications

3.2.1 Electrical

According to the installation manual, the relevant specifications are summarised in table 3.1.

	1 phase	3 phase
Voltage	230 V AC	230/400 V AC
Charging power	1.4-7.36 kW	4.1-22 kW
Current load on each phase	6-32 A	
Mains frequency	50/60 Hz	

Table 3.1: Easee Charging Robot specifications. From installation manual [7].

The charger will automatically adjust the charging power to what the vehicle needs and what is available or scheduled. Note that in the 3 phase configuration, the load on each phase correspond the load on one phase in

the 1 phase configuration. To summarise this, the voltage from each phase to neutral is always 230 V with a maximum current of 32 A.

3.2.2 Protection

The following list summarise protective functions in the charger:

- **Integrated overload protection**: Protects against current draws higher than the electrical equipment are dimensioned for.

- **Overvoltage protection**: Protects against increase in supply voltage higher than what the equipment are designed for.

- **Built-in RCD for ground fault protection**: Protects against electric shock or fires caused by ground faults, when electricity unexpectedly leaks to ground.

- **Thermal protection**: Monitors the increase in temperature higher than what the electronics and enclosure are designed for, and can take actions based on that.

- **Short circuit**: Protects against fire caused by short circuit, when live wires are directly connected together. This function is not integrated in the charger, but all chargers are installed with a dedicated short circuit protection fuse.

3.2.3 Available measurements

The charger is taking various types of measurements in the charger for different purposes. Those that are assumed relevant for the detection algorithm are the voltage on each supply terminal, and the current going through each supply terminal.

Table 3.2 summarises the analogue-to-digital conversion specifications.

Sampling rate	20 kHz
Anti-aliasing filter cut-off frequency	1.6 kHz
Anti-aliasing filter type	1. order RC
ADC resolution	12-bit
Current step size	30.5 mA/sample
Voltage step size	281.7 mV/sample

Table 3.2: Specifications of analogue-to-digital conversion.

3.3   Electric vehicle as an electric load

It is important to understand how an EV act on the charger as a load, because this affects the measurements in the charger that is going to be used to detect arcing. As addressed in section 2.4.2, some equipment naturally generates small non-harmful electric arcs, and it is undesirable that such equipment creates a false trip. From an EV perspective that can be switching relays, ventilation fans or PWM-based light dimmers. Even though the vehicle usually is turned off, it is not unthinkable that some equipment in the vehicle can be used while it is charging.

Most EVs can be treated as a resistive load, that is when the current and voltage are in phase with each other. Figure 3.4 shows a simplified block diagram of the electronics parts in an EV.
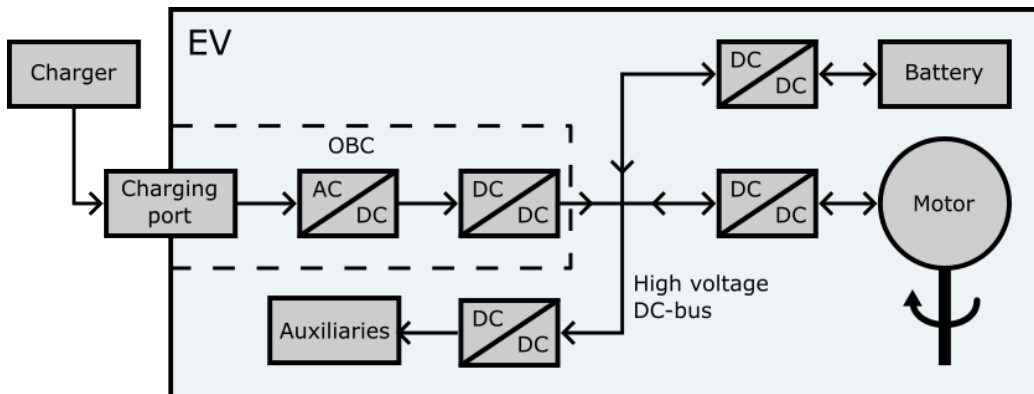

Figure 3.4: Simplified block diagram of the main electronics parts and the current flow in an EV. Most EVs follow this principle.

The EV charger is connected to the vehicle's charging port. Every vehicle contains their own on-board charger (OBC) which rectifies and boosts the voltage into a suitable high voltage for what the vehicle is designed for. It also contains capacitors that smooth the voltage and compensate for transients in the supply or load [17].

A common high voltage DC bus distributes the available power between the parts, for example when the vehicle brakes, energy can be stored in the battery. AC-DC and DC-DC converters creates a galvanic isolation between the parts and separates different voltage amplitudes [23, sec. II].

Because of the available power from the battery and the capacitors in each DC-DC converter, it is assumed that noise from auxiliary devices such as lights, heaters and ventilation fans will have little or no influence on the charger measurements. This simplifies the algorithm structure as it does not need to separate between *dangerous* and *normal* arcs unlike conventional AFDDs.

Chapter 4

Data collection

This chapter goes through the setup of how data from electric arcs are measured using an electric arc generator and transferred from the charger to a PC. The collected data will be used in chapter 5 to develop the algorithm in Matlab which finally will be implemented on the charger's embedded microcontroller. The reason for describing data collection in detail is that there are challenges and considerations regarding the transfer of data from the charger to the PC, and the choices that are made in this chapter has consequences for the accuracy of the collected data.

The microcontroller takes various measurements that may be used to detect arcing and in this chapter it will be chosen which measurements that will be used for the algorithm. Finally, some important observations will be presented.

Figure 4.1 shows the schematics of the data collection setup and will be commented in section 4.2.
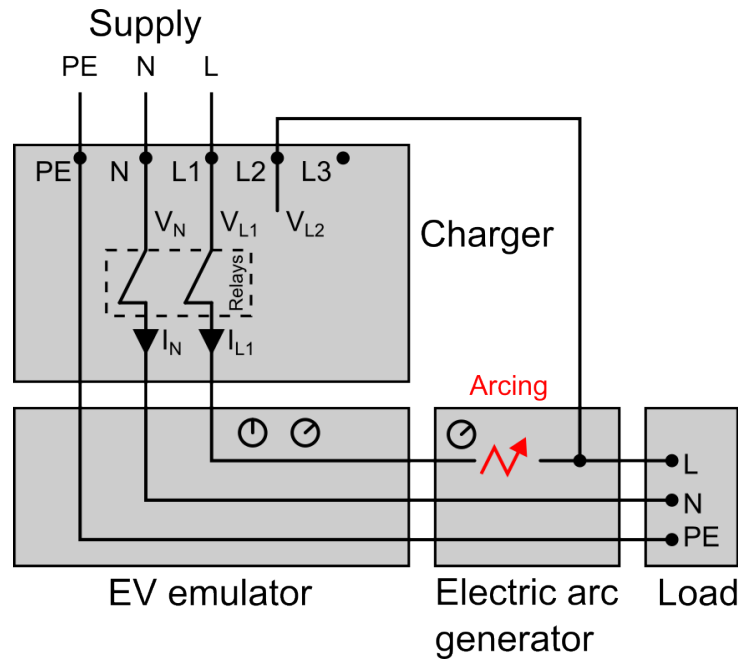
Figure 4.1: Schematics of the electric arc generator setup used to collect data. It consists of a charger, EV emulator, electric arc generator and a load. The EV emulator has two adjustment knobs to emulate that a vehicle is connected (PP and CP signals described in section 3.1.1). The electric arc generator has one adjustment knob for the gap distance.

4.1 Electric arc generator

An electric arc generator is made so that measurements of electric arcs can be collected and used to develop the algorithm for detecting electric arcs.

IEC 62606 [14, sec. 9.9.2.6-7] use a cable specimen and an arc generator to produce electric arcs for testing AFDDs. The cable specimen consists of two parallel wires with a 50 mm split in the insulation, covered with electrical PVC tape. The arc generator consists of two conductors held up by brackets, pointed against each other where the position of one of them can be adjusted, creating an adjustable gap.

Critique has been given to the cable specimen testing method as it typically will give unrealistic results and are not reproducible [37, chap. 5.4]. Because of this, two electric arc generators are made shown in figure 4.2 (one

for low and one for higher currents) instead of a cable specimen. See the attached test reports for details about the development process.
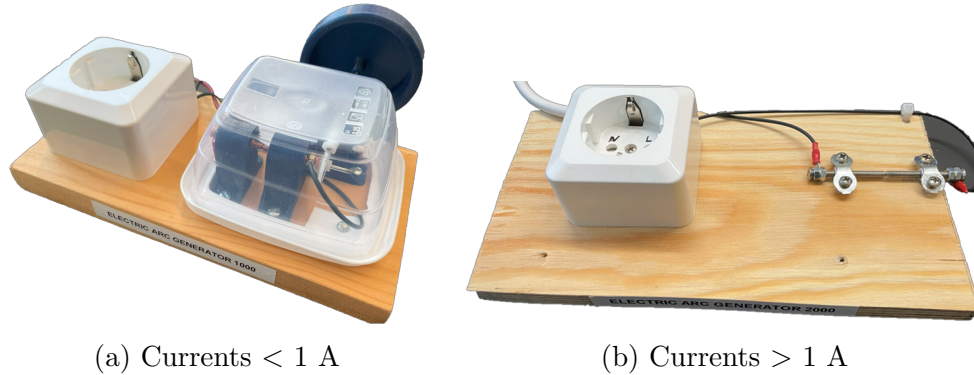

(a) Currents < 1 A (b) Currents > 1 A

Figure 4.2: Electric arc generators.

4.2 Choosing which measurements to collect

It is desired to use the charger for collecting the measurements instead of some other measuring tools, to get the most realistic measurements as possible, since the goal is to make an algorithm that eventually will be implemented on the charger.

Section 4.2.1 highlights an issue with the speed of sampling and transmission which makes it desirable to only transfer the necessary measurements.

Figure 4.3 shows typical current and voltage signals that is possible to measure from the charger during arcing. It emphasizes how the measurements changes depending on the location of arcing.

The current going through the live wire is under normal conditions the same as the current through the neutral wire with opposite sign. So a current signal can be used to detect electric arcs anywhere in the circuit.

If arcing occurs between the charger and load, the charger will not be able to measure it only based on voltage measurements. However, if arcing occurs between the charger and supply (given that enough energy is passed through to keep the charger powered on), the voltage signal will have a similar shape as the current signal.
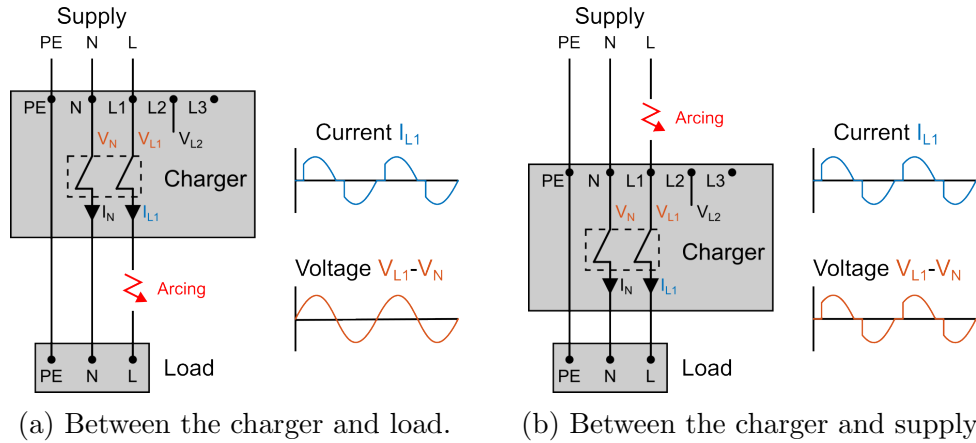
(a) Between the charger and load. (b) Between the charger and supply.

Figure 4.3: How the location of arcing affects the measurements.

It is decided that the current I_{L1} and voltage $V_{L2} - V_N$ from figure 4.1 are transferred to the PC for data collection. $V_{L2} - V_N$ is calculated in the charger before it is transferred (to save the amount of transferred data). This can be used to analyse how the voltage signal would have been if the arcing was occurring between the charger and supply like in figure 4.3b, without the risk of powering down the charger and interrupt the transferring data. It is expected that the current signal can be used to detect electric arcs, and the voltage signal to where the fault is located (i.e. a or b in figure 4.3).

4.2.1 Sampling rate versus transmission rate

As described in section 4.2 two variables have to be transmitted from the charger to the PC. Both of them are 16-bit variables[1] (two bytes) updated 20 000 times per second (see table 3.2). Using a USB to TTL serial adapter to transfer each byte with one start- and stop-bit, each frame constitutes 10 bits. The data rate for the two 16-bit variables ($2 \cdot 2$) is calculated to be:

$$\text{data rate} = 10 \cdot 2 \cdot 2 \cdot 20000 = 800 \, \text{kbit/s} \tag{4.1}$$

Because the data rate is so high there are considered three solutions for transferring the data:

---

[1]The ADC resolution is 12 bit, but the variable is saved as a 16-bit variable in the microcontroller.

1. Use a high enough baud rate, such as 921 600 bit/s.

2. Downsample the measurements and transmit using a lower baud rate.

3. Temporarily save data in a big buffer, and transmit using a lower baud rate whenever the buffer is full.

Alternative 1

A baud rate of 921 600 bit/s is the highest baud rate possible and will theoretically barely satisfy the speed criterion. The UART module will have a low time margin between transmission of bytes and there is a relatively high chance of overflowing the transmission buffer at some point. Based on experience such high baud rate can also lead to unstable data transmission and data loss.

Alternative 2

Downsampling the measurements makes it possible to continuously transfer data, but it also leads to loosing potentially valuable information. It is desired to collect as precise information as possible for the algorithm development, so this is not considered as a good solution.

Alternative 3

There is memory space for making a temporary buffer in the microcontroller of 40 000 bytes (40 kB). By saving two 16-bit variables that is updated 20 000 times per second makes the buffer full in 0.5 seconds. This alternative makes it only possible to take measurements in small intervals at a time, and one have to wait a couple of seconds between the intervals for transmission. But all samples within that interval are collected, and a reliable baud rate is used.

Conclusion

Based on the discussed alternatives, it is decided that alternative 3 is the best solution for transferring the data. The measurements are temporarily saved in a 40 kB buffer which equivalents 0.5 s of measurements and then transferred using a baud rate of 115 200 bit/s when the buffer is full (transmission takes 3.5 s). Measuring 0.5 s will reveal 25 waves in a 50 Hz grid which seems sufficient.

One could argue that the ADC only uses 12-bit values, and in fact only a limited range in this value is used, so dedicating 16 bits during transmission is redundant. But combining bytes before transmission and then having to restore them on reception complicates the task.

4.3 Data collection programs and data flow

Figure 4.4 shows the data flow when collecting data from the charger. A simple program is added to the embedded C source code. A Python program is made to make a general user interface for the user, communicate with the charger and save the dataset. Matlab is used to visualize and analyse the dataset.
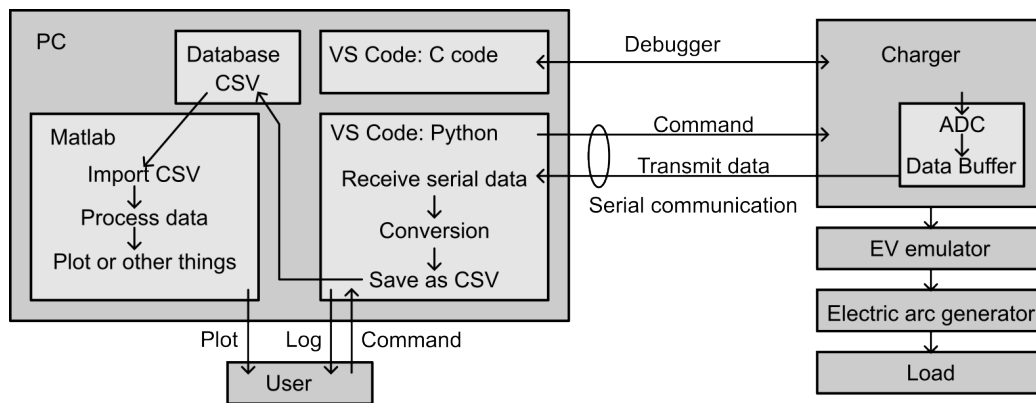
Figure 4.4: Block diagram of the relation between the different programs in the PC and the charger.

Embedded C

Briefly explained, the program waits for a command sent through the serial communication. On reception the chosen measurements will start filling up a temporary data buffer and when it is full it will be transmitted through the serial communication to the PC. The program makes use of flags and non-blocking functions so that the microcontroller has resources to do other tasks as well.

Python

The program consists of two threads running in parallel; one for handling serial communication and one for interacting with the user. Relevant information are printed in the terminal window, and the user can write a command, for instance to make a single measurement. In that case the command is sent to the serial thread using a thread-queue and to the charger through the serial port. On reception of data, it is converted into 16-bit values and stored as a CSV file.

Matlab

Matlab is used to process and visualize the data since it can easily import and plot datasets. It is also going to be used to develop and test the detection algorithm in chapter 5.

4.4   Important observations

In attached test report 3 and 5 measurements of normal and arcing signals were collected and saved. Loads with a current draw of 1-10 A with 1 A increase for each step was used, and four signals were collected for each step. So in total, the collected dataset contains 40 normal and 40 arcing signals.

Figure 4.5a shows measurements during normal charging conditions and 4.5b when electric arcs occurs. They are very similar to what was expected from figure 2.12. The signal is a bit smoother than expected due to the antialiasing filter in the charger. For different current amplitudes, the curve shape is linearly scalable[2], except from 1 A and lower where the low resolution (30.5 mA/sample) becomes visible in that range. The shoulder of the signal (e.g. the time 4-8 ms in figure 4.5) is around 4 ms for all the measured arcing signals.

---

[2]Meaning that the shape of an arcing signal with an amplitude of 3 A multiplied by 2 looks equal to an arcing signal with an amplitude of 6 A.
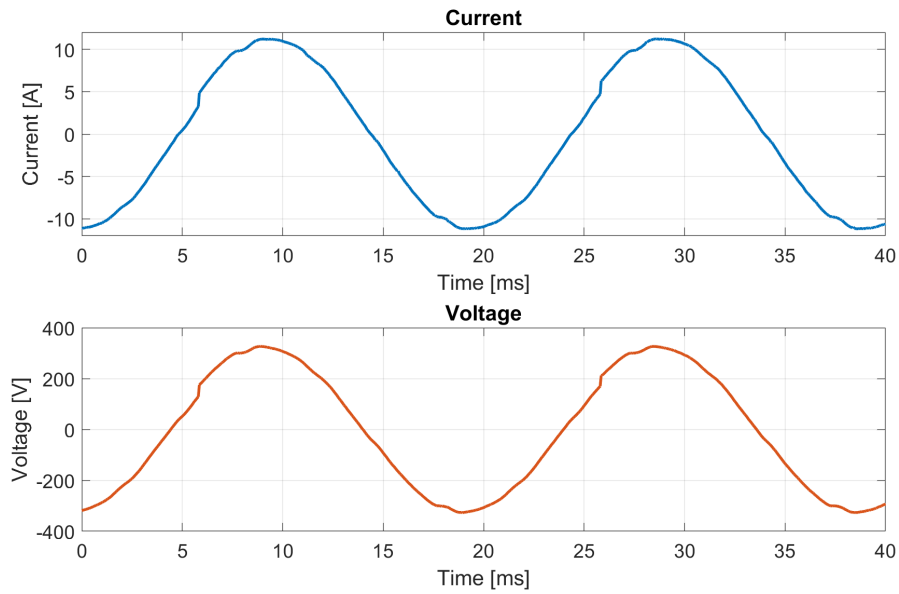
(a) Normal operation
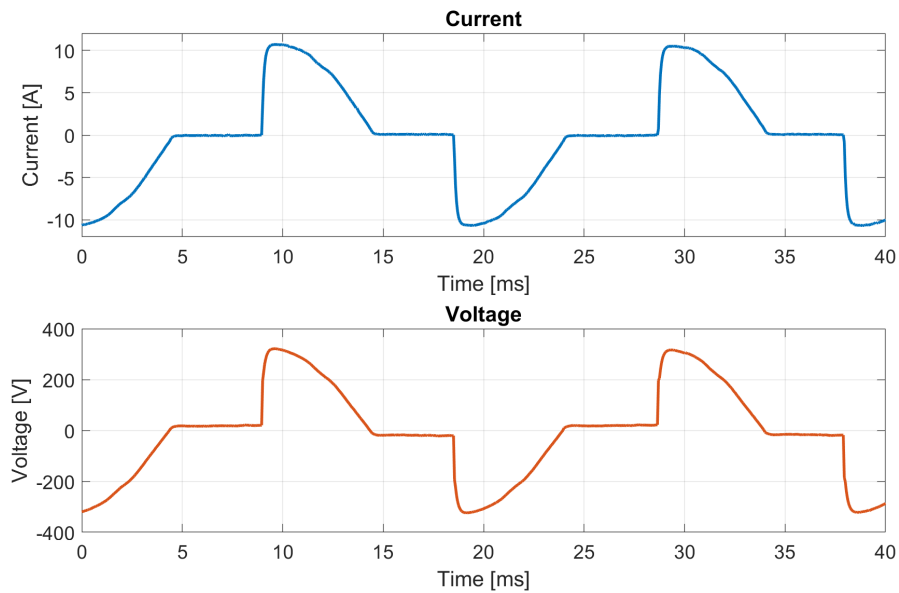
(b) Arcing

Figure 4.5: Measurements during normal operation and when arcing. Measurements are taken at a current draw of 8 A. The unevenness near the tops in figure 4.5a are caused by the electrical grid.

Light colour

Two types of light colours were observed when doing measurements; an orange coloured light and a white slightly blue light as shown in figure 4.6. The white light was much more intense and lasted just for a glimpse when adjusting the gap distance, whereas the orange could easily be held stable. The white light typically occurred in the transition from when the circuit was not leading any current to the orange light when it was leading current.
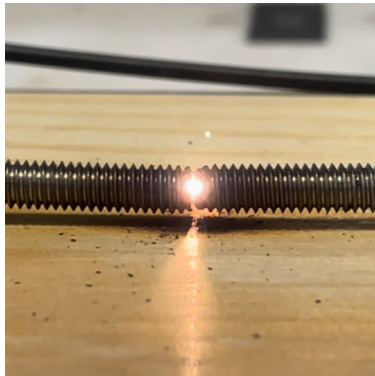
(a) Orange
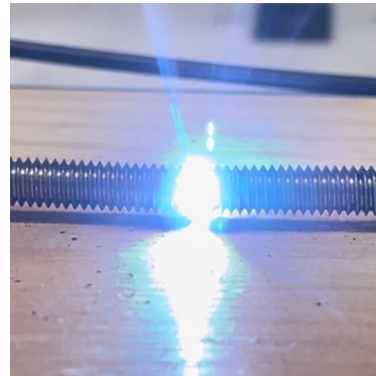
(b) White/blue

Figure 4.6: Different light colours from the electric arc generator. These images are captured at a current draw of 8 A.

Based on theory and measurements, it is assumed that the white light is electric arcs and the extreme heat vaporizes the metal tips of the bolts where some of it ends up in the gap creating contact. But the contact is so small and loose that there is a higher resistance than the rest of the circuit which makes it red-hot glowing (like a glowing bulb). And whenever the gap distance is increased enough, it vaporizes again burning away the contact, and electric arcs occurs in the transition. Vaporized material can be seen underneath the bolts as small black dots in figure 4.6.

During the red-hot metal in figure 4.6a, the measurements looks exactly like the normal conditions in figure 4.5a. Even though the red-hot metal seems dangerous and creates a lot of heat just like electric arcs, it is not possible to detect it using current- and voltage measurements. But it is concluded that since electric arcs are observed to occur in the transition before and after the metal is red-hot, protection against electric arcs will also limit the probability of the red-hot metal.

Chapter 5

Detection algorithm

In this chapter requirements for the detection algorithm are chosen (section 5.1), a mathematical model of typical arcing signals is made (section 5.2) and the detection algorithm is developed (section 5.3) where each step in the algorithm is described in detail (section 5.4-5.7).

The detection algorithm is a classification problem where the purpose of the algorithm is to enhance the properties of electric arcs and distinguish between a normal and an arcing signal. Measurements of arcing and normal conditions are shown in figure 4.5 which is the basis for developing the algorithm.

There are many ways to detect electric arcs and there are new studies on different ways of enhancing the properties of arcing signals [29, p. 3]. Unlike most of these methods (including conventional AFDDs), this study will focus on using the shape of the alternating current waveform during arcing (see figure 4.5b), instead of using high-frequency sensors. The algorithm will use sampled data that is already available on the microcontroller, without extra electronics, and process the measurements.

5.1 Requirements

Based on theory and the collected data, the following list summarises requirements set for the detection algorithm:

- Sampled current measurements should be used as input value as voltage measurements cannot detect all occurrences of series arcs like discussed in section 4.2.

- It should work on different current levels with an RMS value ranging from 1 A to 32 A. It should also notice when the current is below 1 A.

- Designed for 230 V AC circuits which makes the shoulders last around 4 ms as observed in section 4.4.

- Release time of maximum 120 ms from arcing to relay release.

- Use as low processing power as possible so that the microcontroller has capacity to execute all other tasks and still have resources available for future updates.

- It should work on practical 50 Hz AC grids where the frequency can be slightly off or waveforms can contain unevenness and noise.

It is also desired (but not a requirement) to make the algorithm flexible so that it can be used on voltage measurements as well as current as input value. In that case when arcing occurs (using current measurements) it can also be used on voltage measurements to locate the fault (i.e. between the charger and supply or charger and vehicle shown in figure 4.3).

The release time of maximum 120 ms is the requirement for conventional AFDDs according to IEC 62606 (see table 2.3) based on the released energy, and it is desired to use the same principle to protect against damage. The release time for the relays (in this case maximum 10 ms) and processing delays should be included as well.

The algorithm only needs to run whenever a vehicle is charging with a current level above 1 A RMS because if not, the current resolution is too low to be used and arcing in such circumstances has a very low risk of doing any damage (see section 4.4). This needs to be handled when implementing the algorithm in the microcontroller program.

Detection should trigger an alarm which stops any ongoing charging and notify the user.

5.2   Mathematical model of arcing

In attached test report 2 it was discovered that there is noise and unevenness in the waveforms in the local grid voltage as shown in figure 5.1. All data are collected from this grid which impacts the accuracy of the measurements. It is desired to make an algorithm that will work when connected to other grids than the local one, which may have some other kinds of unevenness and noise. To design the algorithm in the most general way, a mathematical model of typical arcing signals without noise is made based on various observations of arcing signal measured from the local grid (described in section 4.4).
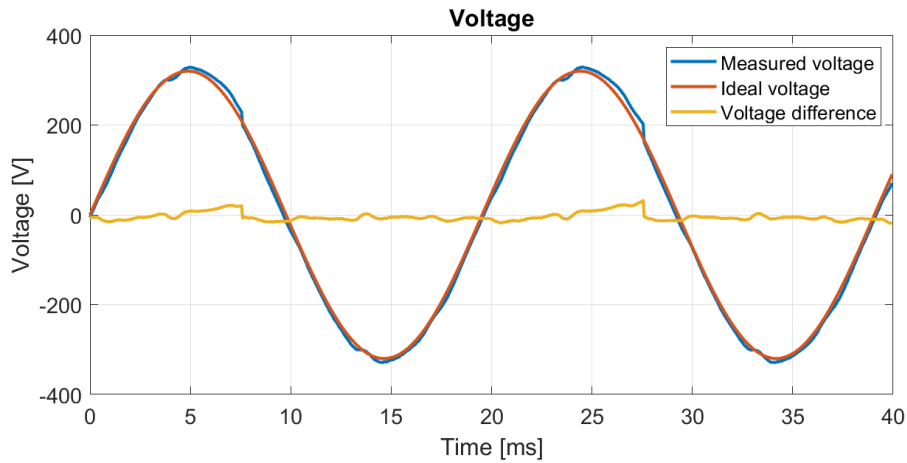
Figure 5.1: Measurements of the local grid voltage shows unevenness and noise in the waveforms.

Figure 5.2 shows an arcing signal along with the mathematical model. The mathematical model consists of three different stages that are put together:

1. 0-4 ms: 0 A.

2. 4-5 ms: 1. order step response with a time constant of $\tau = 150\,\mu s$[1].

3. 5-10 ms: Sine function.

---

[1]Typical arcing signals would have a vertical line, but the model is specifically made for the Easee charger where the anti-aliasing filter constitutes a 1. order step response instead.
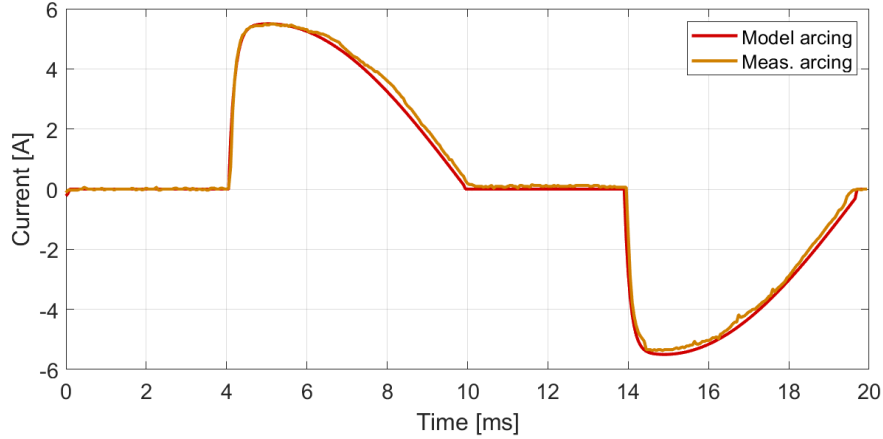
Figure 5.2: Mathematical model of an arcing signal compared to practical measurements.

The mathematical model is implemented as a function in Matlab so that 20 kHz sampled arcing signal can be generated. As the shape is observed to be similar regardless of the current amplitude, the model can be used on all current amplitudes by scaling the amplitude. The similar shape can be explained by the electric arc having a constant breakdown voltage (given that the gap distance is constant) making the shoulder (time from each zero-crossing to breakdown) constant. And as the rounded shape is caused by a 1. order step response, an increase in the step will linearly scale the shape.

Similar as with arcing signals a mathematical model is made for normal signals which is a pure sine wave without any noise.

5.3 Algorithm structure

Figure 5.3 shows the structure of the algorithm. Each block is described in the following sections and the figure also shows the variable name that is used to express the operation of the blocks. The signal is first decimated where the sample rate is reduced from 20 kHz to 4 kHz (section 5.4). Then it is scaled so that the amplitude is normalised to 1 (section 5.5). Feature extraction is the essence of the algorithm where arcing signals constitute a greater feature value than normal signals, and different methods are suggested and discussed (section 5.6). A window is used to pick a recent section of the signal back

in time, the average energy of it is calculated, and arcing is detected if it exceeds a threshold value (section 5.7).
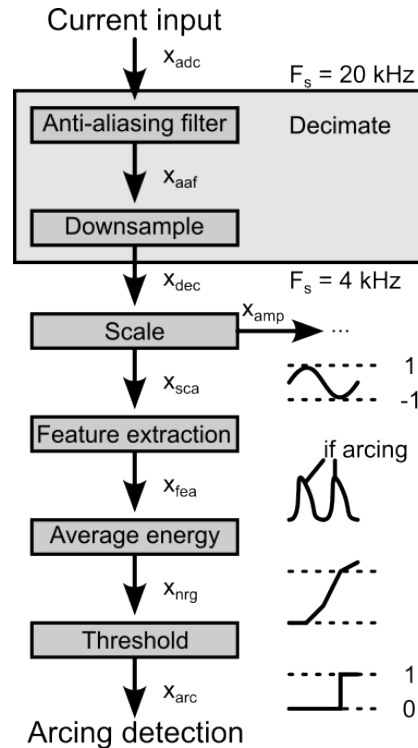
Figure 5.3: Structure of the electric arc detection algorithm along with some plots to visualize what the different blocks do.

Figure 5.4 shows three periods of arcing and normal waveforms both using the mathematical models as well as practical measurements. A variety of data are used when developing the algorithm, but the data shown in the figure will be used in a majority of the figures throughout this chapter to easily compare and limit the number of plots.
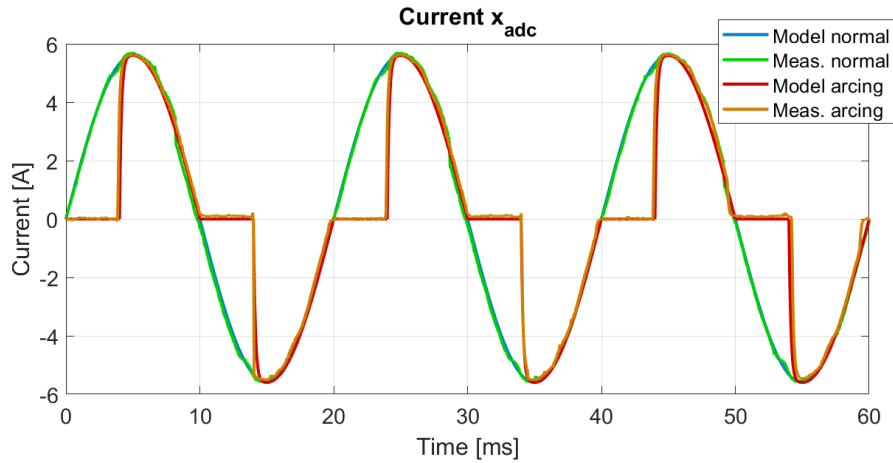
Figure 5.4: Initial current signal of 4 A RMS that is used throughout the documentation of algorithm development. Blue and red are mathematical model of respectively normal and arcing signals, and green and orange are similarly but from practical measurements. It is shown here once to limit the number of figures.

5.4   Decimation

Based on visual observations from figure 5.4 a sampling rate of 20 kHz seems redundant to detect the shape of arcing signals. It is therefore desired to decimate the signal which includes low-pass filtering (anti-aliasing) and downsampling. Decimation will lower the data rate which often lower the computation requirement that is needed for further processing.

There are various considerations that can be taken into account when designing a low-pass filter and downsample factor for decimation. There are no correct answers to this only considerations that need to be assessed against each other.

In general, it is desired to have as low sample rate as possible but taking into account the following considerations:

- Keep the shape of typical arcing signals.

- Sufficient attenuation for frequencies higher than the Nyquist frequency.

- Use a filter that requires as low computational resource as possible.

5.4.1 New sampling rate

Based on experimental testing of low-pass filters with different cut-off frequencies it is known that the shape of arcing signals are well retained if the passband goes up to around 1 kHz.

In section 5.4.2 the low-pass filter type and cut-off frequency is determined which is closely related to determining the new sample rate. There must be a transition from the passband to the stop-band. It is concluded that the stop-band should start from 2 kHz which leaves the area from 1 kHz to 2 kHz as a transition. The new Nyquist frequency is then 2 kHz which gives a sampling rate of 4 kHz, and the downsampling can be executed with a factor of $D = 20/4 = 5$ (pick every fifth element).

5.4.2 Filter suppression at Nyquist frequency

Low-pass filtering is necessary to suppress the effect of aliasing before the data are downsampled [25, chap. 6.1]. This is a standard practice whenever downsampling, whether it is done digitally on a discrete time signal or before sampling an analogue continuous time signal in an ADC.

As specified in table 3.2 the analogue signal is passed through a 1. order anti-aliasing filter with a cut-off frequency of 1.6 kHz before it is sampled in the ADC. Using a standard 1. order transfer function in equation 5.1 the amplitude response at Nyquist frequency ($fs/2 = 20000/2$ Hz) for this filter is -16 dB.

$$H_{RC}(f) = \frac{1}{1 + j\dfrac{f}{f_c}} \tag{5.1}$$

$$H_{RC}(20000/2) = \frac{1}{1 + j\dfrac{20000/2}{1600}} \tag{5.2}$$

$$|H_{RC}(20000/2)| = 0.158 = -16 \text{ dB} \tag{5.3}$$

To not complicate the task even more, it is desired to keep the suppression at the new Nyquist frequency at around -16 dB which is the same as with the previous sampling rate.

5.4.3   Filter type

Some of the main considerations that have to be taken into account when choosing the filter type for this purpose is the filter order and its step response overshoot.

An ideal filter would in the frequency domain have a rectangular shape with a steep transition between the pass- and stop-band. A rectangular shape in the frequency domain corresponds to a sinc-function shape in the time domain. If the input signal is a step signal, convolving this with the filter creates a lot of overshooting and ripple.

The steep curve at $t = 4$ in figure 5.2 is somewhat similar to a step signal, so if the step response of the filter makes overshooting and ripple, this would have an undesired impact on the signal. The downsampled signal would end up distorted like demonstrated in the yellow filter in figure 5.5 and 5.6.

When designing the filter it is essentially a dilemma between a response most similar to an ideal filter versus low overshooting in its step response. There is no correct answer to this problem but two low-pass filter types are suggested based on these factors and their magnitude- and unit step response are shown in figure 5.5:

1. FIR filter with order $N = 15$ designed in Matlab by window-based FIR filter design using a Hamming window.

2. IIR filter with order $N = 2$ designed in Matlab by Butterworth filter design.

Both filters satisfy the criteria set in section 5.4.2 having a minimum suppression of -16 dB at the Nyquist frequency.

In this case the FIR filter does not have any overshoot at all. The IIR filter with $N = 2$ has a small overshoot, but within an acceptable range for this purpose. IIR filters with order $N > 2$ tends to have around 20 % overshoot like the yellow step response in figure 5.5 which is insufficient for this purpose.
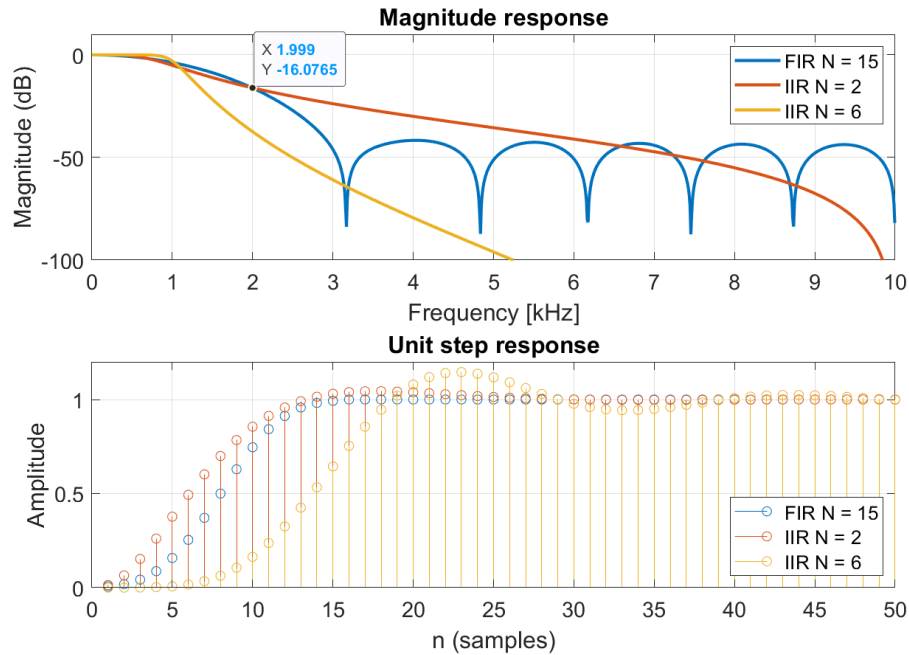
Figure 5.5: Magnitude- and unit step response of some different types of filters. The blue and red lines are suggestions to filters that suffices the requirements, and the yellow line is an example of an inappropriate filter that leads to overshooting and ripple in its step response.

Figure 5.6 shows the arcing signal being filtered by the filters in figure 5.5. One can clearly see the undesired effect of using a filter that makes overshooting and ripples in its step response (yellow), as this distorts the signal. Both the suggested FIR (blue) and IIR (red) keeps the shape of arcing in a sufficient way.
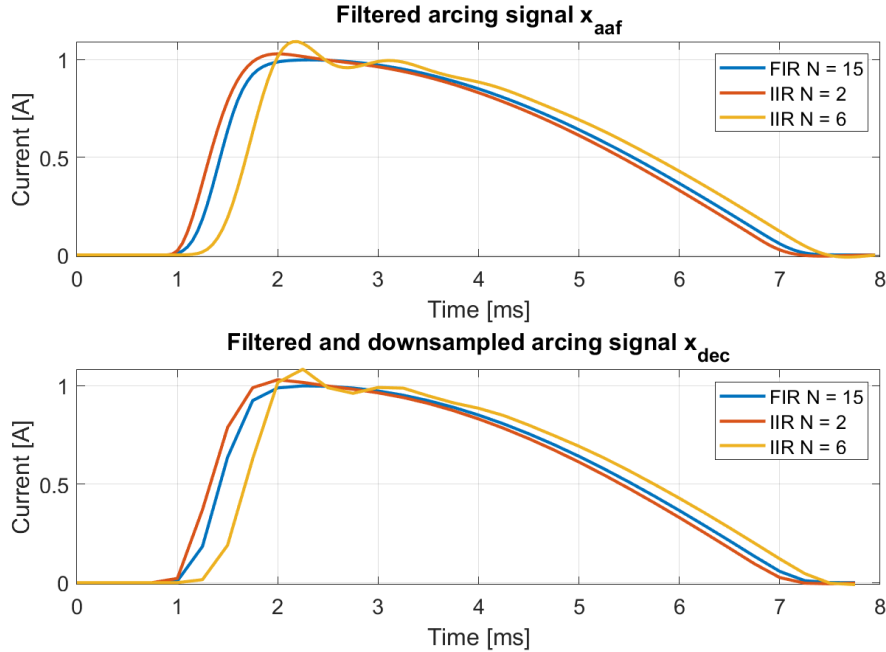
Figure 5.6: Part of an arcing wave passed through the anti-aliasing filters from figure 5.5.

Mathematical expression and computation

The FIR filter of order $N = 15$ consists of $M = 16$ coefficients. The number of multiplications will be used as a measure for the required computation as multiplication and division requires significantly more computation than addition and subtraction. It will in this section be shown how the FIR filter can be realized using an average of 1.6 multiplications per sample instead of 16, by using polyphase structure and the symmetry of the filter coefficients.

If the current signal is expressed as x_{adc} where n is the sample number, the anti-aliasing filtered signal x_{aaf} can be expressed as shown in equation 5.4 where h is the filter coefficients of length $M = 16$. Equation 5.5 express downsampling with a factor of $D = 5$ where m is the sample number and combined they give the equation 5.6.

$$x_{aaf}(n) = \sum_{k=0}^{M-1} h(k)x_{adc}(n-k) \tag{5.4}$$

$$x_{down}(m) = x_{aaf}(mD) \tag{5.5}$$

$$x_{poly}(m) = \sum_{k=0}^{M-1} h(k)x_{adc}(mD-k) \tag{5.6}$$

The principle of a polyphase structure for decimation is to downsample the signal before filtering instead of the opposite, and it can be mathematically proved that it will lead to the same result [25, chap. 11.5.4]. This reduces the rate of filter computation to the downsampled rate instead of the initial rate, with a factor of in this case $D = 5$.

The mathematical expression of polyphase structure for decimation can be a bit complex, but the result will be similar to equation 5.6. The only difference is that the filter coefficients and signal are decimated into chunks in the polyphase structure that are computed for every sample and then summed together every D sample, while in equation 5.6 the entire filter computation is done every D sample. The equation results in an average of $16/5 = 3.2$ multiplications per sample after using polyphase structure.

Because the filter coefficients are symmetric, even more reduction can be achieved in the computation. The symmetry can be expressed as $h(k) = h(M-1-k)$ which means that $x_{adc}(mD-k)$ and $x_{adc}(mD-(M-1-k))$ in equation 5.6 will be multiplied with the same number. Such samples can instead be added together before the multiplication and half of the filter coefficients are used which requires half the number of multiplications. Inserting this into equation 5.6 the final decimated signal is expressed in equation 5.7. It requires $16/2 = 8$ multiplications per sample of m which is equivalent to an average of $8/5 = 1.6$ multiplications per sample n of the original signal.

$$x_{dec}(m) = \sum_{k=0}^{M/2-1} h(k) \cdot [x_{adc}(mD-k) + x_{adc}(mD-(M-1-k))] \tag{5.7}$$

Summary

The FIR filter does not have any overshoot in its step-response while the IIR filter has a small overshoot. By using polyphase structure for decimation and

the symmetry of coefficients the FIR filter can in this case be realized by an average of 1.6 multiplications per sample while the IIR by 5 multiplications per sample. It is concluded that the FIR filter is going to be used as it is the best choice for this purpose.

5.5 Scale

To make the algorithm work with several different current amplitudes it is desirable to scale the signal so that it is normalised with an amplitude of 1. The purpose of this is so that all signals that will be input to the feature extraction block in the next step will be treated similar no matter what amplitude they have. To do so, the amplitude x_{amp} can be estimated, and by dividing the current value x_{dec} with this amplitude x_{amp} it will be normalised like expressed in equation 5.10.

Looking at figure 5.4 the top values are always reached even if arcing occurs or not, so it is a good reference point for the scaling[2].

Let's say that x_{abs} in equation 5.8 is the absolute value of the current x_{dec}. At AC current of 50 Hz a top value will be reached within half a period which lasts 10 ms. A simple way to estimate the amplitude x_{amp} is to pick the maximum value for the past 10 ms of current absolute values x_{abs} like expressed in equation 5.9. $N = 40$ is the number of samples during half a period.

$$x_{abs}(n) = |x_{dec}(n)| \tag{5.8}$$

$$x_{amp}(n) = \max_{m=n-N,...,n} x_{abs}(m) \tag{5.9}$$

$$x_{sca}(n) = \frac{x_{dec}(n)}{x_{amp}(n)} \tag{5.10}$$

x_{amp} can also be used when implementing the algorithm to notice when the current goes below 1 A. According to the set of requirements in section 5.1 the detection algorithm should only look for arcing whenever the current is over 1 A.

Figure 5.7 shows the three variables x_{abs}, x_{amp} and x_{sca} used to scale the current signal as described in the equations 5.8-5.10. The scaling works

---

[2]An alternative to the amplitude is to use a calculated RMS-value, but this will change depending on if arcing occurs or not.

excellent on current signal that has a constant amplitude. In an increase in amplitude the scaled signals are slightly deformed as the x_{amp} are changing, while in a reduction in amplitude the scaled signals are more affected.

Even though there are deformations in the scaled signals when the current changes in amplitude, this method reacts quickly to changes within half a period of time. To avoid the deformation causing false positive detections, it is decided to use a margin in the threshold value which will be described in section 5.7.
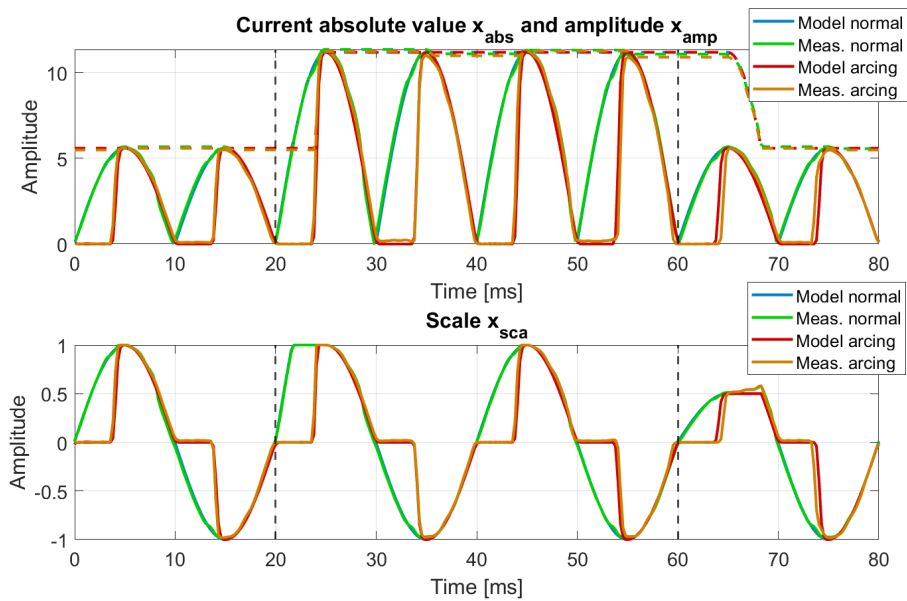
Figure 5.7: Top: Current absolute value x_{abs} (whole lines) together with the maximum absolute value for the past 10 ms x_{amp} (stippled lines). Bottom: Scaled signal x_{sca}. The current signal is doubled in amplitude at $t = 20$ ms and decreased back again at $t = 60$ ms to demonstrate the impact change in amplitude has on the scaled signal.

5.6   Feature extraction

Feature extraction is the core of the detection algorithm where the properties of arcing signals are enhanced and the energy of it (which will be calculated in the next step) can be used to separate red and orange arcing signals from

blue and green normal signals in figure 5.4.

The following sections will discuss five different suggestions of feature extraction methods and test them on the data shown in figure 5.4. To finalize, the different methods are tested on various cases and discussed in section 5.6.6 where one of them will be chosen as the best suited method.

Section	Method
5.6.1	Method 1: Frequency analysis
5.6.2	Method 2: High-pass filter
5.6.3	Method 3: Band-stop filter
5.6.4	Method 4: Trigonometric identities
5.6.5	Method 5: Average energy

Table 5.1: Summary of the different feature extraction methods that are developed.

5.6.1 Method 1: Frequency analysis

Principle

The waveform shape of an arcing signal is different compared to a normal signal like shown in figure 5.4. The deformation is synchronized according to the AC-frequency, and it is expected that by analysing the frequency components of the signal, some properties can be utilized for this feature extraction method.

Discrete Fourier transform (DFT) is an algorithm that converts a finite sequence of a sampled signal from time- to frequency domain. Fast Fourier transform (FFT) is a computation optimized version of DFT available in many programming languages.

FFT computes a set of frequency coefficients that tells the amount of different frequencies in the signal ranging from 0 Hz to $fs/2$ Hz[3]. As both a normal and an arcing signal are periodic, a frequency analysis of one period would tell something about the waveform shape. The frequency resolution depends on the length of the signal and sampling rate. In this case using a length of one period ($N = 80$) the resolution is $fs/N = 4000/80 = 50$ Hz for every coefficient.

---

[3]Technically speaking to fs Hz, but all frequencies over $fs/2$ Hz will be symmetric to the range from 0 Hz to $fs/2$ Hz due to aliasing.

As shown in figure 5.8 every odd coefficient are different between a normal and arcing signal. A normal signal which is a pure sine-wave is zero on all coefficients except the first (50 Hz). The squared difference between a coefficient's value and the value that one would expect from a normal signal can be used as a measure for the feature extraction method. In principle all the odd coefficients could be used, but the first and third coefficient (50 Hz and 150 Hz) are the ones with the greatest difference, so they are chosen to be used.
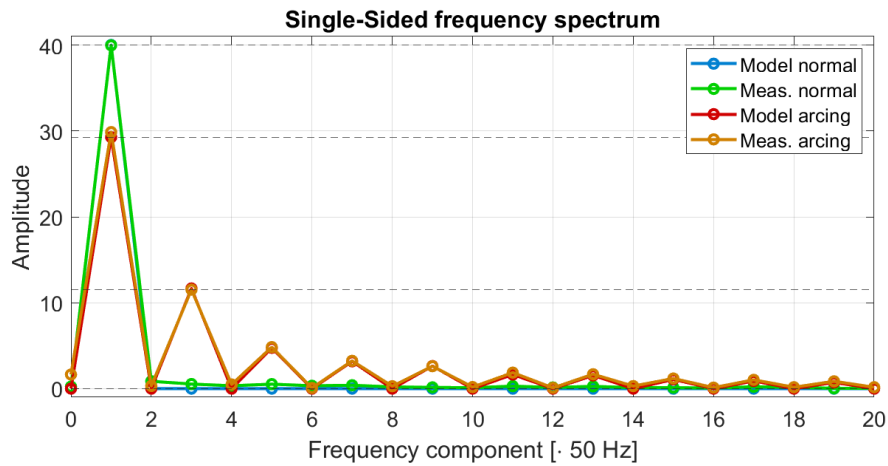
Figure 5.8: Frequency components of one period signals. All even coefficients are zero as both the arcing and normal signal are antisymmetric over one period.

Mathematical expression and computation

Using the x_{sca} as a signal equation 5.11 express the DFT[4] of the past period ($N = 80$). The feature extracted signal from this method x_{fea} can be expressed as in equation 5.12 where $K_1 = 40$ and $K_3 = 0$ is the frequency component value $x_{dft}(k)$ of the normal signal at $k = 1$ and 3 (see figure 5.8).

---

[4]When implementing the method, FFT can be used to calculate DFT as it already exists in many programming languages.

$$x_{dft}(k) = \sum_{n=0}^{N-1} x_{sca}(n)e^{-jk\frac{2\pi}{N}n} \tag{5.11}$$

$$x_{fea}(n) = (|x_{dft}(1)| - K_1)^2 + (|x_{dft}(3)| - K_3)^2 \tag{5.12}$$

The major part of computing x_{fea} will lie in the FFT computation. The number of multiplications for the FFT algorithm can be estimated using $N/2 \log_2 N$[25, chap. 8.1.3] where N is the size of the signal or larger so that the binary logarithm of N is a whole number ($\log_2(N) \in \mathbb{N}$). In this case $N = 80 \to N = 128$ which gives the number of multiplications:

$$\frac{128}{2} \log_2 128 = 448 \tag{5.13}$$

448 multiplications is a very high computation requirement and may not be realizable if it is going to be computed for every sample. But doing that is redundant as the method separates the arcing from normal signals very well (see figure 5.9) and the computation of $x_{fea}(n)$ is not dependent on previous computations $x_{fea}(n-1)$ (like for instance an IIR-filter would be).

DFT has the property that a time shift in a signal corresponds to a phase shift in the frequency domain which is not noticeable in this case as only the magnitude is analysed. So as long as the whole period of the input signal has an arcing shape, it does not matter when the computation is done. This gives more flexibility to determine how often the computation should be done and in section 5.7 it will be chosen that computation should happen at least two times for each period. This results in an average computation of $448 \cdot 2/80 = 11.2$ multiplications per sample.

The FFT algorithm computes all $N = 80$ coefficients while x_{fea} only uses two of them. FFT is designed to compute all coefficients, however there are alternative algorithms so called *single-bin FFT algorithms* (for instance *Goertzel algorithm*) that efficiently computes single frequency components of DFT [24] and may save computation. Due to the complexity of such algorithms and lack in theory on the subject, it is treated as out of the scope for this thesis and set as further work in section 6.2.

Test on data

Using the data provided in figure 5.4 the output of this feature extraction method is shown in figure 5.9. Notice how the method manages to separate the normal and arcing signals for all samples n because of the time shift property of DFT. The plot shows x_{fea} calculations for every sample n, and it is concluded that this is redundant for this method.
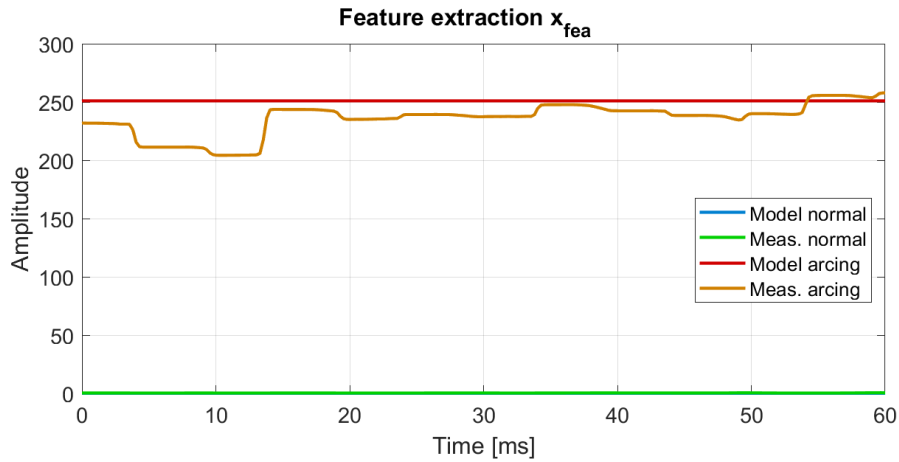
Figure 5.9: Feature extraction x_{fea} by using method 1.

5.6.2 Method 2: High-pass filter

Principle

Based on frequency analysis of the signals in figure 5.8 a normal signal only contains the 50 Hz component while an arcing signal contains higher frequency components as well. The principle of this method is to suppress the low 50 Hz waveform and let the higher frequencies from 100 Hz and upwards pass making the arcing signal stand out from the normal in forms of peaks and transients.

Figure 5.10 shows different suggestions to high-pass filters designed in Matlab that can be used. They have a stop-band from 0-50 Hz and pass-band from 100 Hz and upwards with a transition from 50-100 Hz. Based on different tests it is concluded that the filters should have an attenuation of at least -40 dB in the stop-band and maximum 5 dB transients in the pass-band.

Using Matlab, the minimum order filters that satisfy those requirements is found and shown in the legend in figure 5.10.
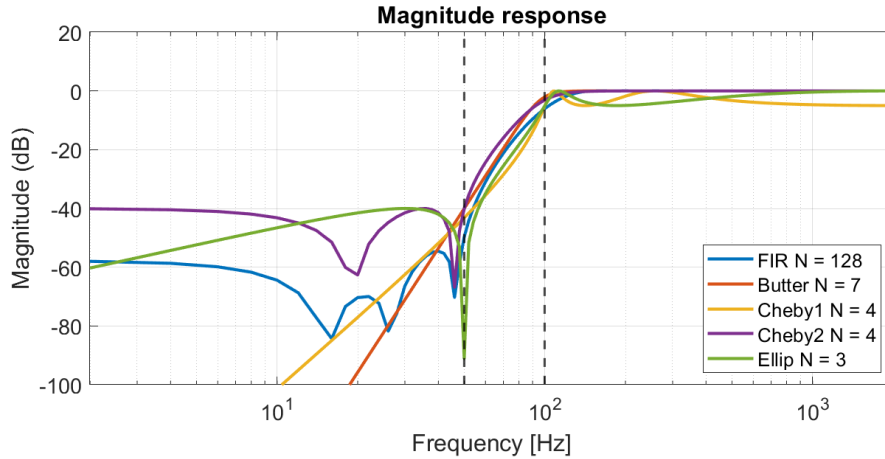
Figure 5.10: Magnitude response of different types of filters.

The blue line in figure 5.10 is a FIR filter while the other are IIR filters. Using an IIR filter it can generally be realized using much fewer coefficients than a FIR which saves computation. The Butterworth filter (red line) requires more coefficients than the other IIR filters, but has the property of having a smooth monotonic response, which is not a requirement in this case. The two Chebyshev filters uses an equation that creates a filter where the magnitude response is similar to the response of an ideal filter. Type 1 has a maximally flat stop-band and the ripple in pass-band can be specified, while type 2 opposite. Finally, elliptic filter contains ripple in both stop- and passband, but has the steepest transition and therefore often requires the lowest order like in this case [25, chap. 10.3.4].

As there is not that much difference in all the IIR filter characteristics the elliptic filter is chosen as it has the fewest coefficients and requires the lowest computation of them all.

Mathematical expression

An IIR filter can be expressed by equation 5.14 where a and b are the filter coefficients where b acts on the input signal x_{sca} and a acts on previous output signals x_{fea}. $N = 3$ is the order of the filter and in this case a is of length 3 and b of length 4 making a total of 7 multiplications per sample.

$$x_{fea}(n) = \sum_{i=0}^{N} b(i)x_{sca}(n-i) - \sum_{i=0}^{N-1} a(i)x_{fea}(n-1-i) \qquad (5.14)$$

Test on data

Using the data provided in figure 5.4 the output of this feature extraction method is shown in figure 5.11.

Figure 5.11: Absolute value of feature extraction $|x_{fea}|$ by using method 2. The absolute value is plotted as x_{fea} will contain negative values, but will disappear when computing the energy in next step. As the filter has an infinite impulse response it is initialised using four periods of normal sine waves to avoid turn-on transients of the filter.

5.6.3 Method 3: Band-stop filter

Principle

The principle of this method is similar to method 2 but replace the high-pass filter with a band-stop filter. The band-stop filter focuses on suppressing the frequencies around 50 Hz and let all other frequencies pass.

Just like decided for the high-pass filter described in section 5.6.2 the filter should have a minimum attenuation of -40 dB in the stop-band. To ensure

sufficient suppression for some changes in the AC-frequency, the stop-band
is set from 48-52 Hz.

Figure 5.12 shows a suggestion for a band-stop filter together with the
high-pass filter from method 2 from section 5.6.2. The band-stop filter is
designed in Matlab using a Butterworth filter of 2. order. The advantage of
using the band-stop filter is that the transition is steeper than the high-pass
filter and there is no ripple in any of the pass-bands.
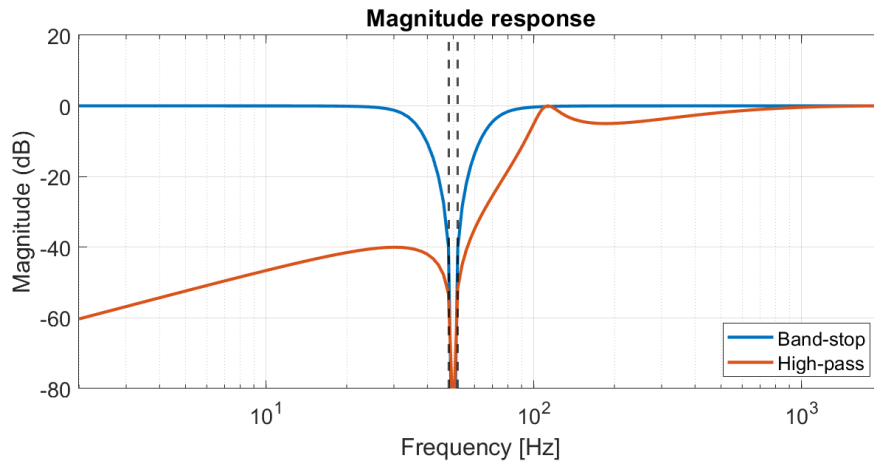
Figure 5.12: Comparison of the magnitude response to the chosen high-pass
filter from method 2 with a suggested band-stop filter from this method. The
stippled lines marks the stop-band from 48-52 Hz.

Mathematical expression

The band-stop is a type of IIR-filter and can be expressed in the same way
as the high-pass filter in equation 5.14. a is of length 4 and b of length 5
making a total of 9 multiplications per sample.

Test on data

Using the data provided in figure 5.4 the output of this feature extraction
method is shown in figure 5.13.
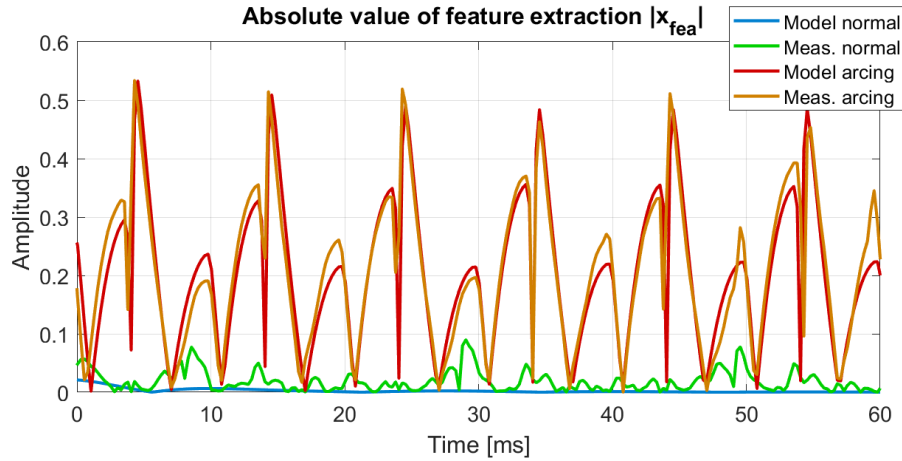
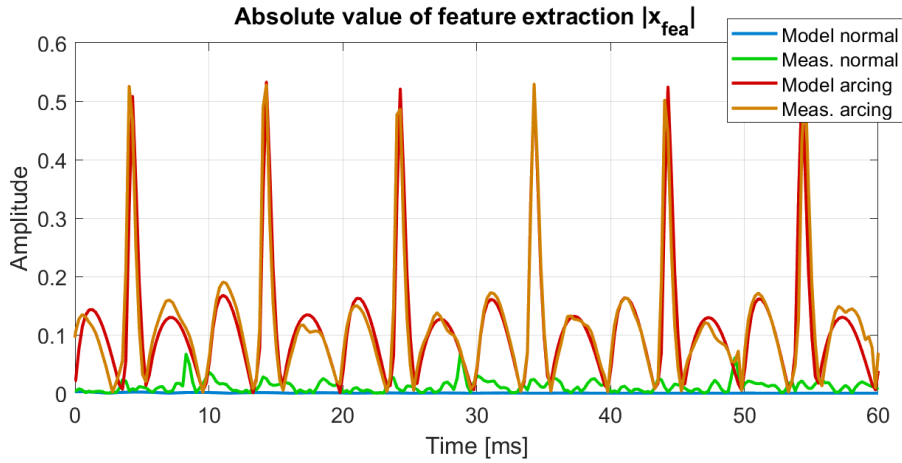Figure 5.13: Absolute value of feature extraction $|x_{fea}|$ by using method 3.

5.6.4   Method 4: Trigonometric identities

Principle

The measured AC current should in theory be alternating with the shape of a 50 Hz sine wave which is a trigonometric function. Trigonometric identities can be applied to such functions and are true for all values of the variables. The principle for this method is to apply trigonometric identities on the signal and compare the result with what would be expected from a normal sine wave.

The two identities that is going to be used is the phase shift identity shown in equation 5.15, Pythagorean identity in 5.16 and circle equation in 5.17.

$$\sin(\theta) = \cos(\theta - \frac{\pi}{2}) \tag{5.15}$$

$$\sin^2(\theta) + \cos^2(\theta) = 1 \tag{5.16}$$

$$x^2 + y^2 = r^2 \tag{5.17}$$

Assume that the input signal x_{sca} is a perfect 50 Hz cosine-function like expressed in 5.18. From equation 5.15 by looking at the signal back in time (i.e. phase shifting), with quarter of a period which in this case is $n = 20$ it can be expressed like in 5.20 using a sine-function.

$$x_{sca}(n) = \cos(2\pi f \frac{n}{F_s}) \tag{5.18}$$

$$x_{sca}(n - 20) = \cos(2\pi f \frac{n}{F_s} - \frac{\pi}{2}) \tag{5.19}$$

$$= \sin(2\pi f \frac{n}{F_s}) \tag{5.20}$$

So if $x_{sca}(n) = \cos(2\pi f \frac{n}{F_s})$ then $x_{sca}(n - 20) = \sin(2\pi f \frac{n}{F_s})$. Plotting these in a 2D plot shown in figure 5.14 gives a unit circle from the normal signals as they satisfy the circle equation 5.17 where $r = 1$ by Pythagorean identity 5.16. For the arcing signals there are clearly a deviation from the unit circle as such waveform does not satisfy the identities. This can be used as a measure for this feature extraction method.

Inserting $x_{sca}(n)$ and $x_{sca}(n - 20)$ into 5.17 gives equation 5.21 where r is the radius of the circle (e.g. the distance from origin to the data points). The deviation distance from the unit circle to the data points are $1 - r$ which is expressed in 5.22. The squared deviation distance used as the output from this feature extraction method is expressed in 5.23.

$$r^2 = x_{sca}(n)^2 + x_{sca}(n - 20)^2 \tag{5.21}$$

$$1 - r = 1 - \sqrt{x_{sca}(n)^2 + x_{sca}(n - 20)^2} \tag{5.22}$$

$$x_{fea}(n) = (1 - r)^2 = [1 - \sqrt{x_{sca}(n)^2 + x_{sca}(n - 20)^2}]^2 \tag{5.23}$$
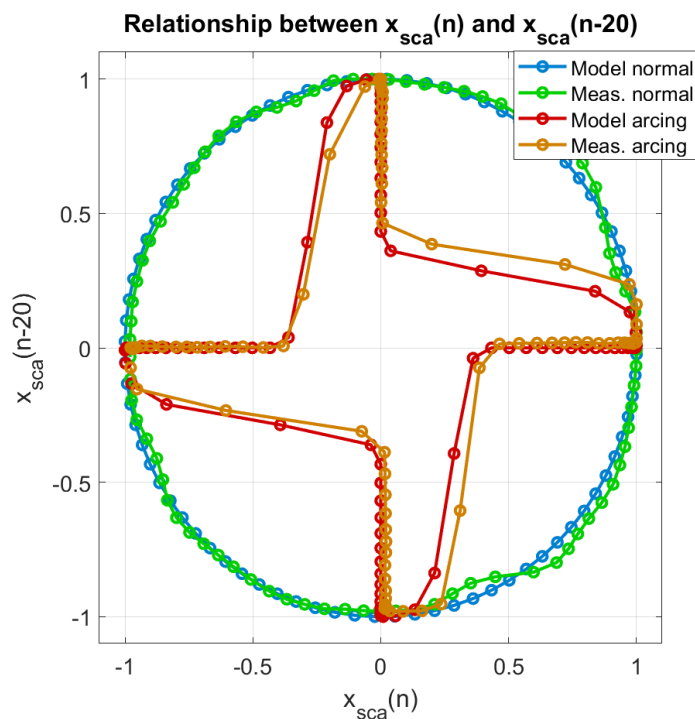
Figure 5.14: Relationship between $x_{sca}(n)$ and $x_{sca}(n-20)$ during one period of signals.

Computation

The method requires low computation compared to other methods. When neglecting additions and subtractions the method consists of 3 multiplications and 1 square root per sample.

Test on data

Using the data provided in figure 5.4 the output of this feature extraction method is shown in figure 5.15.
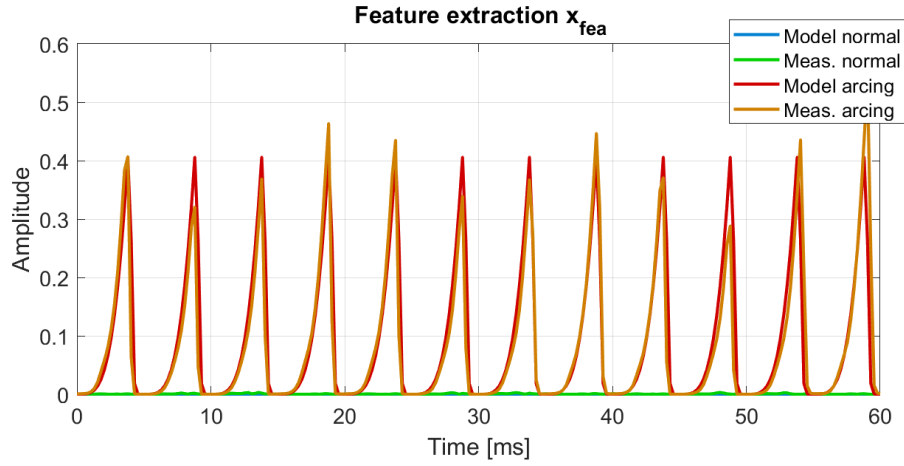
Figure 5.15: Feature extraction x_{fea} by using method 4.

5.6.5 Method 5: Average energy

Principle

Comparing normal and arcing signals (from figure 5.4) one can see that the energy in arcing signals are lower than normal ones. This is the basis for this method, and it takes advantage of the fact that the amplitude of normal and arcing signals are the same even though their energy changes.

Mathematical expression and computation

During one period of an arcing signal, two electric arcs occur, one for each half-wave. The average energy of a signal during the past half period will differ from a normal signal. The reduction in average energy in the signal x_{sca} from what one would expect from a normal signal is used as an output for this feature extraction method. It can be expressed as in equation 5.24 where in this case $E = 0.5$ is the average energy of a normal signal during one half-wave (where $N = 40$ samples).

$$x_{fea}(n) = E - \frac{1}{N} \sum_{k=0}^{N-1} x_{sca}(n-k)^2 \tag{5.24}$$

$$E = \frac{1}{N} \sum_{k=0}^{N-1} \sin(2\pi f \frac{k}{f_s})^2 \tag{5.25}$$

$$= \frac{1}{40} \sum_{k=0}^{39} \sin(2\pi 50 \frac{k}{4000})^2 \tag{5.26}$$

$$= 0.5 \tag{5.27}$$

Looking at equation 5.24 there are $N = 40$ multiplications by $x_{sca}(n-k)^2$ in the summing notation. But increasing n to $n+1$ for the next sample will result in increasing the indexing to $x_{sca}(n+1-k)^2$ which means that $N-1$ of the multiplications in the summing notation is equal to the previous summing notation. By saving the values of $x_{sca}(n-k)^2$ in a memory, they can be used in the next computation and the total complexity is reduced from $N+1$ multiplications per sample to 2. One can also argue that the multiplication of $1/N$ is redundant as it is a constant, which is true from the computation perspective. Removing $1/N$ will calculate the energy instead of the average energy which can also be used, and the complexity of equation 5.24 is reduced to 1 multiplications per sample.

Test on data

Using the data provided in figure 5.4 the output of this feature extraction method is shown in figure 5.16. Just like method 1 from section 5.6.1 the normal and arcing signals are separated for all samples of n. Because of this, it can be considered to reduce the rate of how often x_{fea} is calculated like method 1, but since it only requires 1 multiplications per sample it is not considered necessary.
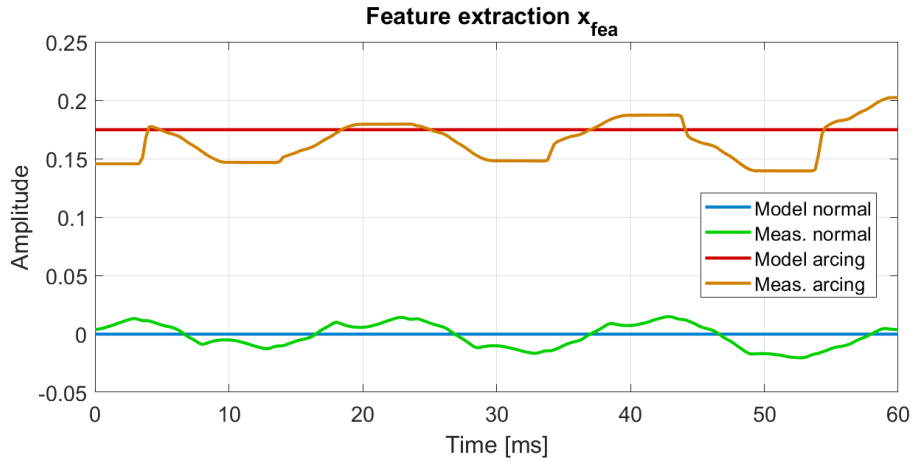
Figure 5.16: Feature extraction x_{fea} by using method 5.

5.6.6   Robustness and comparison

In this section the different feature extraction methods are compared using six tests. The tests are made considering the requirements described in section 5.1. Finally, it will be discussed and chosen which feature extraction method is the most suitable for the algorithm based on the tests and requirements.

The measure for the tests are the average energy of x_{fea} as this will be computed in the next step after feature extraction. It will in section 5.7 be chosen to use a window length of $t = 60$ ms for computing the average energy.

Normalisation

To make it easier to compare the methods, their values are normalised according to table 5.2 so that the average energy of an arcing signal from the mathematical model constitutes 1. This will not be a part of the algorithm, it is just done for comparison reasons in this section.

Method	Normalisation constant
1	$63.0 \cdot 10^3$
2	$22.7 \cdot 10^{-3}$
3	$56.5 \cdot 10^{-3}$
4	$23.1 \cdot 10^{-3}$
5	$30.5 \cdot 10^{-3}$

Table 5.2: Average energy of x_{fea} of arcing from the mathematical model which will be used to normalise the values in table 5.3-5.5 for comparison reasons.

Test 1: Comparing mathematical model and practical measurements

From the requirements in section 5.1 the algorithm should work on practical measurements that may contain unevenness and noise. Table 5.3 compares the mathematical model with one instance of practical measurements.

Method	Model		Measurements	
	Normal	Arcing	Normal	Arcing
1	≈ 0	1	$1.71 \cdot 10^{-6}$	0.889
2	$21.3 \cdot 10^{-6}$	1	$11.0 \cdot 10^{-3}$	1.062
3	$372 \cdot 10^{-6}$	1	$11.9 \cdot 10^{-3}$	1.041
4	≈ 0	1	$27.1 \cdot 10^{-6}$	0.935
5	≈ 0	1	$3.51 \cdot 10^{-3}$	0.898

Table 5.3: Average energy of x_{fea} of normal and arcing for the different methods. The table show values for both the mathematical model and practical measurements normalised according to table 5.2.

Mathematical model: As all the values are normalised according to arcing signals from the mathematical model, they result in a value of 1 for all methods. Method 2 and 3 are based on IIR-filter which will have a value greater than 0 for normal signals. While method 1, 4 and 5 are designed to output a value based on the difference from a normal signal and will therefore have a value approximately 0.

Practical measurements: All the methods manages well to separate normal and arcing signals using the practical measurements as well. It is

noticed that method 1 and 5 has a decrease in arcing value right below 90 % of what one could expect, but it is also worth noticing that method 1 has the lowest normal value for the practical measurements as well.

Test 2: Other frequencies than 50 Hz

Ideally the grid frequency is 50 Hz and the algorithm is designed for that, but in practical grids it can change depending on the connected load. From the requirements in section 5.1 the algorithm should also work on practical grids where the frequency is slightly off 50 Hz, and table 5.4 tests the methods using a frequency of 48 Hz and 52 Hz.

	48 Hz		52 Hz	
Method	Normal	Arcing	Normal	Arcing
1	$22.2 \cdot 10^{-6}$	0.956	$26.3 \cdot 10^{-6}$	0.932
2	$149 \cdot 10^{-6}$	1.070	$196 \cdot 10^{-6}$	0.943
3	$3.75 \cdot 10^{-3}$	1.023	$796 \cdot 10^{-6}$	0.998
4	$15.7 \cdot 10^{-6}$	1.013	$16.2 \cdot 10^{-6}$	0.983
5	$7.11 \cdot 10^{-3}$	0.977	$5.93 \cdot 10^{-3}$	0.967

Table 5.4: Average energy of x_{fea} of normal and arcing from the mathematical model where the frequency is 48 Hz and 52 Hz. The values are normalised according to table 5.2.

Method 1 is the one that is most affected by the change in frequency for the arcing signals (4-7 %), while method 5 is most affected for the normal signals (6-7 %). Other than that, in general a slight change in frequency result in a low impact in the values.

Test 3: Change in amplitude

According to section 5.1 the algorithm should work on current signals with different amplitudes. For this, the scaling function in section 5.5 was made, but as mentioned in the section and shown in figure 5.7 the scaling that is used for the algorithm may have an impact on the signal when there is a change in amplitude from one level to another. The test in table 5.5 shows how much a change in amplitude affects the signal.

	Increase		Reduction	
Method	Normal	Arcing	Normal	Arcing
1	$849 \cdot 10^{-6}$	0.965	$29.7 \cdot 10^{-3}$	1.260
2	$50.2 \cdot 10^{-3}$	1.018	$45.8 \cdot 10^{-3}$	0.899
3	$68.1 \cdot 10^{-3}$	1.009	$193 \cdot 10^{-3}$	0.947
4	$11.8 \cdot 10^{-3}$	0.974	$236 \cdot 10^{-3}$	1.377
5	$94.4 \cdot 10^{-3}$	0.964	$508 \cdot 10^{-3}$	1.603

Table 5.5: Average energy of x_{fea} (normalised according to table 5.2) of the mathematical model right after a change in the amplitude of the current signal. The amplitude is increased and reduced by multiplying or dividing by 2.

In general method 1 and 2 are relatively low affected by change in amplitude while method 3 and especially 4 and 5 are greatly affected. Especially when there is a reduction in the amplitude, a normal signal can be detected as an arcing signal (false positive) where method 5 results in a value of 51 % compared to arcing.

The probability for a change in current amplitude at the same time that arcing occurs is very low, and one can discuss if it is any purpose for taking this into account. The critical purpose of the test is to measure the risk of making a false positive alarm, that is when a change in amplitude causes the algorithm to trigger an alarm during a normal signal.

The origin of this error is from the scaling part of the algorithm, and it can also be discussed whether scaling should be improved, instead of using the error as a measure for comparing the feature extraction methods. It will therefore be listed in the further work in section 6.2.

Test 4: Feature extraction delay

A requirement in section 5.1 is that the charger should have a release time of maximum 120 ms. In section 5.7 the timing of the different parts of the algorithm will be discussed, and it will be concluded that all feature extraction methods should have a maximum delay of 20 ms from when arcing is available in the signal to when the x_{fea} is at a typical arcing level.

Method	Time [ms]
1	14
2	4
3	1
4	3
5	4

Table 5.6: Typical time from when a signal changes from normal to arcing before the energy of x_{fea} is around the typical average energy for arcing from table 5.3.

All the methods satisfy the criteria of a maximum feature extraction delay of 20 ms.

Test 5: Computation complexity

From section 5.1 the algorithm should use as low processing power as possible. Table 5.7 summarises the average number of multiplications per sample for the methods.

Method	Multiplications per sample
1	11.2
2	7
3	9
4	4
5	2 or 1

Table 5.7: Average number of multiplications per sample for all the methods. Method 4 approximates that a square root requires the same as a multiplication. As described in 5.6.5 method 5 initially requires 2, but one variant of the method can be implemented that requires 1 multiplication per sample.

Initially method 1 was very computational heavy compared to the other ones. But as described in section 5.6.1 it did not need to be computed for each sample[5], and the result is comparable to the other methods. Table 5.7

---

[5]In addition to that, a single-bin FFT algorithm may lower the computation complexity even further. But this is out of the scope of this thesis and will be set as further work in section 6.2.

shows that all of the methods are relatively light weighted, where method 4 and 5 requires the least.

Test 6: Voltage measurements

It is desirable (but not a requirement) to have an algorithm that is flexible where voltage measurements also can be used to detect arcing, as described in section 5.1.

Method	Voltage measurements	
	Normal	Arcing
1	$105 \cdot 10^{-3}$	$62.9 \cdot 10^3$
2	$274 \cdot 10^{-6}$	$21.6 \cdot 10^{-3}$
3	$937 \cdot 10^{-6}$	$53.1 \cdot 10^{-3}$
4	$644 \cdot 10^{-9}$	$33.2 \cdot 10^{-3}$
5	$14.0 \cdot 10^{-6}$	$37.1 \cdot 10^{-3}$

Table 5.8: Average energy of x_{fea} of practical voltage measurements (not normalised).

The measures in table 5.8 looks in general very promising as expected. There is a slight increase in the normal value above 0, but that is also the case for the practical current measurements. The same yields for arcing signals by comparing them to the arcing values in table 5.2.

Conclusion and choosing feature extraction method

Doing an overall evaluation method 5 is rejected as a possible method as several tests especially test 1-3 distinguishes it from the other ones in a negative way. Other than that, all the resulting methods shows promising results.

Method 1 changes value a bit when testing on practical measurements in test 1 and there is an uncertainty of how much it will change on other practical measurements. It is also the one requiring most computation resources, and therefore not chosen as the best alternative.

Method 3 and 4 compared to method 2 has a high risk of triggering a false positive alarm on a normal signal when there is a change in current amplitude shown in test 3. An overall evaluation of method 2 based on the tests concludes that this will be the recommended feature extraction method.

When that is said it can be considered if the scaling part from section 5.5 should be improved which contributes to choosing method 2. This consideration will be listed in further work in section 6.2 and future development may conclude that one of the other methods will be chosen instead.

5.7 Average energy and threshold

To determine if arcing occurs or not based on the feature extracted signal x_{fea} a way of comparing the signal to a threshold value should be done. A straight forward way of doing this is to compare x_{fea} directly with a threshold value. But noise or unexpected shapes in the current signal may affect the signal creating peaks that can trigger the alarm. To make the algorithm reliable and robust it makes sense to compute the average energy over a given time frame and compare this with a threshold. This requires consecutive electric arcs to occur for an alarm to trigger but also lower the probability of false alarms.

5.7.1 Timing and window size

One of the requirements from section 5.1 specify a release time of maximum 120 ms from when arcing starts to relay release. This requirement is essential for determining the window size used to compute the average energy. It is desired to use as large window size as possible which makes the algorithm more reliable as more periods of a signal is used to determine if arcing occurs or not, as long as the total release time is under 120 ms. In this section all delays that can occur before the relays are tripped is addressed, and a window size is chosen.

Initially the algorithm is intended to be computed for all samples n. But it was mentioned in section 5.6.1 how the computation requirement for feature extraction method 1 could be lowered by lowering the computation rate. But doing that also introduces a delay as the signal can transit from normal to arcing right after a computation, let's call this *Computation rate delay*. Although it was concluded in section 5.6.6 that method 2 is going to be used, it is desired to take the delay into account as future development of the algorithm may choose to use method 1. It is concluded that the maximum time between computations should be 10 ms. There is no correct answer to this, but it seems as a good starting point as 10 ms is the same time as

half a period where one typically would see an arcing shape. Note that only method 1 would take advantage of this as the other ones would need to be calculated for every sample n.

Feature extraction method 1 is based on frequency analysis over one period of time (20 ms), so it requires the whole period to have an arcing shape to ensure that the output has the value of an arcing signal. This creates a delay of maximum 20 ms, let's call it *Feature extraction delay*.

The relays have a maximum release time of 10 ms from section 5.1 which can be called *relay release*.

By using a window size of $N = 240$ which corresponds to a time of $t = 60$ ms three periods of the signal are used calculate the average energy. The detection algorithm will be based on three periods which contains six half-waves that can be of arcing shapes. Looking back at figure 5.4 six periods of current signal was used to document the feature extraction methods which corresponds to the decided windowing size. To detect an arcing signal using the average energy of this window creates a delay of maximum 60 ms, let's call this *window delay*.

All the described delays and the chosen window size leads to a final *margin* of $120 - 10 - 20 - 10 - 60 = 20$ ms. The margin includes unpredicted or other minor delays that is not described in this section.

Figure 5.17 shows a timeline where all the maximum delays are summarised and emphasize that the maximum 120 ms release time requirement is satisfied.
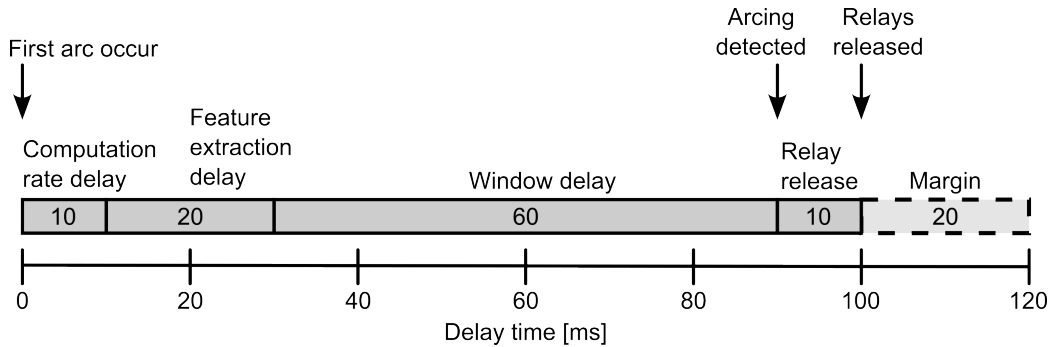

Figure 5.17: Summary of various delays introduced in the algorithm.

5.7.2 Average energy

The average energy x_{nrg} during a period of $t = 60$ ms can be calculated using equation 5.28 where $N = 240$.

$$x_{nrg}(n) = \frac{1}{N} \sum_{k=0}^{N-1} x_{fea}(n-k)^2 \tag{5.28}$$

Figure 5.18 shows the average energy (using a 60 ms window which was chosen in section 5.7.1) of the x_{fea} signal from figure 5.11[6]. The figure shows how the average energy x_{nrg} reaches the typical average energy of an arcing signal from table 5.2 in about 60 ms as expected.

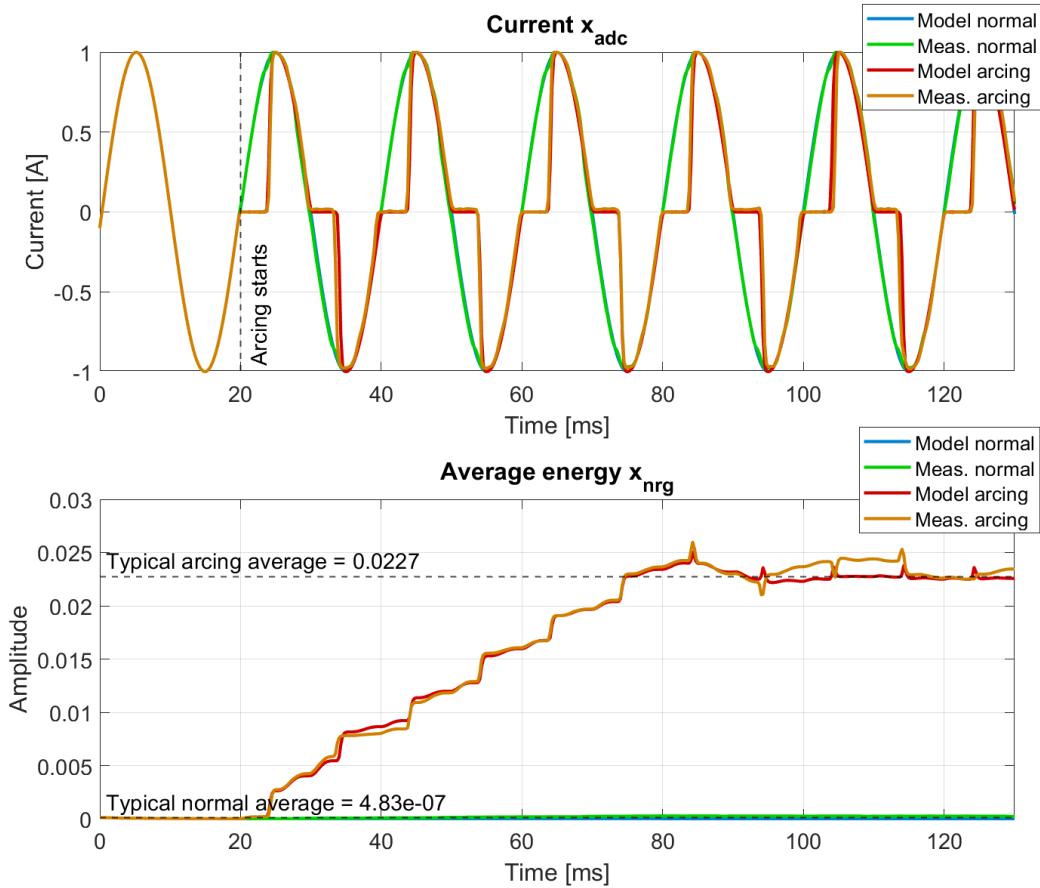[6]by using feature extraction method 2 which was chosen in section 5.6.6

Figure 5.18: Average energy x_{nrg} of the feature extraction signal x_{fea}. The current signal starts arcing at $t = 20$ ms.

5.7.3   Threshold

The average energy of feature extraction x_{fea} will by using the mathematical model for normal be $483 \cdot 10^{-9}$ and for arcing $22.7 \cdot 10^{-3}$. The threshold should lay somewhere between those values. Alternatively the signal can be mapped to 0-1 so that the values makes more sense using equation 5.29 where $K_{low} = 483 \cdot 10^{-9}$ and $K_{high} = 22.7 \cdot 10^{-3}$.

$$x_{map}(n) = \frac{x_{nrg}(n) - K_{low}}{K_{high} - K_{low}} \qquad (5.29)$$

There are various considerations that need to be addressed when choosing a threshold value. Setting a too low value may result in falsely tripping the relays even though no arcing occurs. While setting a too high value may not trip the relays even though arcing occurs leading to danger associated with electric arcs. There is no correct answer to the optimal threshold value and the risks should be balanced against each other.

This thesis covers development of the electric arc detection algorithm and will not determine a suitable threshold value. The threshold value is a parameter of the algorithm and choosing this should be based on statistics from a large amount of measured data. It will therefore be listed as further work in section 6.2.

Even though the threshold value is not chosen at this time, it is desired to test the algorithm with an example threshold to get a measure of how good it works. Test report 6 tests the algorithm with a threshold value of $18 \cdot 10^{-3}$ which was a guess for a suitable threshold based on figure 5.18. The test uses the collected data described in section 4.4 as measurements. The algorithm does not raise any false positive alarms on the normal signals and manages to detect all the arcing signals within 110 ms (120 ms requirement minus the 10 ms relay release, see figure 5.17). However, the dataset is too small to conclude that the algorithm works sufficiently (more testing will be listed in further work in section 6.2), but it indicates very promising results.

Chapter 6

Discussion

This chapter summarises the content of the thesis and what is left for further work.

6.1 Conclusion

In this thesis electric arcs were studied with the focus on measurements that can indicate arcing in a circuit. An electric arc detection algorithm was developed that can be implemented on the embedded microcontroller in Easee chargers to detect series electric arcs. It uses current measurements as input and releases relays if arcing is detected to stop the current in the charging circuit and protect against further damage.

Unlike conventional AFDDs that uses high-frequency sensors, the algorithm uses digital signal processing and detects the special shape of an arcing signal on each half-wave of the AC-current measurements, that already are available on the microcontroller. The algorithm is specifically developed for Easee chargers with respect to its hardware and software structure. However, the principle may be converted into other electrical equipment or measuring systems as well.

The algorithm is designed to have a maximum release time of 120 ms which was discussed in the thesis to be a sufficient time where arcing can not do any critical damage. The algorithm handles change in the current level from 1-32 A where current levels less than 1 A are associated with low or no danger.

The core of the algorithm is the feature extraction part, and five methods of feature extraction was developed. One of the methods, based on high-pass filtering was chosen to be used for the algorithm based on various tests of its robustness. However, several of the methods are showing promising results and future development may conclude that one of the other is better suited.

A dataset of measurements taken by the charger was collected from the lab of normal and arcing signals using an electric arc generator on current levels ranging from 1-10 A. The measurements contained noise and unevenness in the waveforms that was specific for that electrical grid. Based on the dataset a mathematical model of an arcing signal was made that does not include any noise or unevenness, and the algorithm was mainly developed using the model.

The algorithm uses a threshold value as a parameter which is yet to be determined in further work based on comprehensive testing and a risk analysis. However, it was tested on the normal and arcing signals from the dataset using an example threshold and managed to detect all the arcing signals without any false positive alarms on the normal signals. This can only be treated as an indication as the dataset containing only 40 normal and 40 arcing signals is too small to conclude that the algorithm works sufficiently.

A greener future requires smarter and safer electronics, and implementing electric arc detection will work as an extra safety function in the charger. There are still work to be done which will be listed in section 6.2. Therefore, the algorithm was never implemented on a microcontroller and tested in real-time, it was only tested in Matlab using the dataset and mathematical model as measurements. This thesis forms a basis for further development and is a step towards realizing built-in series electric arc detection in Easee chargers.

6.2 Further work

Further work is listed as follows:

1. Consider improving the scaling part of the algorithm, as it was the cause of rejecting some of the feature extraction methods as mentioned in section 5.6.6.

2. Consider using one of the other feature extraction methods described in section 5.6, as several of them showed promising results. Further development may conclude that one of the other methods are better suited

for the algorithm than what was concluded in section 5.6.6 (especially method 1 where a single-bin FFT algorithm may lower the computation complexity of the algorithm as mentioned in section 5.6.1).

3. Consider if it is desirable to expand the algorithm to detect parallel- and ground arcs in addition to series arcs.

4. Implement the algorithm in embedded C on the microcontroller.

5. Do more testing including:

   - Loads up to 32 A which is what Easee chargers are designed for. Maximum load tested in this study was 10 A.

   - Charging EV, both to see if generated arcing is detected but mostly to see if normal is not inducing false positive alarms. A variety of different vehicle brands and models should be tested.

   - Different electrical grids. As pointed out in section 5.2 the collected measurements contained noise and unevenness in the waveforms that was specific for that grid.

   - Arcing produced by realistic cases like damaged cable, loose wires or Chargeberry not sufficient attached instead of using an electric arc generator.

   - Voltage measurements. As described in section 4.2 it is possible to use voltage measurements to determine the location of the fault. The main focus in the thesis was using the current measurements to detect arcing in general.

6. Choose a suitable threshold value. As discussed in section 5.7.3 it needs to be set to a suitable value based on a large number of tests and a risk analysis.

7. Consider if Easee chargers can be certified as an arc fault detection devices (AFDD) according to IEC 62606 for an extra quality stamp.

Bibliography

[1] Davy_lamp.png (500×600). `https://upload.wikimedia.org/wikipedia/commons/3/38/Davy_lamp.png`. (Accessed on 16.01.2023).

[2] Pga-ls10 - littelfuse. `https://www.littelfuse.com/products/protection-relays-and-controls/protection-relays/arc-flash-detection/pga-ls10.aspx`. (Accessed on 02.13.2023).

[3] Tmp126 — ti.com. `https://www.ti.com/product/TMP126/part-details/TMP126NDCKR`. (Accessed on 02.13.2023).

[4] Voltabattery.jpg (1536×2048). `https://upload.wikimedia.org/wikipedia/commons/5/54/VoltaBattery.JPG`. (Accessed on 16.01.2023).

[5] Nek 400:2022, elektriske lavspenningsinstallasjoner. Technical report, May 2022.

[6] André Anders. Tracking down the origin of arc plasma science. Technical report, 2003.

[7] Easee AS. Manuals - easee international. `https://easee.com/manuals/`. (Accessed on 14.02.2023).

[8] Easee AS. Smart ev charging solutions - small. smart. full of power - easee. `https://easee.com/uk/`. (Accessed on 02.13.2023).

[9] (NFPA) National Fire Protection Association. National electrical code 2020. Technical report, sep 2019.

[10] Hertha Ayrton. *The Electric Arc*. Cambridge library collection. publisher not identified, place of publication not identified, 1902.

[11] Vytenis Babrauskas. Electric arc explosions—a review. *Fire safety journal*, 89:7–15, 2017.

[12] J. Banks and R. L. Rardin. Seleeted international comparisons of fire loss. Technical report, Dec 1980.

[13] Tony Cafe. T.c. forensic: Article 10 - physical constants for investigators. `https://www.tcforensic.com.au/docs/article10.html`, 2007. (Accessed on 02.02.2023).

[14] International Electrotechnical Commission. Iec 62606:2013, edition 1.0. Technical report, 07 2013.

[15] H. Davy. *Elements of Chemical Philosophy*. Number pt. 1, v. 1. J. Johnson and Company, 1812.

[16] Elfa Distrelec. Afdd-32/2/b/003-a — eaton arc fault detection device 32 a 2 — distrelec norway. `https://www.elfadistrelec.no/en/arc-fault-detection-device-32-eaton-afdd-32-003/p/30092189?no-cache=true&marketingPopup=false`. (Accessed on 06.02.2023).

[17] evexpert.eu. On-board charger. `https://www.evexpert.eu/eshop1/knowledge-center/on-board-charger`. (Accessed on 03.14.2023).

[18] Markus Fagerås. Ntnu open: Testing av lysbuevern. Master's thesis, may 2016. (Accessed on 10.02.2023).

[19] Flagstaffotos. Lightning_simulator_questacon02.jpg (1600×1067). `https://upload.wikimedia.org/wikipedia/commons/f/fa/Lightning_simulator_questacon02.jpg`. (Accessed on 03.02.2023).

[20] Direktoratet for samfunnssikkerhet og beredskap. Brannstatistikk. `https://www.brannstatistikk.no/brus-ui/search?searchId=19AEA323-63D3-4090-B00E-625147E78F72&type=RESTRICTED_SEARCH_DEFINITION`. (Accessed on 03.02.2023).

[21] Deutsche Fotothek. Fotothek_df_n-08_0000383.jpg (800×796). `https://upload.wikimedia.org/wikipedia/commons/6/6d/Fotothek_df_n-08_0000383.jpg`. (Accessed on 03.02.2023).

[22] Alexander A. Fridman. Plasma physics and engineering, 2011.

[23] Ahmed M. A. Haidar and Kashem M. Muttaqi. Behavioral characterization of electric vehicle charging loads in a distribution power grid through modeling of battery chargers. *IEEE Transactions on Industry Applications*, 52(1):483–492, 2016.

[24] Md. Asif Iqbal and Md. Saifur Rahman. Development and performance analysis of a novel single-bin fft algorithm. page 316 – 319, 2022. Cited by: 0.

[25] Dimitris G. Manolakis John G. Proakis. *Digital Signal Processing: Principles, Algorithms, and Applications*. Pearson Education, Inc., fourth edition edition, 20.

[26] William M. Plate Jr. Gmaw.welding.af.ncs.jpg (1960×2213). `https://upload.wikimedia.org/wikipedia/commons/a/aa/GMAW.welding.af.ncs.jpg`. (Accessed on 03.02.2023).

[27] Ippei Kiyohara. Characteristics of the electric arc. Master's thesis, University of Illinois, 1913.

[28] Dongwei Li, Zhengxiang Song, Jianhua Wang, Yingsan Geng, Huilin Chen, Li Yu, and Bo Liu. A method for residential series arc fault detection and identification. In *2009 Proceedings of the 55th IEEE Holm Conference on Electrical Contacts*, pages 8–14, 2009.

[29] Teng Li, Zhijie Jiao, Lina Wang, and Yong Mu. A method of dc arc detection in all-electric aircraft. *Energies*, 13(16), 2020.

[30] Mliu92. Iec 62196 type 2 r1.svg. `https://upload.wikimedia.org/wikipedia/commons/c/cb/IEC_62196_Type_2_r1.svg`. (Accessed on 03.14.2023).

[31] Alexis Peschot, Christophe Poulain, Nelly Bonifaci, and Olivier Lesaint. Electrical breakdown voltage in micro- and submicrometer contact gaps (100nm - 10μm) in air and nitrogen. In *2015 IEEE 61st Holm Conference on Electrical Contacts (Holm)*, pages 280–286, 2015.

[32] Jean-Francois Rey. Iec 62606: A first step towards standards for arc fault protection. `https://blog.se.com/energy-management-energy-efficiency/energy-regulations/2013/07/09/iec-62606-`

`a-first-step-towards-international-standards-for-arc-fault-protection/`, July 9 2013. (Accessed on 09.02.2023).

[33] Ralf Schumacher. Spark-plug01.jpeg (1000×1005). `https://upload.wikimedia.org/wikipedia/commons/c/c3/Spark-plug01.jpeg`. (Accessed on 03.02.2023).

[34] Siemens. 5sm6 afd unit. Technical report, 2012. (Accessed on 10.02.2023).

[35] E. Sili, F. Koliatene, and J. P. Cambronne. Pressure and temperature effects on the paschen curve. In *2011 Annual Report Conference on Electrical Insulation and Dielectric Phenomena*, pages 464–467, 2011.

[36] K. Srinivasan and G. Jason. Lightning as atmospheric electricity. Technical report, 2006. Cited By :17.

[37] Ørnulf Nordseth (Institute for Energy Technology). Status of the use of arc fault detection devices in norway. Technical report, 2021 (English version 2022).

Attachments

Test reports

Number	Title
1	Making of electric arc generator 1000
2	Setting up charger and computer for testing and programming
3	Generating electric arcs
4	Making of electric arc generator 2000
5	Collecting data of electric arcs
6	Testing the algorithm

Table 6.1: List of attached test reports.

Test report number 1
Title: Making of electric arc generator 1000

Description: To understand the properties of electric arcs, an electric arc generator has to be made. This will later be used to generate electric arc so that current and voltage measurements can be done. The design is inspired by various electric arc generators from literature where two terminals are placed against each other and one of them can be finely screwed to adjust the gap length. Copper terminals are used as this is a standard metal for wires.

Note: In the aftermath it is known that this electric arc generator 1000 was only capable of generating arc with a current draw of max 1 A. At a higher current draw the plastic brackets melted and a new improved version had to be made.

Date: 28.02.2023

Participants: Espen Myrset

List of equipment:

- 2x M3-25 copper bolts
- 2x M3 copper nuts
- 4x M3 5mm insert nuts
- 2x 3mm cable shoes
- 2 mm metal shaft
- Various DIY plastic cog wheels in module 0.5 size
- 2x 2x5x2.3mm bearings
- Wall socket
- See-through shielding
- Wooden plate
- Wire
- 3D printer
- 3D modelling and slicing software, in this case Adobe Fusion 360 and Cura
- Soldering iron
- Heat adhesive glue

Risk analysis

Risk	Probability	Severity	Action to minimise risk
Time consumption when having to redo work	Medium	Low	Carefully design the 3D model. Check the physically dimensions of the cog wheels. Include people with experience in the 3D-printing process. Planning and follow the step-by-step procedure.
Burn marks on skin when inserting the insert nuts	Low	Medium	Place the insert nut on top of the hole before start heating it. Do not touch the soldering iron nor the insert nut. If it doesn't insert properly, wait for it to cool before trying again.

Breaking of plastic brackets or cog wheels. Delays until getting new parts.	Low	Medium	Carefully mount the brackets and only tight more if it still is loose. Use a 2.5 mm hole for the metal shaft to attach parts on the shaft and only use hammer on the shaft.
Accident when using wood cutting tools	Medium	Medium	Use of protection equipment like safety glasses, ear protection and gloves. Use clamps to keep the wood in a fixed place.

Procedure

1. Consider the adjustment accuracy: M3 bolts are chosen because of their small threads as well as it can hold high current. M3 bolts have a thread pitch of 500 um which means it will move 500 um per turn. As an electric arc theoretically can occur in distances under 12.5 um in 230 V AC circuits it is desired that distances easily can be set in this range, so a gear ratio must be used. By using a worm gear (one tooth per turn) with a 40-tooth gear, a 40/1 ratio is established. Turning the knob one round will change the gap distance with 500/40 = 12.5 um which is more than sufficient.
2. Design of brackets and knob in 3D modelling software:
   a. 3D printing design rules are followed for the entire design: https://www.hubs.com/get/3d-printing-design-rules/.
   b. Bracket size of 16x16 mm as low in hight as possible for strong stability.
   c. Foots extensions on each side with screw hole and two supporting walls.
   d. Holes with space for insert nuts and 2 mm shaft.
   e. The hight of the bracket from the adjustment knob is calculated according to the reference diameter of the cog wheels according to the equation $ref\ diameter = module \cdot nr\ of\ teeths$ (where in these parts module = 0.5). It is higher than the two other ones so that a clockwise turn on the adjustment know also leads to a clockwise turn on the bolt. It has holes for two bearings to be inserted in each side.
   f. The adjustment knob has a diameter of 60 mm so that it can be used to finely adjust. It has rounded edges to make it comfortable to use. A hole extension is included so that it can be tightly attached to the metal shaft in a fixed position.
3. The 3D parts are printed.
4. Insert nuts are inserted in each side of two of the brackets. A soldering iron is used to heat up the nuts and plastic. When they are almost fully inserted a hard, flat object is used to press them inside so that the angle is as accurate as possible.
5. Bearings are inserted to the last bracket using a hammer.
6. The 40T cog wheel are attached to one of the bolts using a small part of the metal shaft and heat adhesive glue.
7. Two bolts rounded in the edge so that their centre point will be closest each other. Wires are attached to them using cable shoe and nut.
8. The bolts are screwed into their corresponding brackets and the brackets are screwed into the wooden plate.
9. A metal shaft is inserted through the cog wheel, bearings and knob as close as possible, but still space for the shielding in between.
10. The last bracket is screwed to the wooden plate. Care must be taken as the bolt will move 500 um per turn. The bolt is screwed so that the parts touch and the upper cog wheel is placed slightly to the side on top of the other one, so that it has some space for movement.

11. A small plastic food box is used as shieling. The lid is cut out and screwed to the wooden plate. A 3 mm gap is cut out for the 2 mm metal shaft, so that the box can be put upside down on top of the un-isolated parts and into the fixed lid.
12. The socket is mounted to the wooden plate and everything wired up according to figure 1. Live and neutral pins are marked on the sockets so that the electric arc generator always is connected the same way.
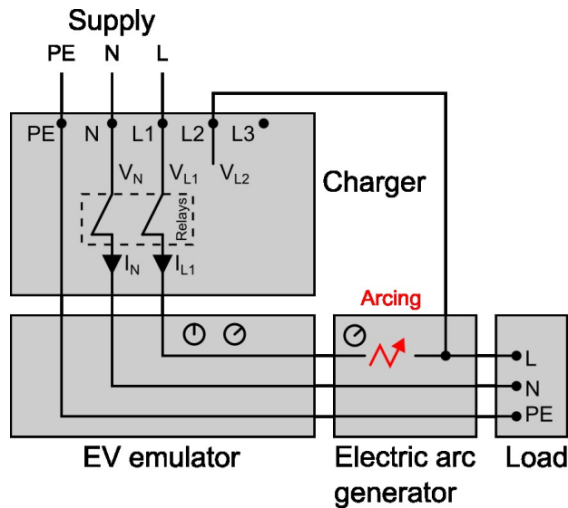

Figure 1: Schematics of the electric arc generator setup.

13. After everything were connected, it was found that it had a low accuracy because of a small gap between the cog wheels. This made a dead zone of half a turn when changing direction. Although it is not going to be used as an accurate tool, it was desired to fix this problem to get more control of the adjustment. One of the brackets were unscrewed and a small solid mass were laid underneath before it was screwed again, making the bracket tilt so that the gap of the cog wheels were removed.

Results and evaluation

An electric arc generator was made. Just like it was designed, it has a very high resolution. To beginning with it had a low accuracy because of a small gap between the cog wheels, but this problem was eliminated after adjusting the brackets.
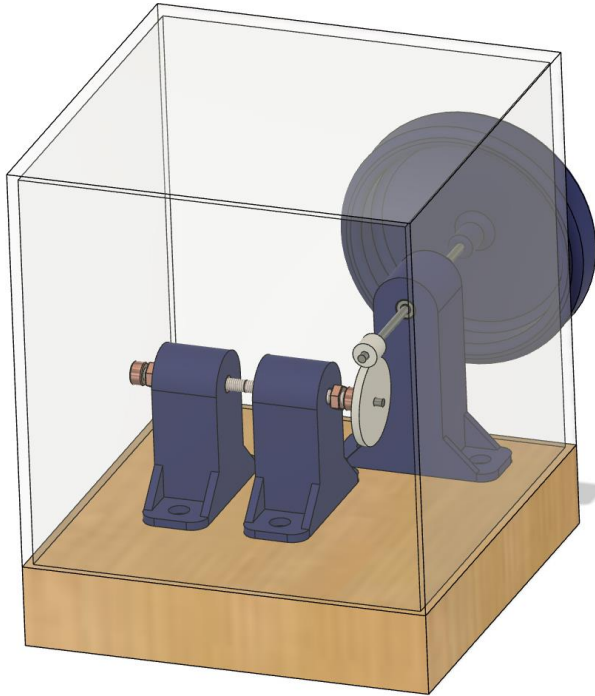
Relevant images

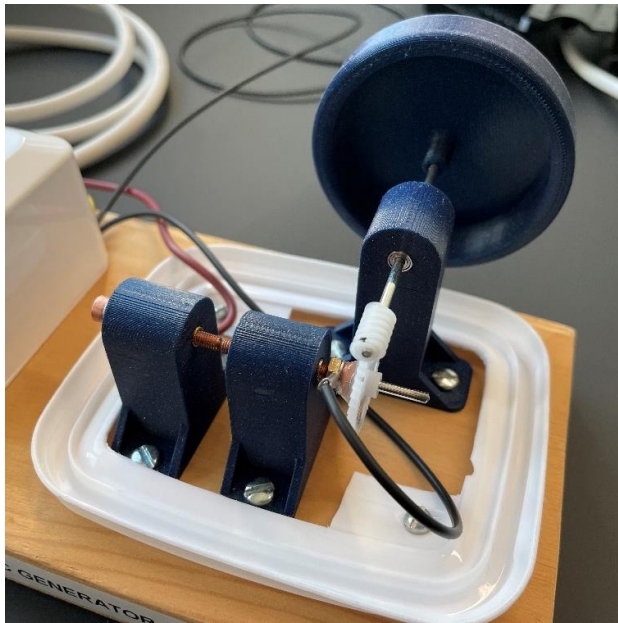*Figure 2: 3D model of the electric arc generator 1000.*

Figure 3: The finished electric arc generator without shielding 1000.

Figure 4: The finished electric arc generator 1000.

Figure 5: The data collection setup.

Test report number 2

Title: Setting up the charger and equipment for collecting data

Description: Before the charger can start collecting data using the electric arc generator, the system needs to be set up for this task. The charger is going to be connected together with the electric arc generator and necessary test-equipment. The charger is going to be programmed so that it can send measurements to a PC and a serial communication have to be set up. The PC needs a program to collect these measurements, save it as csv, and an easy general user interface so that the user can control how and when measurements are going to be made.

Date: 13.03.2023

Participants: Espen Myrset

List of equipment:

- Easee charger
- EV emulator with male type 2 socket to standard EU socket
- Electrical load, in this case a 2 kW heat fan
- PC and USB hub
- Debugger module for STM microcontrollers
- USB to TTL serial adapter
- Multimeter

Risk analysis

Risk	Probability	Severity	Action to minimise risk
Electrical shock	Low	High	See section "Prevention against electrical shock".
Power on a load is constantly on, without being able to turn it off on the EV emulator because of a bug or when debugging	Medium	Low	Use a load that has a built-in switch. Be ready to disconnect the supply plug. Be careful when debugging and stepping through the uc program. Disconnect the supply when leaving after a day.
Unnecessary time consumption when installing software	Medium	Low	Ask for help with standard setup of uc and programming. Include others in the programming process.
Transmission of wrong data or faults in the conversion calculations	Medium	Low	Verify the measurements using measuring tools like a multimeter using at least two different values.
Movements of equipment disconnects debugging or communication wires	Medium	Low	Use some sort of strain relief on the wires.

Prevention against electrical shock

- Always be at least two people on the lab when working on systems where the voltage is over 50 VAC.
- Use the Chargeberry cover to protect the electronics in the charger and against electrical shock. Drill a hole in the cover to insert wires that is needed to program and send data through so that the electronics still are covered.

- Always disconnect the supply when leaving after a day so that no one else starts working on the equipment.
- Make sure the Chargeberry is correctly inserted into the back plate.
- Disconnect the supply every time the Chargeberry is going to be removed, so that no screw terminals are visible without being disconnected.

Procedure

1. Connect the equipment together according to schematics in figure 1 and image in figure 2. Note for this thesis the electric arc generator is not going to be used, so the male socket from the load can be directly connected to the female EV emulator socket.
2. Test that the charger can start charging, by connecting a load and adjust the EV emulator. The EV emulator simulates (see figure 3) that an electric vehicle is connected to the charger so that other loads can be tested. The EV emulator provides PP and CP signals through the cable which tells the charging cable capacity and status of the car. Status A is used for no charging and C for charging:

Base status	Charging status	Resistance, CP-PE	Resistance, R2	Voltage, CP-PE
Status A	Standby	Open, or ∞ Ω		+12 V
Status B	Vehicle detected	2740 Ω		+9±1 V
Status C	Ready (charging)	882 Ω	1300 Ω	+6±1 V
Status D	With ventilation	246 Ω	270 Ω	+3±1 V
Status E	No power (shut off)			0 V
Status F	Error			−12 V

3. Connect the USB to TTL serial adapter and debugger module:
   a. Remove glue and open the cover of the Chargeberry so that access to the PCBs are given.
   b. Drill a 10 mm hole in the Chargeberry
   c. Connect the debugger module to the powerboard PCB according to the schematics (not shown in this report because of restrictions).
   d. Connect the USB to TTL serial adapter to the powerboard PCB according to the schematics (not shown in this report because of restrictions).
   e. Insert the wires through the hole and mount the Chargeberry cover. Use some tape to attach the wires to the charger so that movements of the equipment don't disconnect the wires. See figure 4.
4. Install programming software:
   a. Get help from Easee members to set up the PC for programming.
5. Prepare the uc software:
   a. The uc program is modified so that measurements can be taken and sent to PC on commend. See the thesis for more information and code.
   b. There is already existing code in the uc program that log certain events. Because fast transmission of data is critical and the mix of sending ASCII-characters and values, all existing code for logging are commented out. This removes the risk of receiving unexpected values which potentially can lead to the use of wrong values without noticing it

6. Prepare programs for receiving serial data and visualizing it (See the thesis for more information and code):
   a. A simple Python program was made where the user can interact with the uc using the text in the terminal. As the measuring time is relatively low and transmission time high, those events are marked with green text to highlight what is going on (se figure 5). The program receives data, do some conversions and saves it as a csv-file so that it easily can be imported into matlab.
   b. Matlab is used to visualize and process the raw data from the csv-file.
7. Verify **current measurements**. A is connected in series with the supply wire L1 and measures the current drawn from the charger.
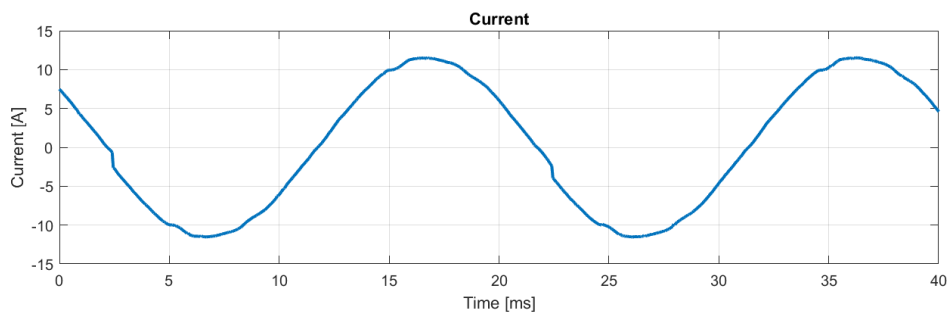   a. **No load connected**: Multimeter: 0.00-0.01 A. Data name: c_standby.csv.
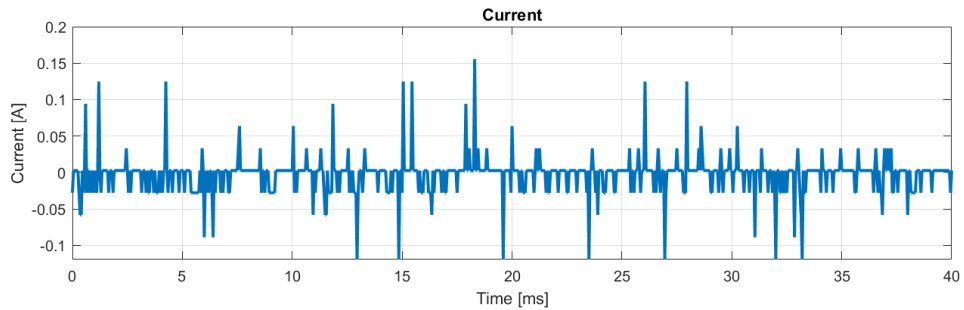
Matlab rms: 0.02 A.

   b. **1 kW load connected**: Multimeter: 4.22 A. Data name: c_1kW.csv.
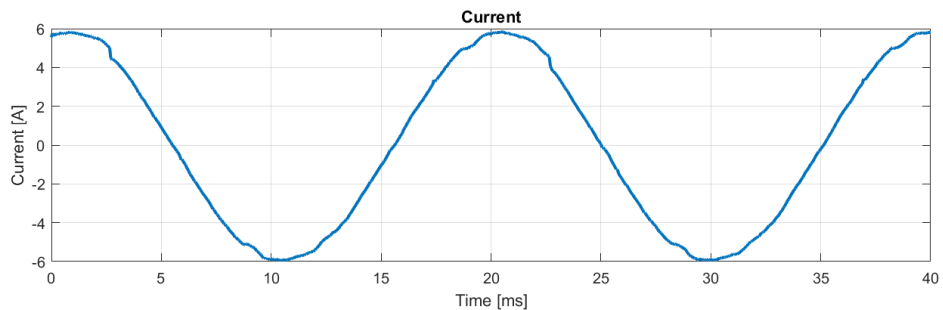

Matlab rms: 4.17 A.

   c. **2 kW load connected**: Multimeter: 8.24 A. Data name: c_2kW.csv.

Matlab rms: 8.15 A.

8. Verify **voltage measurements**. The voltage grid that is used in the lab is 230 VAC IT. The uc program is slightly modified (by uncommenting two lines under "Measure voltages" in function save_data for this test only) so that the voltages at terminal N and L1 can be collected. A multimeter measures the voltage at a parallel connected socket at the same time as the measurements.

    a. **No load connected**: Multimeter: 234.0 V. Data name: vN_vL1_standby.csv.
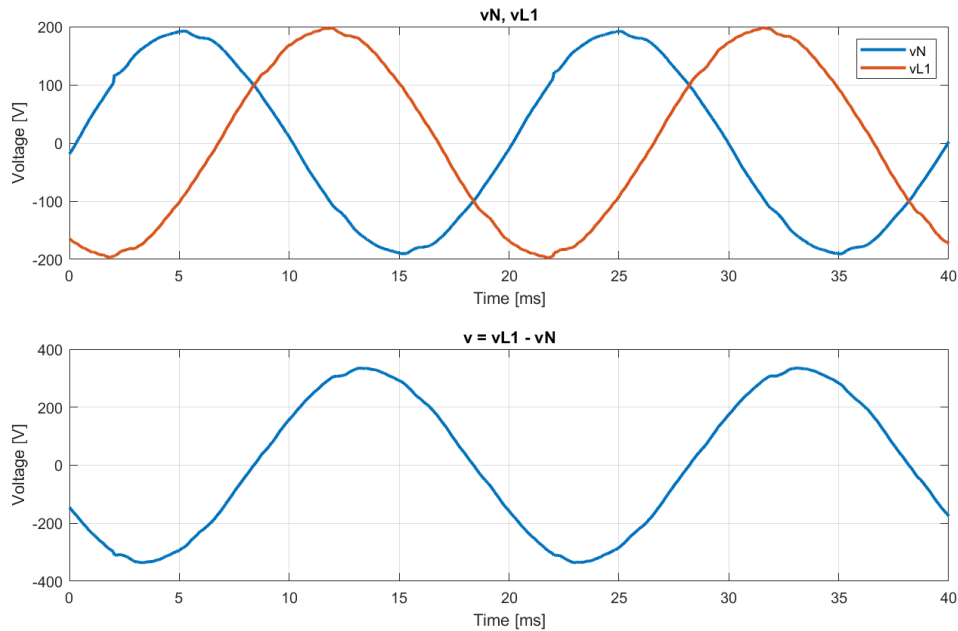
vN and vL1 have a max value of about 195 V, 120 ° according to each other, which is expected in an IT supply. The voltage $vN - vL1$ is calculated and according to matlabs rms function this signal has an rms value of 234.7 V.

    b. **2 kW load connected**: Multimeter: 230.7 V. Data name: vN_vL1_2kW.csv.
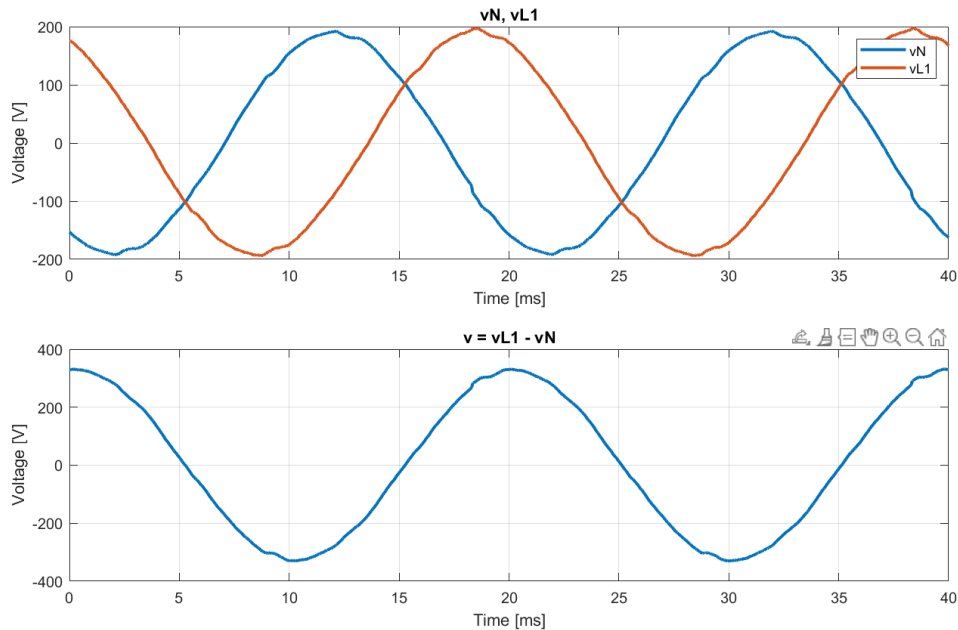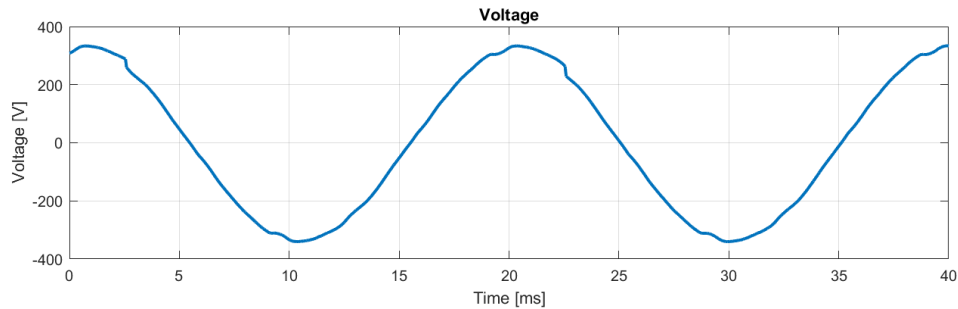
Matlabs rms function measures 231.3 V.

9. Verify **voltage measurement at L2 terminal**: L2 terminal is going to be used in later test reports to measure the voltage after the electric arc generator, as if the electric arc were located in the supply before the charger (tiny black wire in figure 4). In the uc program (which is going to be used in all later tests) the voltage is calculated relative to the neutral wire: $v = vL2 - vN$.

   a. **L2 connected to N**: It is expected that the voltage should be around 0 V. Data name: vL2_to_vL1.csv.
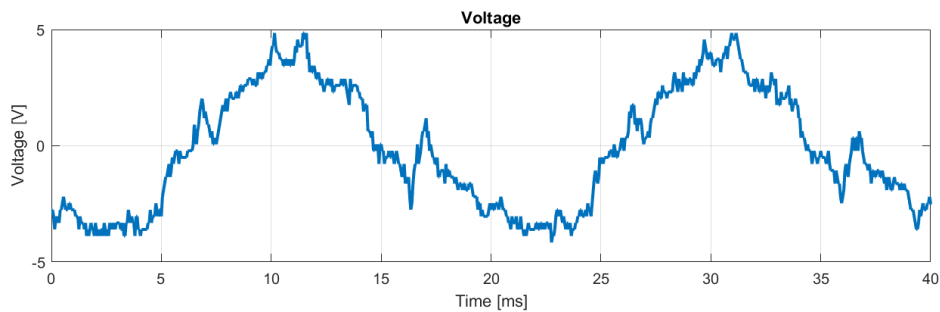
Matlabs rms function measures 2.5 V.

   b. **L2 connected to L1**: It is expected that the voltage should be the same as a multimeter shows connected in t a parallel connected socket at the same time as the measurements. Multimeter: 235.5 V. Data name: vL2_to_vN.csv.

Matlabs rms function measures 235.7 V.

Programs

All relevant programs are attached to the thesis. See "attachments". Name of the programs:

- Uc program: log_data.c, log_data.h (A separate program file are made for this system called log_data.c with the helper file log_data.h. This contains functions that are called from other parts of the program which is not shown in this report because of restrictions).
- Python: serialcom.py
- Matlab: import_data.m

Results and evaluation

Current measurements from the charger corresponds with the values from the multimeter. The highest deviation measured was 0.09 A which is acceptable for this purpose.

Voltage measurements indicates that the measurements from the charger are slightly higher than what are measured by a multimeter in parallel. The highest deviation measured was 0.7 V. This is acceptable for this purpose.

Voltage measurements from L2 terminal to N was expected to be around 0 V, but is measured to be 2.5 V. It is discussed together with Easee members that this is a result of noise on the PCB and variation in the values of measuring components on L2 and N terminal. When used to measure 230 V this will lead to a 1.1 % deviator. This is acceptable for this purpose.

All measurements show waveforms at around 50 Hz frequency. The waveforms are slightly uneven, but it is already known from earlier that there is some noise or unevenness in this power grid.
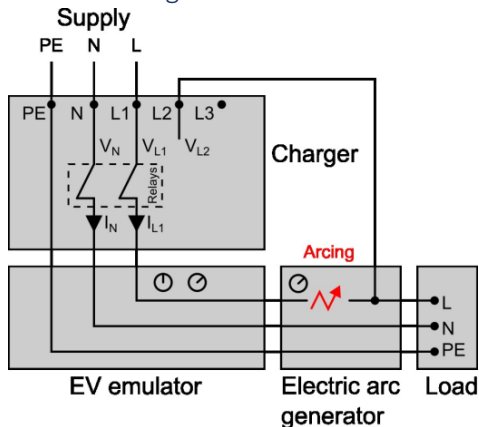
Relevant images

Figure 1: Schematics of data collection system.

Figure 2: Finished setup for testing data collection from the charger.
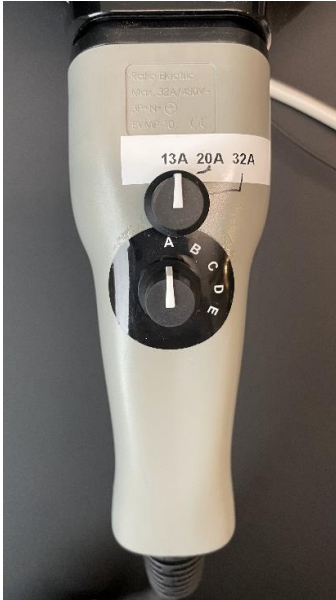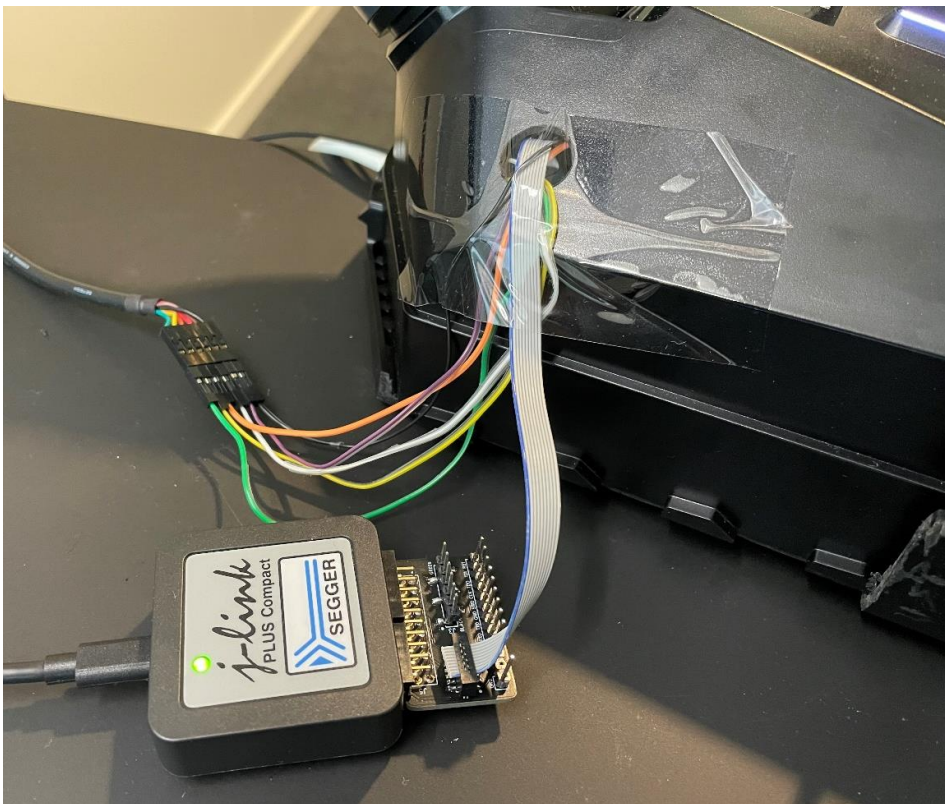
Figure 3: EV emulator.

Figure 4: Connection of USB to TTL serial adapter (upper) and debugger module (lower) through the hole in the Chargerberry.

```
Warning: File "data.csv" already exsist. Press <enter> to overwrite:
Starting thread
Port opened
Type a command:
        <enter>/m = Measure
        c = Continuous measurements
        e = Exit
m
Measurements started
Measurements done
Measurements received
Total intervals received: 1
Type a command:
        <enter>/m = Measure
        c = Continuous measurements
        e = Exit
e
User is happy!
Port closed
Total intervals received: 1
Data saved in "data.csv"
Thread terminated
```

Figure 5: Example of GUI in the Python program. One interval of measurements are taken before it is exited.

Test report number 3

Title: Generating electric arcs

Description: Start collecting data when electric arcs occurs by using the electric arc generator 1000. Current draw used in this report is 0.11-2 A.

Date: 16.03.2023

Participants: Espen Myrset

List of equipment:

- Electric arc generator 1000
- Easee charger
- EV emulator with male type 2 socket to standard EU socket
- Various electrical loads: 25 W lightbulb, 2 kW heat fan and an adjustable load for lab testing
- PC and USB hub
- USB to TTL serial adapter
- 2x 74271142 ferrite bead

Risk analysis

Risk	Probability	Severity	Action to minimise risk
Electric shock	Low	High	Do not work on powered equipment. Always be at least two people on the lab when working with voltages over 50 V. Attach all enclosures before powering up.
Unexpected small flames or explosions	Low	Medium	Start with low loads and stepwise increase to the desired load. Locate the fire extinguisher. Use protection glasses. Use an easily available socket. Keep some space to the electric arc generator except for one hand.

Procedure

1. This test report makes use of the data collection setup described in test report 2. The electric arc generator is connected between the charger and the load, like described in that test report. An image of the setup is shown in figure 1.
2. As low load as a 25 W lightbulb (0.11 A) is used to start with to minimize the outcome of unexpected events.
   a. When taking the first measurements of electric arcs the Python program froze from time to time. When restarting the Python program, the charger responded which indicated that something in Python or the serial communication was the problem. After some troubleshooting it was discovered that the electric arcs make high-frequency noise which propagates through the air or wires and to the charger. This disturbed the serial communication and not all the bytes are successfully transferring. When python waits for a certain number of bytes, it freezes. A solution for this problem was to attach one ferrite bead to each of the wires that comes from

the box where the electric arcs are generated which reduces the noise, and to physically separate and have distance between the communication line and the rest.

b. The test creates very small electric arc that can be seen with the eye and the 50 Hz net frequency could be heard. It was not possible to adjust the gap distance to generate constant electric arcs, rather adjustments had to be done exactly when the measurements were taken to make it visible in the measurements. But the current is too small to see the typical electric arcs properties in the measurements because of low current resolution.
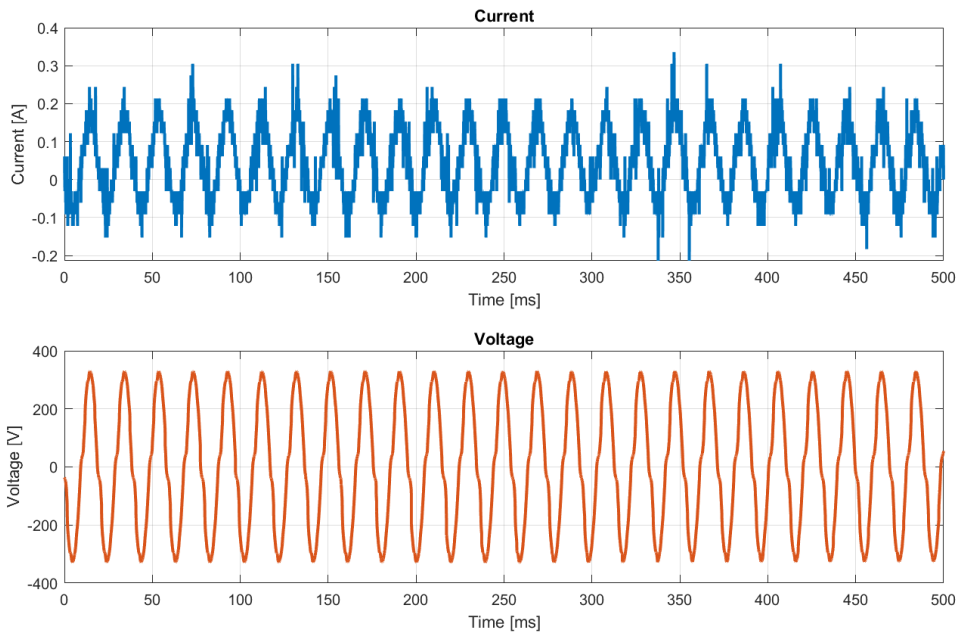
Filename: lamp.csv.

3. The heat fan is connected, first directly to the charger so that the current draw of the heat fan can be adjusted, then with the electric arc generator in between. The result is similar to the one with the lamp.

4. The adjustable load is connected. It can be adjusted to draw 0-10 A with 1 A per step. First it is set on drawing 1 A. After many measurements one of them shows the typical properties of electric arcs with nearly vertical spikes in each waveform. But since the load is so low it is

assumed that there is not enough heat to maintain the arc for many waves when the gap distance is moving.
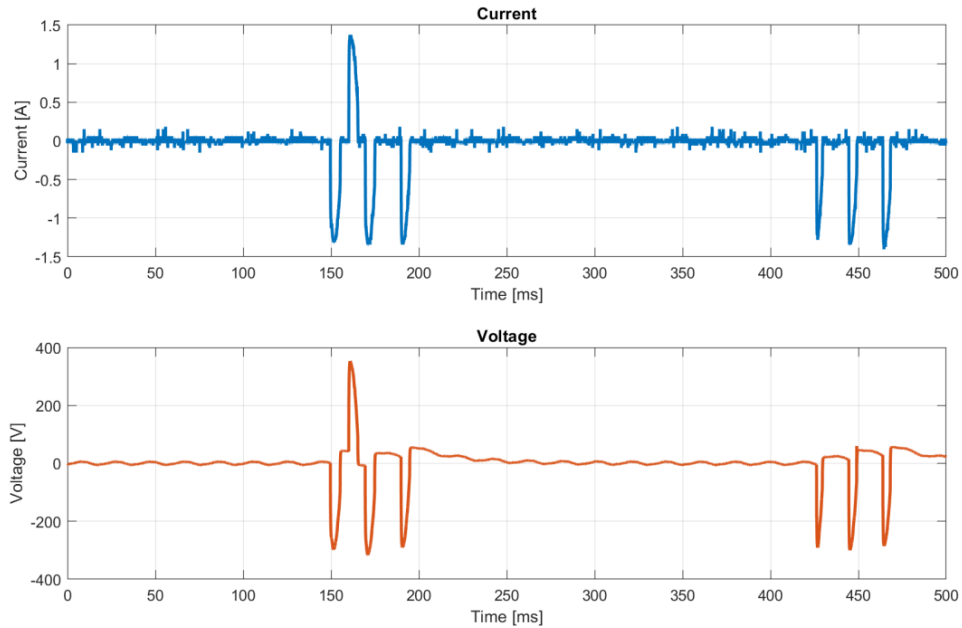
Filename: load_1A.csv.

5. The adjustable load is then set to draw 2 A. No electric arcs were observed in the measurements. The plastic bracket holding the bolts started melting because of the heat and the electric arc generator eventually broke.

Filename: load_2A.csv.

Results and evaluation

Loads were tested with a current draw of 0.11-2 A.

Arcing often resulted in a fault in the serial communication due to high-frequency noise in the cables and/or through air. This was fixed by connecting a ferrite bead to each of the wires that comes from the box where the electric arcs are generated, and separate the placement of communication cable and the rest.

From the shining light between the bolt in the electric arc generator, it looks like electric arcs were produced. Only one of the measurements from a 1 A current load showed typical electric arc properties. It is thought from the other measurements that the observations are a combination of electric arcs and red-hot metal, and by increasing the current, electric arcs may be easier to observe.

When drawing a current of 2 A the heat produced by the electric arcs/red-hot metal was enough to melt the plastic bracket holding the bolts so that the electric arc generator got broken.

Relevant images

Figure 1: Test setup for data collection using the electric arc generator 1000.

Test report number 4

Title: Making of electric arc generator 2000

Description: Because the electric arc generator 1000 was broken when a current load higher than 1 A was used, a new one needed to be made that can hold higher currents.

Date: 21.03.2023

Participants: Espen Myrset

List of equipment:

- 2x M6-30 stainless steel bolts
- 10x M6 stainless steel nuts
- 2x 6mm cable shoes
- Wooden plate
- Wire
- Stainless steel strap

Risk analysis

Risk	Probability	Severity	Action to minimise risk
Accident when using wood cutting tools	Medium	Medium	Use of protection equipment like safety glasses, ear protection and gloves. Use clamps to keep the wood in a fixed place.

Procedure

1. Considerations: The accuracy of the electric arc generator 1000 seemed redundant for this purpose, therefore no gears are used in the new version. M6 bolts instead of M3 bolts are used so that the bolts are more solid which hopefully better dissipate the heat so that electric arcs instead of red glowing metal occurs. The copper bolts are replaced by stainless steel which has a little bit higher melting point.
2. Wires are connected to each of the bolt using a cable shoe and two nuts. Three nuts are then inserted to the bolts. See figure 1.
3. The three nuts are not tightened on one of the bolts. A strap is used to attach them to the wooden plate with the bolt head outside the plate. This is the adjustment bolt.
4. The three nuts on the other bolt is tightened and a strap is used to attach it so that the bolt touches the adjustment bolt.
5. The wire are connected in the same way as with the electric arc generator 1000, se test report 1.
6. **Note** that the adjustment bolt is under voltage when powering on, so operating this must be done in a proper way to avoid electric hazard.
7. As a shield a plexiglass box is used at the lab. This has a small gap in it allowing adjustment of the bolt during testing.

Results and evaluation

An improved version of the previous electric arc generator 1000 was made. It is called the electric arc generator 2000.
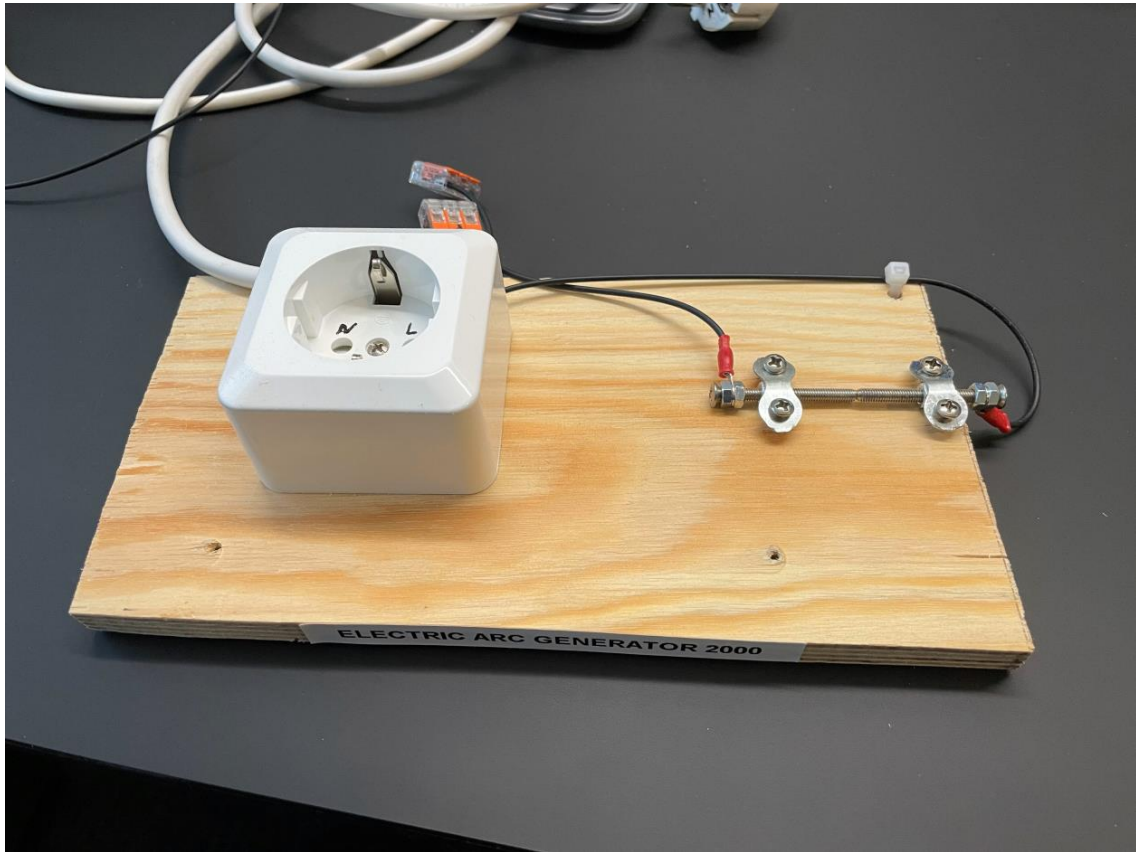
Relevant images

Figure 1: The finished electric arc generator 2000.

Test report number 5

Title: Collecting data of electric arcs

Description: Collecting data of electric arcs by using the electric arc generator 2000. Current draw used in this report is 1-10 A.

Date: 22.03.2023

Participants: Espen Myrset

List of equipment:

- Electric arc generator 2000 placed in a plexiglass protection box
- Easee charger
- EV emulator with male type 2 socket to standard EU socket
- Adjustable load for lab testing
- PC and USB hub
- USB to TTL serial adapter

Risk analysis

| Risk	Probability	Severity	Action to minimise risk
Electric shock	Low	High	Always be at least two people on the lab when working with voltages over 50 V. Attach all protection equipment before powering up. Get assistance from others with certification in live line working. Use at least two safety barriers.
Unexpected small flames or explosions	Low	Medium	Attach the electric arc generator into the plexiglass box in a safe manner. Start with low loads and stepwise increase to the desired load. Locate the fire extinguisher. Use protection glasses. Use an easily available socket.
Burnt skin when touching the adjustable load	Medium	Medium	Block off the testing area and notify other people that testing is ongoing.

Procedure

Safety first: The adjustment bolt is a live wire when powering up and needs to be turned to generate electric arcs. This procedure is defined as live-line working, and only personnel with certification in live line working can do this task. Personnel protection equipment is barrier 1, and proper isolated tools is barrier 2. In this case isolating gloves, isolating floor mat and isolating screwdriver was used.

1. This test report is more or less a continuation of the work that was done in test report 3, but now with a more robust electric arc generator. See test report 2 and 3 for setting up and figure 1.
2. First measurements are taken with the adjustable load during normal conditions. The current levels that are going to be tested is 1-10 A with 1 A increase for each step. Four normal signals for each step are collected and saved.

3. Electric arcs are generated, and measurements are taken using the adjustable load. The light and the measurements are observed. Four arcing signals that lasts at least 120 ms are collected and saved. Some of the measurements are shown:
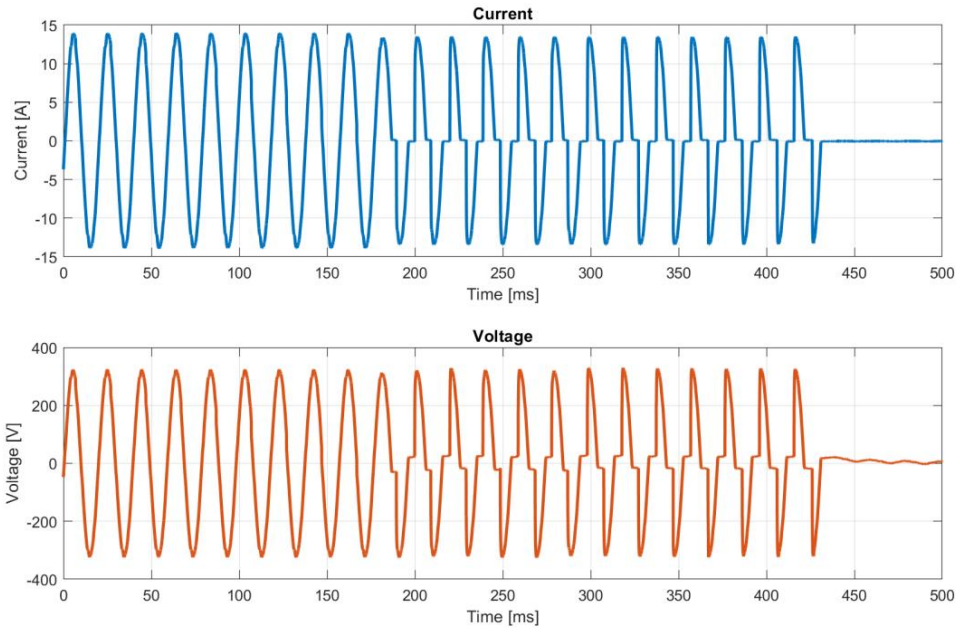
   a. 4 A current load. Filename: load_4A.csv:
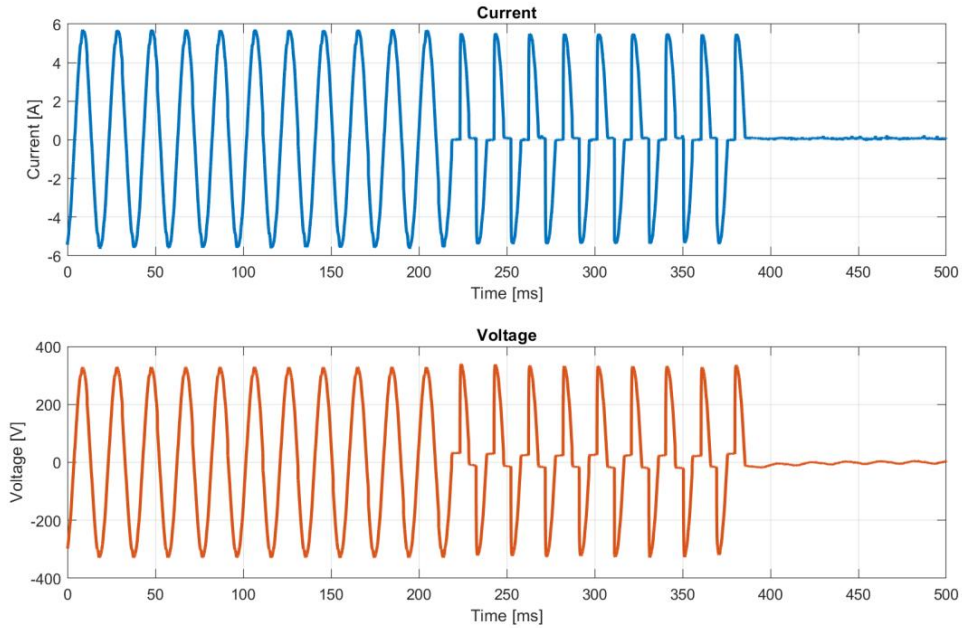
   b. 7 A current load. Filename: load_7A.csv:
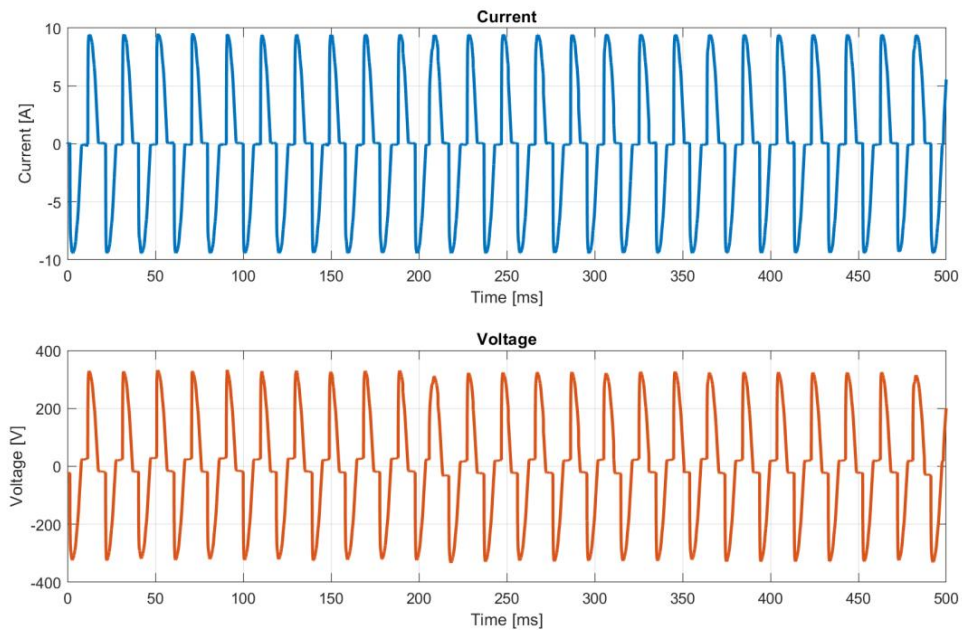
   c. 10 A current load. Filename: load_10A.csv:

Results and evaluation

Loads were tested with a current draw of 1-10 A. For each step four signals of normal and arcing that lasted at least 120 ms were collected and saved. The higher current the easier it was to generate arcing.

The gap distance needed to be very small or none (so that the bolts touched each other) before electric arcs occurred. Then the distance could be increased a bit before the arcing stopped, probably because the high temperature to the bolts and surroundings during arcing makes it easier to trigger new ones.

Two types of light were observed (See figure 2):

1. Bright white/blue light: Looks like they are electric arcs because of the light intensity and measurements.
2. Glowing orange light: Often occurred after electric arcs. It was impossible to separate this state from the normal conducting state using the measurements. It is assumed that this light came from vaporized metal from the bolts caused by the intense heat from the electric arc nearly welding the bolts together. But because of the small amount it was acting just like a small glowing bulb.

Relevant images

Figure 1: Test setup for data collection using the electric arc generator 2000.
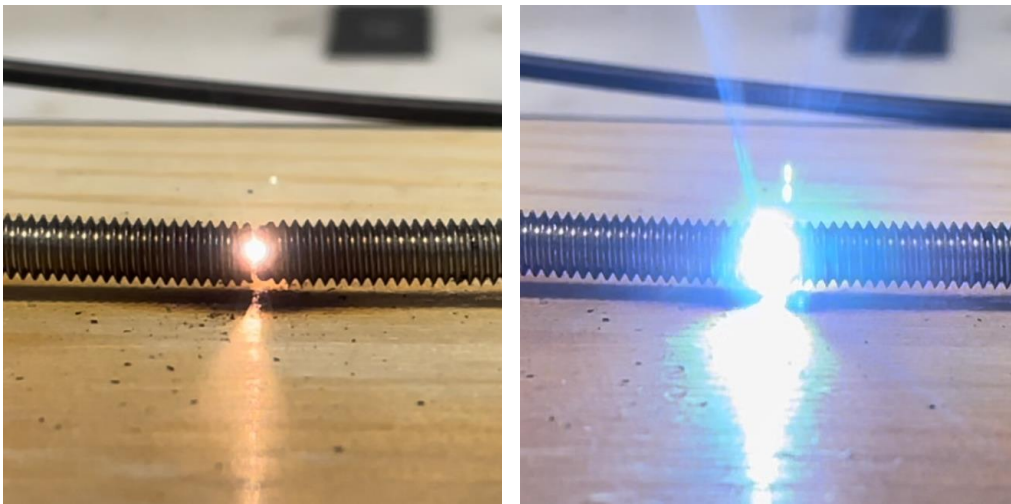

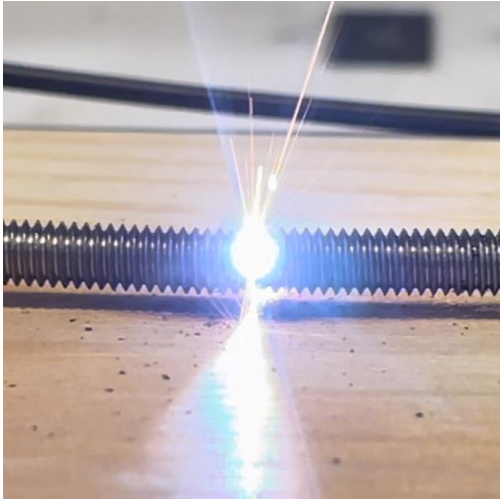*Figure 2: Two types of observed light; glowing orange and a bright white/blue light.*

Figure 3: Transition between the orange and white light.

Test report number 6

Title: Testing the algorithm

Description: In the thesis it is described that a threshold should be chosen in further work as this is a comprehensive task out of the scope for the thesis. However, the algorithm is in this test report tested with an example threshold to get a measure of how good the resulting algorithm is.

Date: 29.05.2023

Participants: Espen Myrset

List of equipment:

- PC with Matlab and the collected data from test report 5

Procedure

1. From the thesis it is found that the threshold should be between $483 \cdot 10^{-9}$ and $22.7 \cdot 10^{-3}$. As an example, the threshold is set to $\mathbf{18 \cdot 10^{-3}}$ in this test report.
2. The collected data from test report 5 contains measurements for loads of 1-10 A with 1 A increase for each step. Four measurements of both normal and arcing are available for each of the steps.
3. Using the algorithm with the example threshold, it is observed on the collected data if it manages to classify the signals correctly within the 110 ms requirement (120 ms minus the 10 ms relay release). Table 1 shows how many of the four signals it manages to classify correctly for each step (see figure 1 for an example):

	Nr. of correctly classified	
Current level [A]	**Normal**	**Arcing**
1	4	4
2	4	4
3	4	4
4	4	4
5	4	4
6	4	4
7	4	4
8	4	4
9	4	4
10	4	4

Table 1: How many of the 4 collected signals that is classified correctly within the time requirement.

Results and evaluation

The algorithm manages to classify 100 % of both the normal and arcing signals correctly within the time requirement.

The normal signals have barely any change in the average energy x_{nrg} and is approximately 0 all the time. The arcing signals are usually detected within 40-50 ms from when the arcing starts.
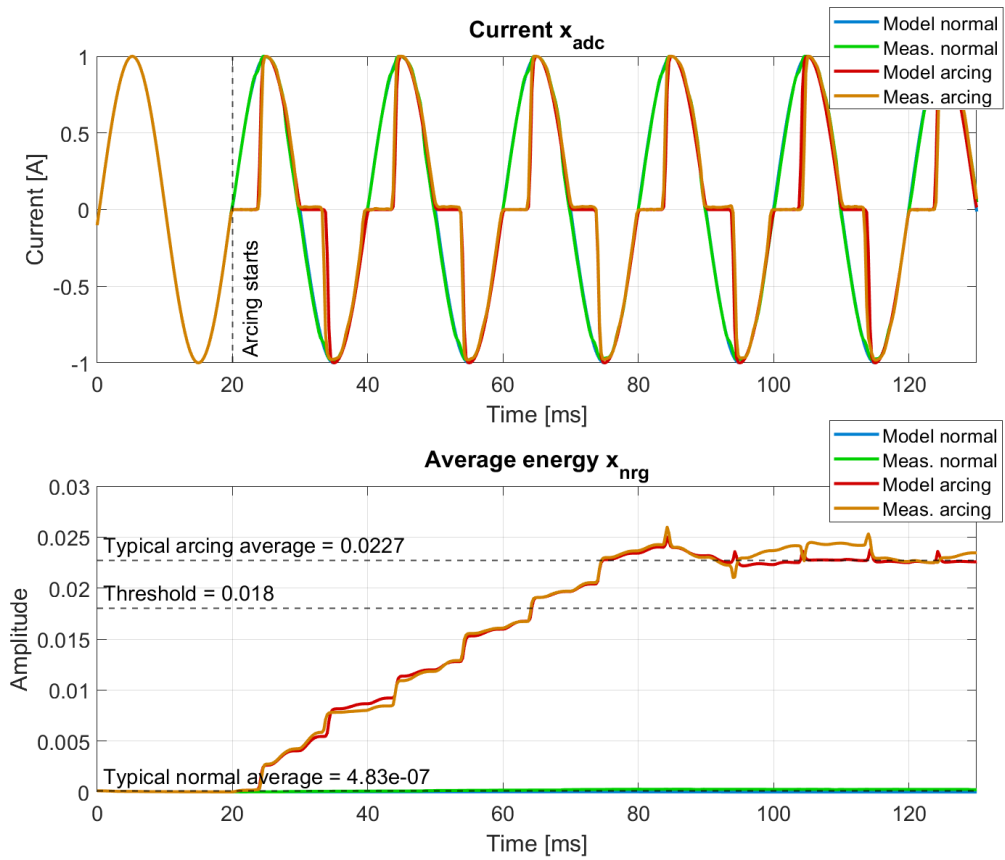
Relevant images

Figure 1: Example of a test of the collected data with a threshold value of 0.018. The mathematical model is also included for comparison reasons. The algorithm manages in this case to detect arcing in 45 ms which is within the requirement.